EXPERIMENTAL STUDY ON BOND BEHAVIOUR OF CFRP SHEETS EXTERNALLY BONDED TO REINFORCED CONCRETE

by

Emmanuella O. Atunbi

B.Sc.E. (Civil Engineering) University of Ilorin, Nigeria, 2014

A Thesis submitted in Partial Fulfillment of the Requirements for the Degree of

Master of Science in Engineering

In the Graduate Academic unit of Civil Engineering

Supervisors: Alan Lloyd, PhD, Department of Civil Engineering
Peter H. Bischoff, PhD, P.Eng, Department of Civil Engineering

Examining Board: Kaveh Arjomandi, PhD, P.Eng, Department of Civil Engineering
Gobinda Saha, PhD, P.Eng, Department of Mechanical Engineering
Xiomara Sanchez, PhD., P.Eng., Department of Civil Engineering

This thesis is accepted by the Dean of Graduate Studies

THE UNIVERSITY OF NEW BRUNSWICK

January 2018

ABSTRACT

Fiber reinforced polymers (FRP) have become widely used in retrofitting existing reinforced concrete (RC) structures because of their high strength and stiffness-to-weight ratio. An important aspect in the design of this composite element is determining the bond behaviour of the FRP sheet-to-concrete interface. Previous studies have involved the use of conventional instrumentation (typically strain gauges) that provide limited data to work with. This study presents an experimental investigation to determine the effect of bond length and stress on the bond behaviour of FRP-to-concrete interface under static loads using a digital image correlation (DIC) technique. Twelve double lap shear specimens bonded with carbon fiber reinforced polymer (CFRP) sheets were tested with varying bond lengths. Development length, longitudinal strains and bond stress and slip relationships were obtained and compared with values computed from existing models. Comprehensive results were obtained from the DIC technique which allowed for proper monitoring of the progression of failure and the effect of shear lag on the distribution of stresses in the FRP sheet.

ACKNOWLEDGEMENTS

I would like to extend my gratitude to the following people:

- My supervisors, Dr. Alan Lloyd and Dr. Peter Bischoff, for their guidance and advice throughout the completion of my program. I really appreciate their help and support.
- The administrative staff of the Civil Engineering department, Joyce Moore, Angela Stewart and Alisha Hanselpacker and the laboratory technicians for their assistance all through my stay as a Master's student at UNB.
- My parents, Emmanuel and Elizabeth and my siblings, Francis, Cecilia and Gregory for their unconditional love, motivation and assistance during my studies in Canada.
- My friends and colleagues who have contributed in one way or the other towards the successful completion of my Master's program.

TABLE OF CONTENTS

LIST OF TABLES

LIST OF FIGURES

1.0 INTRODUCTION

1.1 General

The need to repair and improve the strength of existing reinforced concrete (RC) structures has become a significant topic for engineering researchers. Reinforced concrete structures deteriorate due to ageing, corrosion, poor maintenance, increase in load, and unforeseen situations like impact, blasts and earthquakes (Setunge et al. 2002). Before now, steel sheets were the most common when it comes to the improvement and rehabilitation of these structures. These sheets or plates were externally bonded to the existing reinforced concrete members to improve their load carrying capacity and strength. This method is simple, cheap to maintain, and has a high mechanical performance but possesses certain disadvantages such as; maneuvering difficulty, steel corrosion, requirement of a temporary support system (scaffolding), and the limitation in available plate lengths resulting in the need to join more than one sheet to get a longer length (Meier, 1997).

Fiber reinforced polymers (FRPs) are known to gradually replace the use of steel in the rehabilitation of RC structures. This is because of their excellent strength capacity, stiffness-to-weight-ratio and corrosion resistance. In addition to increasing the ultimate capacity of the structure, the application of externally bonded FRP sheets for the flexural strengthening of RC elements is also known to mitigate the development of cracks under low and high magnitude loads. The most commonly used FRP materials are carbon FRP (CFRP), glass FRP (GFRP), aramid FRP (AFRP) and basalt FRP (BFRP) which is still new when it comes to its use in the industry. Each of these materials has its own advantages and disadvantages which will be discussed further in the literature. Depending on the kind

of application and outcome that is to be achieved, a choice of material can be made to yield the desired premium results.

To properly design the FRP strengthening system, the capacity of the bond (bond strength) between the FRP sheet and the concrete substrate must be known. FRPs are bonded to the concrete substrate using adhesives commonly known as resins (examples are epoxy, vinyl ester and polyester). There are certain material and structural factors that affect the bond between the concrete substrate and FRP sheet such as the material properties of the FRP sheet and concrete, the type of load the structure is subjected to, the surface condition as well as geometric shape of the structural element (Shen et al., 2015).

Researchers have found that FRP sheets perform well as a strengthening retrofit for static load applications up to the point of failure which most times is due to debonding. Experimental and analytical investigations on the FRP-concrete composite properties such as bond strength and other aspects of the layup of externally bonded FRP sheet to RC structures under static and quasistatic load rates have been carried out by many researchers (Chiew et al., 2007, Smith and Teng, 2001, Ahmed et al., 2011 and many more) and the results have been incorporated into many models used for present day design guidelines. The need to still revisit this study is important because varying test setups and analytical programs have been employed by different researchers that have led to different and sometimes conflicting results.

Since there are discrepancies in results obtained by previous researchers in the study of FRP strengthened beams under static loads, the proposed study aims to improve on existing knowledge and results. In order to achieve this, previous literature will be extensively explored. A series of double lap shear tests will be carried out on FRP sheet bonded to

concrete prisms under static load to investigate the behaviour and strength of the bond between the FRP-to-concrete interface. CFRP sheet is to be investigated in the proposed experimental research. A Digital Image Correlation (DIC) software will be used in determining the strain values along the length of the bonded FRP sheet. Static test results obtainedfrom this study will then be compared to experimental and analytical results obtained from existing literature.

1.2 Aim and Objectives

The core aim of this study is to assess and determine the material properties of FRP-to-concrete bond subjected to static loads. This research is limited to a study of strengthened prisms where the concrete, externally bonded FRP sheet and embedded steel are in tension. The work carried out in this thesis forms the first part of a more extensive research program investigating the bond behaviour of FRP strengthened members under static, dynamic and impact loading.

The objectives of this study include:

- Understanding the static behaviour of FRP bonded reinforced concrete prisms
- Review of both experimental and analytical results from previous studies to determine the interfacial bond response of FRP composite elements under static and dynamic loads
- Performing experiments under static load and comparing results with those stated by other researchers including those included in the standard design codes.
- Use of the Digital Image Correlation (DIC) analysis technique in determining strain values on FRP sheets bonded to concrete.

1.3 Scope of Study

The scope of this study includes the experimental and analytical investigation of FRP sheet bonded RC prisms comprised of the following procedures:

1. Review and collation of previous experimental studies on the effect that both static and dynamic loads have on the bond between FRP-to-concrete interface.
2. Review of techniques used to bond FRP sheets to concrete.
3. Study of proposed analytical models to determine the behaviour and characteristics of FRP bonded concrete.
4. Design, build, and test FRP bonded reinforced concrete prisms using the double lap shear test method. The tests are carried out using various development lengths of CFRP sheets under static load.
5. Evaluate test data and compare with test results obtained by previous researchers.
6. Compare experimental results with results obtained from previously designed models including those recommended in the design standards.
7. Report results obtained from the study and presentation of design recommendations.

1.4 Review of Thesis Content

Previous studies on FRP bonded RC structures are reviewed. The uses, advantages and disadvantages of the various types of FRP materials are discussed in Chapter 2. Previous studies on FRP strengthened concrete under static, quasistatic and high strain rates are discussed in this chapter as well. Chapter 3 gives details about the setup and methodology of the experimental research carried out to determine the effect of static load on the bond strength of FRP-to-concrete interface. The test results are then presented in Chapter 4 and compared with models previously proposed based on various concrete parameters and FRP

parameters (length, thickness, width and so on.). Chapter 5 is a journal that gives the detailed comparison of stress, slip and development length results obtained from the experiments and those obtained based on calculations using existing models. Conclusions and recommendations on how to improve the bond strength of the FRP-to-concrete interface based on results obtained from the experimental investigation are presented in Chapter 6.

2.0 LITERATURE REVIEW

2.1 General

Seismic effects as well as the possibility of a high explosive attack on structures has become a significant topic in research and design all over the world. It is critical that load bearing RC elements can withstand high lateral loads and retain some degree of post-load capacity. Hence, the need to improve existing RC structures to meet these service demands. One of the ways this can be achieved is by bonding FRP sheet to the face of the RC element (Lloyd et al, 2011). This is a reliable way to improve and strengthen existing structures as opposed to complete reconstruction. Externally bonded FRP sheets have been successfully applied to reinforced concrete beams and other structural elements to increase their strength and load carrying capacity (Ahmed et al, 2011). In addition to the fact that FRP sheets delay the appearance of visual cracks, its attractive use is due to its excellent strength, high stiffness-to-weight properties, and corrosion resistance (Maalej and Leong, 2005).

In this section, the various types and properties of FRP materials are discussed, and the mechanism of debonding is considered. The various methods in which bond between FRP sheet and concrete can be understood experimentally are discussed, as well as past studies carried out on the bond between FRP sheet and concrete in structures are highlghted.

2.2 Types and Properties of Surface Bonded FRP Materials

FRP consists of two main composite materials which are fiber (such as carbon or glass) and resin (such as epoxy, vinyl esters or polyesters). The four most common types of FRP materials as earlier stated are; carbon FRP, glass FRP, aramid FRP and basalt FRP. Basalt FRP have been introduced in the structural industry in recent times. Surface bonded FRP

sheets have both advantages and disadvantages. They are linearly elastic, undergo brittle failure, and fail at large strains (Correia, 2013). FRP sheets consist of high strength fibers bonded together by a resin matrix which include epoxies, polyesters and vinyl esters (Berver et al., 2001). The properties of FRP Sheets (or laminates) depend on the orientation, type, and volume of fiber used. The type of resin and the quality control used during their manufacturing process affect the behaviour of the laminates when used for strengthening or repair (Setunge et. al, 2002). Figures 2.1(a) to (d) show pictures of the various types of FRP sheets available for use.

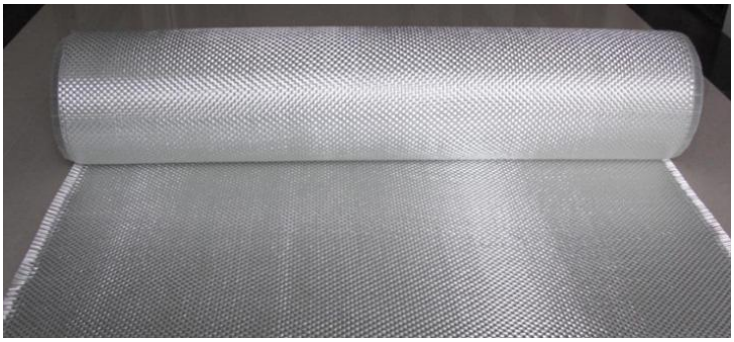

Figure 2.1(a): Glass FRP sheet

(Retrieved from: http://www.kripainternational.com)

Figure 2.1(b): Carbon FRP Sheet

(Retrieved from: http://www.sp-reinforcement.eu)

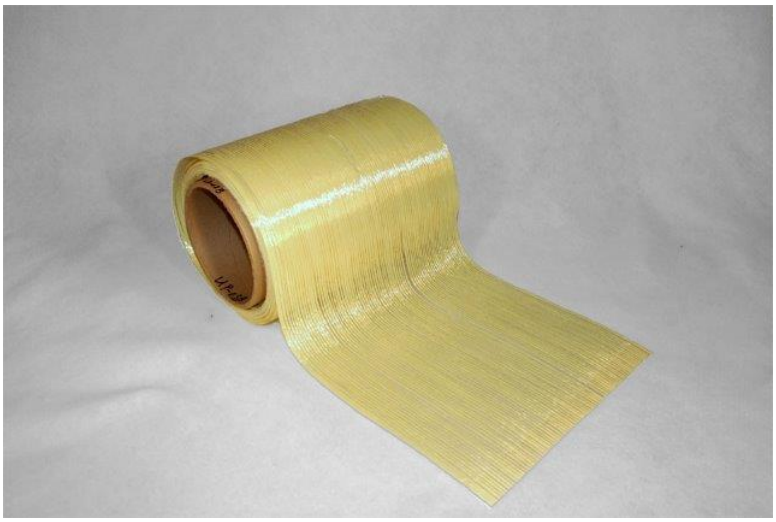

Figure 2.1(c): Aramid FRP Sheet

(Retrieved from: http://www.acpsales.com)

Figure 2.1(d): Basalt FRP Sheet

(Retrieved from: http://www.eas-fiberglass.com)

As stated earlier, fiber and resin make up the FRP composite and each component gives the composite material certain characteristics or properties. The fibers provide the necessary tensile strength and stiffness while the resin serves as the binder for the fibers (Berver et al., 2001). Details of the advantages and disadvantages of the types of fibers and resins will be discussed in subsequent subsections.

2.2.1 Fibers

Fibers can be manufactured as either a woven roving or a chopped strand mat depending on the FRP properties desired by the user. Correia (2013) described some of the drawbacks and benefits of the different reinforcing fibers with glass fibers being the cheapest and most commonly used. Glass fibers are usually affected by creep and are likely to degrade under high temperature and in an alkaline environment. Carbon fibers are expensive and have good creep resistance. Aramid fibers also have good creep and fatigue resistance. Basalt fibers have similar properties to glass fibers, but they are non-abrasive and biodegradable.

Physical and mechanical properties of the different types of FRP fibers are provided in Table 2.1.

Table 2.1: Properties of Reinforcing Fibers:

Property	E-Glass	Carbon	Aramid	Steel
Elastic Modulus (GPa)	73 - 88	200 - 400	70 - 90	200
Ultimate Strength (MPa)	2350 - 4600	2600 - 3600	2800 - 4100	400
Ultimate Tensile Strain(%)	2.5 - 4.5	0.6 - 1.5	2.0 - 4.0	0.2
Density (Kg/m^3)	1200 - 2100	1500 - 1600	1200 - 1500	7900

2.2.2 Resins

As indicated by Setunge et al (2002), manufacturers use resins that are resistant to environmental conditions such as salt, moisture and extreme temperatures. They are expected to be workable, compatible with both the concrete substrate and the fiber and must have mechanical properties that suit the FRP composite system. There are two major types of resins; thermoset and thermoplastic polymer resins.

Thermoset polymer resins are those types of polymers that cannot be amended or reversed by reheating. They are injected into the molds in the case of pultruded shapes in liquid form and then solidify after curing. Examples include: epoxies, vinyl esters and polyesters. Thermoplastic polymer resins on the other hand, solidify at room temperature and liquefy when heated. Hence, a thermoplastic polymer resin can be reformed or reversed by heating. The resin in its melted form is infused into the reinforcing fiber bundles and then cooled under pressure for it to become solid. Examples include; semi-crystalline, amorphous and poly ether-ether ketone resins (Correia, 2013).

2.3 FRP Manufacturing Techniques

Commercial FRPs can be manufactured through various methods such as: pultrusion method, hand lay-up method, and the filament winding method. They are simple to manufacture but require a careful application and good workmanship during installation. The pultrusion method is used to manufacture FRP composites of definite shapes such as rods, beams, channels and plates in the factory. In this method, fibers are saturated with resin and then pulled through a heated die to form a definite shape. Hand lay-up method involves pre-pregnating the fibers with resin manually before installation. They are mostly used when FRP sheets are to be installed. Filament winding is generally used in the production of spherical and circular FRPs in the factory. It involves winding the saturated fibers round a mandrel to produce a circular shape. The pultrusion and filament winding method are simple to use and produce higher quality FRPs compared to the hand lay-up method (Ballinger 1991, Campbell, 2010).

For FRP sheet installation, the FRPs are made into laminates by layering single sheets of fibers in various orientations to obtain the desired strength and stiffness properties required. The strength and stiffness properties of the laminate depend on the direction and system in which the plies are laid. It is required that the right ply orientation is selected to provide a structurally efficient design. When fibers are laid such that each layer of the composite is in one direction such that its strength and stiffness are provided only in that direction, it is called a zero-degree direction laminate or one-direction lay-up of FRP sheet. They have high elastic modulus and increase the load bearing capacity of the structure. When fiber plies are arranged in two directions perpendicular to each other, the product is known as a ninety-degree direction FRP or bi-directional laminate. Bi-directional laminates are more

suitable for increasing the ductility rather than the load bearing capacity of the structure, they can be stacked in either a 0º, -45º, +45º and 90º sequence or in a 0º, -60º, and 60º sequence also known as quasi-isotropic sequence (Campbell, 2010).

The strength and load-bearing capacity of FRP sheets greatly depend on the fiber orientation. It is therefore important to place as many layers of FRP sheets as possible in the main load bearing direction required. Figure 2.2 shows a unidirectional layup and a quasi-isotropic layup sequence of FRP sheet having equal numbers of plies in all directions:

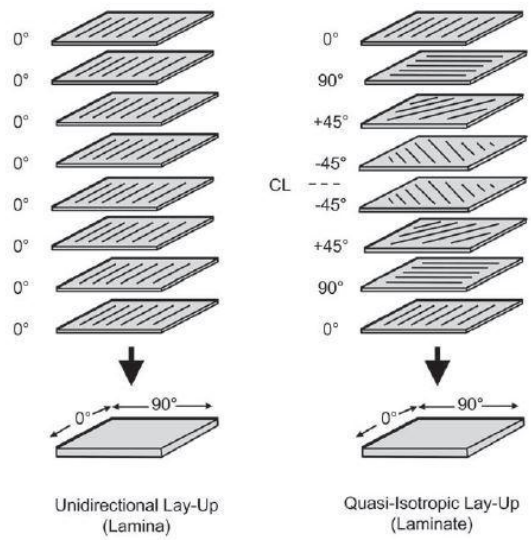

Figure 2.2: Laminae and Laminate Lay-up Sequence of FRP Sheet (Campbell, 2010)

2.4 Strengthening of Reinforced Concrete Beams with FRP Sheets

Although FRP sheet enhances the stiffness and load bearing capacities of RC structures, the effect of the failure modes found in the FRP bonded RC structure is one of the salient areas to be addressed (Wu and Niu, 2000). Different types of failure modes have been identified from previous studies. The failure modes identified include; flexural failure by

FRP rupture, failure by crushing of compressive concrete, shear failure, plate (sheet) end interfacial debonding failure, intermediate crack induced interfacial debonding failure, and failure due to concrete cover separation (Teng et al., 2002).

The first three failure modes are regarded as sectional failures and are like those that occur in normal RC structures (RC structures without externally bonded materials). The other three types can be termed as debonding failures. They cannot be found in normal RC structures and usually occur before the concrete fails or the FRP ruptures. For this reason, they are termed as a premature failure (Pham et al., 2016). According to results from tests and analysis from past studies, debonding failures can occur due to the number of layers of FRP sheet bonded to the concrete, the bond length of FRP sheet as well as the compressive strength of concrete. According to Pan et al. (2009), Smith and Teng (2001) and Lu et al. (2007), debonding failure can be classified into two broad types: plate end debonding failure that originates at the sheets or plates near the supports and then propagates to other parts of the bonded structure and intermediate crack induced interfacial stress debonding caused by the development of flexural cracks that propagate towards the plate ends.

Interfacial stress debonding failures are caused by high stresses developed at the sheets and transmitted to the concrete. The stress causes intermediate cracks to originate at the critical section (which is usually the midspan for beams) which then propagates towards the sheet ends. This mechanism tends to affect the strength of a substantial part of the FRP strengthened beams (Smith and Teng, 2001, Sebastian, 2001). There are two stages of the debonding process as stated by Sebastian (2001), they are the initiation phase and the propagation phase. In the initiation phase, a flexural crack at midspan causes the

development of inclined cracks around it. As the inclined cracks widen, the FRP sheet bends (dowel action), causing the FRP sheet to pull the adhesive and concrete cover on one side of the crack thereby causing failure along a horizontal plane. Just a thin layer of concrete cover is detached from the main original beam; the delaminated concrete, adhesive and sheet remain as a single entity. In the second stage, the inclined cracks gradually increase in length as additional load is applied on the beam. The inclined fracture continues to increase until the bonded FRP sheet is completely detached from the beam. The energy released during this process is sometimes enough for concrete wedges limited by flexural or inclined crack to be dislodged from the beam. Figure 2.3 shows the crack induced interfacial stress debonding process.

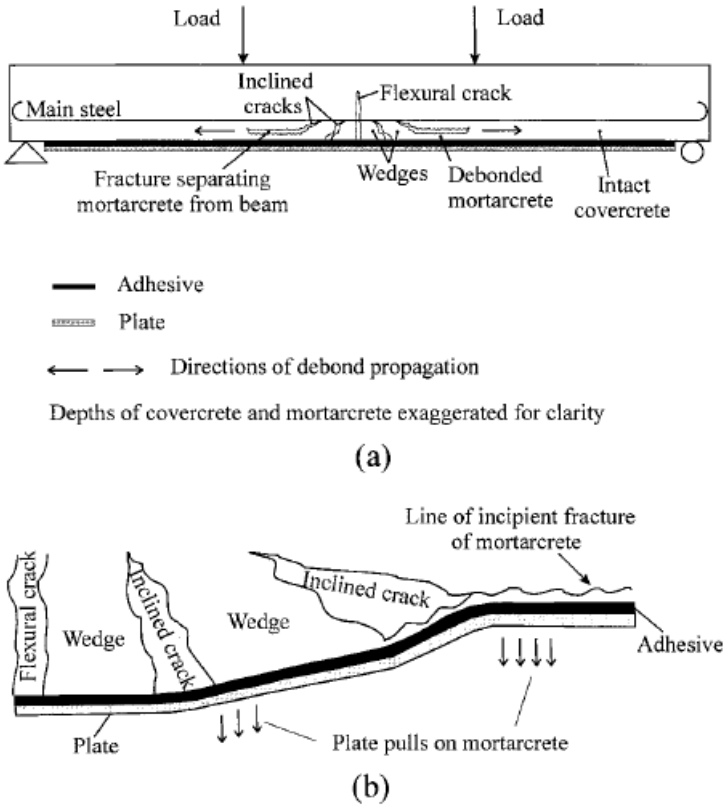

Figure 2.3: Interfacial Stress Debonding: (a) Mode of Failure (b) Dowel Effect in Plate. (Sebastian, 2001)

Plate end debonding failure originates at the ends of the FRP plates or sheets because of the formation of a crack that spreads inwards into the beam, away from the plate end. The abrupt termination of the plate near the support causes the initiation of high shear and normal stresses to occur at this location thereby causing inclined cracks that propagate horizontally to the level of the tension reinforcement. This causes the concrete cover to break away from the beam while firmly attached to the FRP sheet (Sebastian, 2001). It is generally believed that this type of debonding failure comes into existence when the interfacial shear and normal stresses exceed the strength of the weakest material which is usually the concrete (Smith and Teng, 2001). Figure 2.4 shows the plate end debonding process and the mechanism of development of vertical stresses at the plate ends.

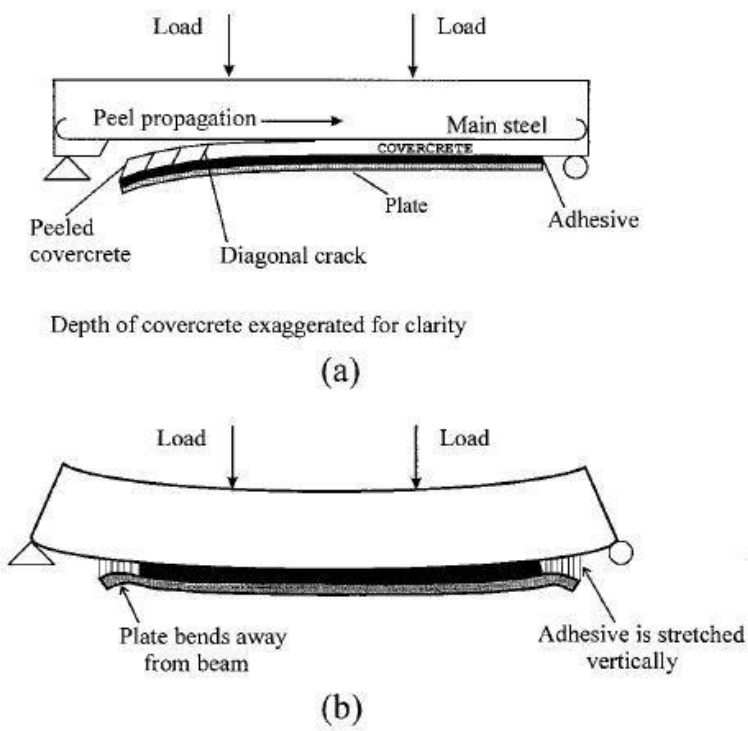

Figure 2.4: Plate End Debonding in Concrete Beam (a) Mode of Failure (b) Mechanism of Development of Vertical Stresses Near Ends of Plate (Sebastian, 2001)

2.5 Tests to Assess the Bond Behaviour Between FRP-to-Concrete Interface

Previous studies have shown that the flexural strengthening of RC using FRP sheets or laminates often develop premature failure due to debonding (as stated earlier). This has been observed experimentally (using various types of tests) and analytically. Some of the test methods include; the flexural beam test (bending test), the pull-out test, and the push test (direct shear tests). These test methods help to determine the bond behaviour between the FRP-to-concrete interface as well as assess the mechanism behind the debonding process. It has also been observed that different test set-ups can yield significantly different results (Bizindavyi and Neale, 1999, Chen et al. 2001, Yao et al. 2005).

The flexural beam test can be used to determine the bond behaviour between concrete and FRP laminates. Bonded specimens are subjected to three or four-point bending. Pham et al. (2016) employed this method to investigate the debonding failure mechanism of reinforced concrete beams retrofitted with CFRP sheets. Figure 2.5 shows the setup for a three and four-point bending test carried out on an FRP-to-concrete composite beam by pham et al. (2016). Other researchers such as Cheng et al. (2001) and Lee and Moy (2007) also used this method to determine the bond strength between the FRP sheet and reinforced concrete. Lee and Moy (2007) carried out an experiment using the flexural beam test method to determine the behaviour of RC beams strengthened with CFRP sheets. The test results obtained were like results obtained from other designed models.

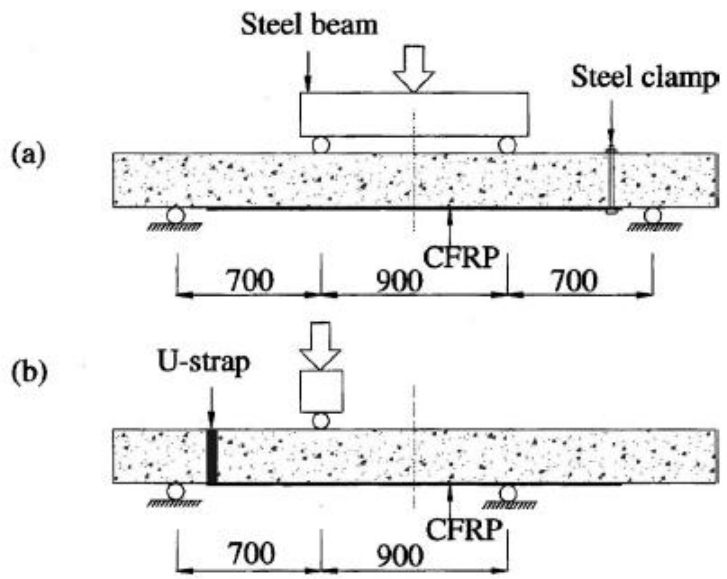

Figure 2.5: (a) Four-point Bending Test (b) Three-point Bending Test (Pham et al.,2006)

The tensile test used to access FRP bond strength can be either a double or single lap pull or push test. This type of test is commonly used because of its simplicity and ability to produce similar stresses to those encountered in actual beams (Shadravan, 2009). The pull test is carried out by bonding FRP laminates to either one side (single lap) or opposite sides (double lap) of a concrete prism as shown in Figure 2.6(a) and (c). Tension is applied on the concrete at a constant loading rate until failure. The capacity of the specimen is determined from the maximum load (CSA S806, 2012). The double lap pull test has been found to be the most suitable for standard universal testing machines because they allow for the varying of different parameters like loading rates and bond lengths. It also allows for variations in testing procedures (Shadravan, 2009).

In the push test, pressure is applied on the concrete using a hydraulic jack. As in the pull test, FRP sheets can be bonded to either one or two opposite sides of the concrete prism.

According to Shadravan (2009), this test method has been used by many researchers like Bizindavyi and Neale (1997), Chajes et al (1996) and Yao et al (2005). Force is transferred to the specimen at a constant loading rate or strain rate. Results obtained are then used to determine the capacity of the FRP bonded specimen (CSA S806, 2012). Illustrations for the double and single lap push tests are shown in Figure 2.6(b) and (d). Other methods of testing include subjecting the FRP-to-concrete interface to a combination of tension and shear force or simply subjecting it to an out-of-plane tension force (Ueda et al., 2003).

The pull test method as recommended in Annex N of the Canadian Standard Association's CSA S806 (2012) will be used in this literature to determine the bond strength and behaviour of FRP sheets bonded to concrete. The effect of the various properties such as effective bond length of the FRP sheet, strain rate, bond-slip relationship at the FRP-to-concrete interface as well as loading conditions will be investigated and reported in this literature.

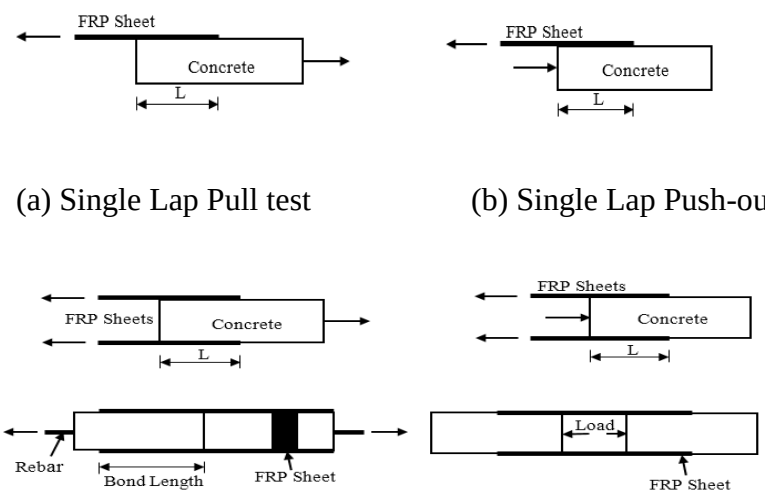

(a) Single Lap Pull test (b) Single Lap Push-out Test

(c) Double Lap Pull Test (d) Double Lap Push test

Figure 2.6: Types of Direct Shear Bond Tests

(Shadravan, 2009)

2.6 Previous Studies

Reinforced concrete structures are affected by high strain rate induced loads caused by high energy effect such as extreme impact, blast, and earthquake. These types of loads can cause the affected structure to fail in tension and, hence the need to strengthen and stiffen some of the structure's elements to control deformation. Surface-bonded FRP sheet is an exceptional material in deformation control in reinforced concrete structures subjected to strain because of their high impact resistance. They are also very stiff and are therefore not intended to improve ductility in their applications (Shadravan, 2009 and Khalighi, 2009).

Concrete, steel and FRP sheets have special responses to the effect of loads. This is because these materials have sole properties and provide unique contributions to the construction and use of FRP strengthened reinforced concrete structures. In order to analyze the bond between FRP-to-concrete bond under both static and dynamic impact loading, the stiffness, inertia, strain rate effect, strain energy, bond strength and bond-slip relationships of the structure must be duly studied and clarified. Bond properties are very important when it comes to externally rehabilitating RC members with FRP sheets (Otani, 1979). Past experimental and analytical research on FRP-to-concrete bond slip relationships under both static and dynamic loads is discussed and summarized in this part of the chapter, highlighting and comparing their advantages and limitations.

2.6.1 Experimental Research

A substantial amount of experimental research has been carried out over the years regarding structural repair using externally bonded sheets. Older studies carried out were based on using steel plates as the repair material which was recognized to be considerably effective. However, in recent times, more experimental studies are being carried out to

determine the effectiveness of using FRP laminates instead of steel plates because FRP sheets have shown better qualities in many strengthening applications compared to steel plates (Quantrill et al., 1996). Experimental study is still the most used method in determining the behaviour of FRP bonded RC structures, and this has led to many test data being developed for various structural elements.

A range of tests previously carried out by researchers on the behaviour of FRP bonded RC elements under static and dynamic loading will be discussed in this section. The test methods used, and various fundamental bond properties considered in each study will also be discussed, highlighting the behaviour of specimens and results obtained in these investigations.

2.6.1.1 Stress, Strain and Strain Rate Effect on FRP-to-concrete Bond Interface

When force is applied on an FRP-to-concrete specimen, bond stresses in the adhesive between the FRP sheet and the concrete serve as a medium through which tensile stresses are transferred from the FRP to the concrete (Cheng and Teng, 2001). Bizindavyi and Neale (1999), Buyukozturk et al. (2004) and many others in their tests and theories have proved that the bond between the FRP sheet and the concrete in a composite element causes bond stresses to develop and these stresses are not distributed equally along the bonded area. Bond stress decreases exponentially as the distance away from the critical section increases. That is, higher bond stresses develop in the FRP sheets in regions near the critical section (loaded end of the FRP sheet).

Figure 2.7 shows a graphical representation of bond stress results obtained by Shen et al. (2015) on two of their test specimens. This figure also provides a schematic representation of the shear specimen with dimension details and position of strain gauges. As observed in

the graphs, the location of maximum bond stress moves along the length of the FRP sheet as the load (P) is increased.

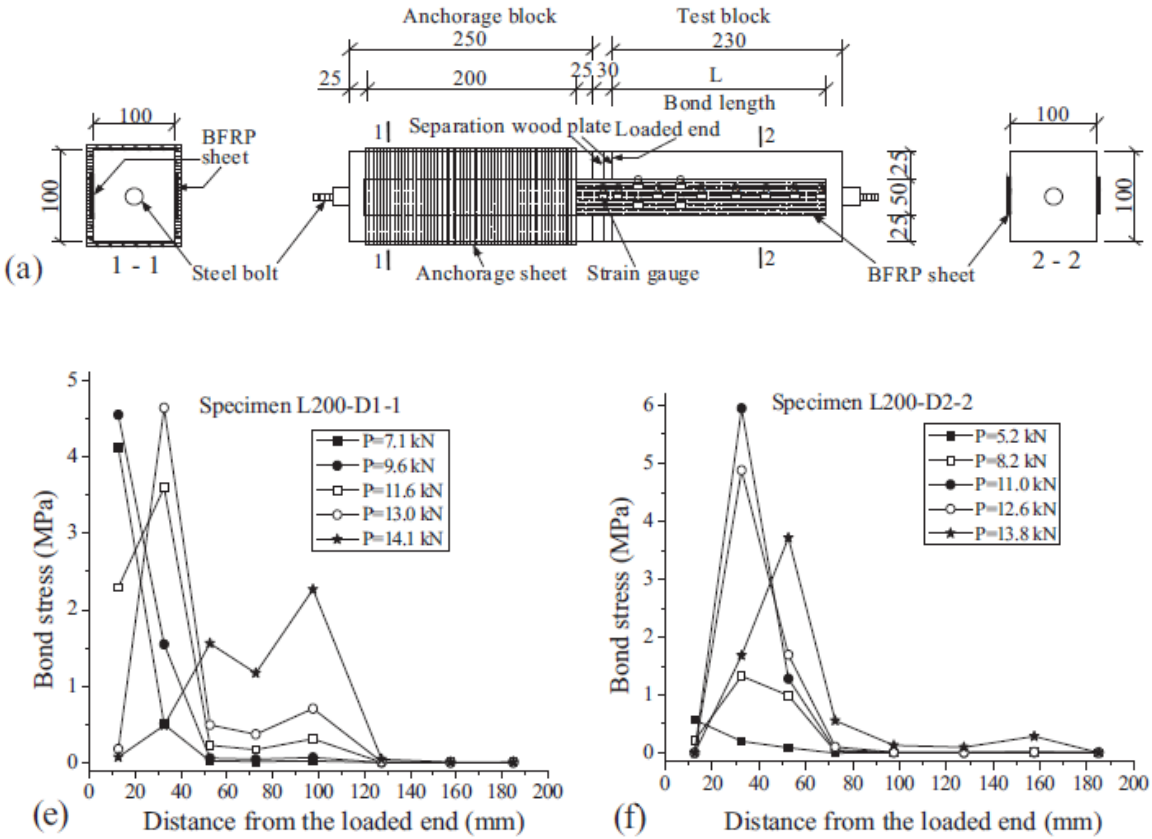

Figure 2.7: Relationship between Distance from the Loaded End and Bond Stress (Shen et al., 2015)

Huo et al. (2016) in their tests, subjected CFRP bonded beams to three-point bending under both static and impact loads. Higher strain values of the CFRP sheet were recorded under impact than in static tests. Stress and strain were found to be linearly proportional up to the point of failure under both static and dynamic loads. Stress and strain values under impact were higher than those obtained in the static tests. Shen et al. (2015) also performed similar experiments but only under dynamic loading by bonding BFRP sheets with different bond lengths on to concrete prisms. Strain values of the FRP sheet decreased along its bond

length with maximum strain occurring near the critical section of the FRP sheet. Maximum stress values of the FRP sheet moved along its bond length over time during the experiment. These observations signify the propagation of debonding failure along the bond length of the FRP sheet. It was also concluded that an increase in strain rate caused a subsequent increase in the FRP-to-concrete bond stress and strain. Figure 2.8 shows the strain values of the CFRP sheet recorded at various distances away from the loaded end at different loading rates. Plots in this figure show that strain decreased as the distance from the loaded end increased after impact. F_D and F_{DU} are the dynamic load and ultimate dynamic load respectively, while ε represents the strain.

Shen et al's results also showed that the strain in the laminate is dependent on the magnitude of loading. That is, as the load is increased, strain values increased as well.

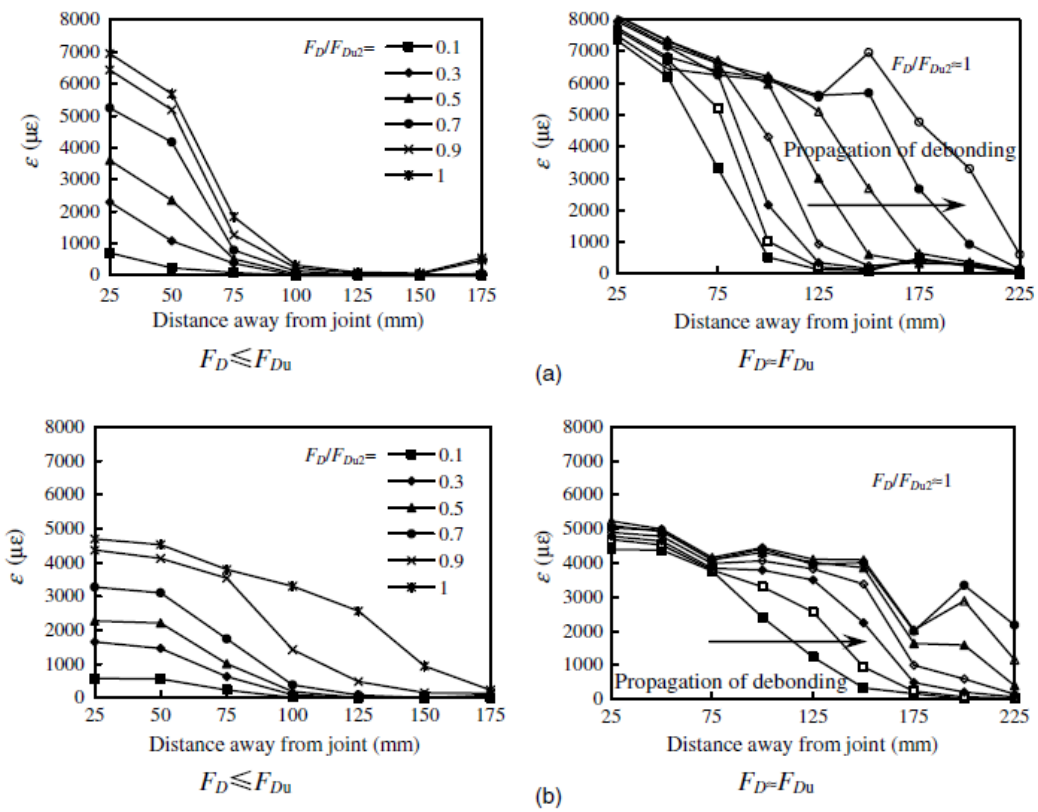

Figure 2.8: Strain Distributions of CFRP Sheet after Impact

(Huo et al., 2016)

In FRP strengthened beams, for very large loads up to ultimate capacity, the strain distribution begins to deviate from the regular descending tendency (nonlinear distribution). This is due to the slip that occurs at the FRP-to-concrete bond interface (Esfahani et al., 2007).

Shi et al. (2012) studied the effect of strain rates on the stress and strain behaviour of FRP sheets bonded to reinforced concrete using the double lap pull-out method. They also observed that higher strain rates increased the maximum strain (as strain rate increases, maximum strain of FRP sheet increases) of the FRP sheet. It also increased the shear stresses being transferred from the FRP sheet to the concrete. Figure 2.9 shows and

compares the results obtained from quasi-static and dynamic tests. S and D stand for quasi-static and dynamic loads respectively.

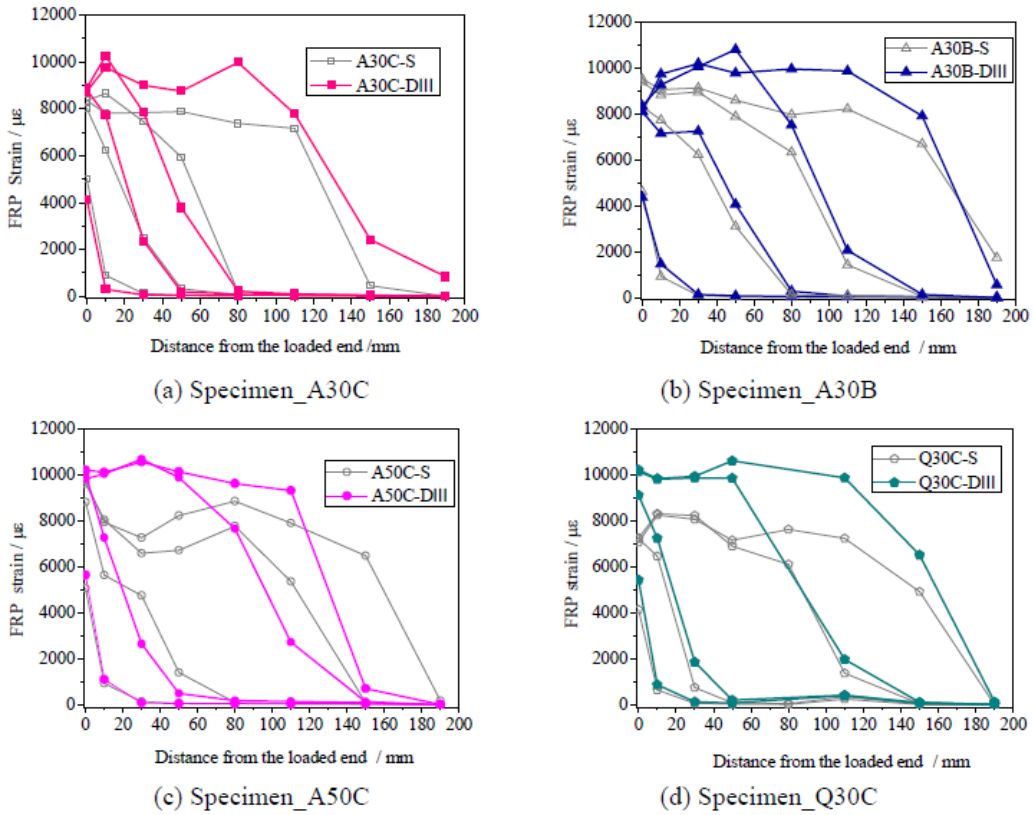

Figure 2.9: FRP Strain Distribution under Quasi-static and Dynamic Loading (Shi et al., 2012)

Pham and Hao (2016) carried out a review on past studies to determine the behaviour of FRP strengthened reinforced concrete structures under varying strain rates. They observed that past studies have so far yielded contradicting results in terms of how strain rate affects FRP stress-strain relationship and their corresponding strain distribution along its bond length. It was stated that Eskandari and Nemes (2000), Shokrieh and Omidi (2009) and Huo et al. (2013) all observed an increase in the FRP strain as the strain rate increased. Foroutan et al. (2013), Benloulo et al. (1997) and Rodriguez et al. (1996) all observed a

decrease in FRP strain as the strain rate increased. However, Lifshitz and Leber (1998) and Daniel et al. (1981) did not observe any change in the FRP strain values in relation to an increase in strain rate. Based on this, Pham and Hao (2016) could not conclude as regards the effect of strain rate on the failure strain of FRP sheets bonded to concrete.

As stated in the literature, it has been observed that high strain rate (greater than $10^2\ s^{-1}$) affects the stress-strain response of FRP sheets. FRP stress-strain response reported by Rodriguez et al. (1996), Benloulo et al. (1997) and Gilat et al (2002) all showed nonlinear behaviour at high strain rates. Strain rates lower than that stated ($10^2\ s^{-1}$) gave a linear stress-strain relationship (Pham et al., 2016).

Shen et al. (2015) evaluated the performance of existing FRP bond stress models developed in the past by comparing the model results with their experimental data using Equation 2.1. The equation gives the integral absolute error (IAE) which is used to model assessments.

[2.1] $$IAE = \sum \frac{[(Expe. - Theo.)^2]^{1/2}}{\sum |Expe.|}$$

where Expe. and Theo. represent the experimental and theoretical data, respectively. Table 2.2 shows the theoretical static and dynamic stress results obtained from previous studies and their accuracy when compared to Shen et al’s experimental results.

Table 2.2: Performance of Bond Stress Models

Reference	Equation	Consideration factors	Theoretical result (MPa)	IAE (%)
Neubauer and Rostasy	$\tau_{max} = 1.8f_t$	f_t	4.72	44.3
Tanaka	$\tau_{max} = 6.13 - \ln L$	L	3.13	4.3
Hiroyuki and Wu	$\tau_{max} = 5.88\,L^{-0.669}$	L	0.79	75.8
Pellegrino et al.	$\tau_{max} = 3.1(n_f E_f t_f)^{0.32}$	E_f, t_f	6.99	113.8
Cao et al.	$\tau_{max} = 1.64\sqrt[4]{f_{cu}}$	f_{cu}	4.06	24.2
Yang et al.	$\tau_{max} = 0.5f_t$	f_t	1.31	59.9
Maeda et al.	$\tau_{max} = 110.2 \times 10^{-6} E_f t_f$	E_f, t_f	1.40	57.2
Khalifa et al.	$\tau_{max} = 110.2 \times 10^{-6} E_f t_f \left(\frac{f_{co}}{42}\right)^{2/3}$	E_f, t_f, f_{co}	1.11	66.1
Nakaba et al.	$\tau_{max} = 3.5f_c'0.19$	f_c'	6.66	103.7
Sato et al.	$\tau_{max} = 2.68 \times 10^{-5} E_f t_f (f_c')^{0.2}$	E_f, t_f, f_c'	0.67	79.5
Lorenzis et al.	$\tau_{max} = 0.0182(n_f E_f t_f)^{0.5}$	E_f, t_f	2.05	37.3
Ko et al.	$\tau_{max} = 0.165f_c'$	f_c'	4.88	49.2
ISO model	$\tau_{max} = 0.93f_{co}^{0.44}$	f_{co}	4.13	26.3
Average value			3.22	57.0

(Shen et al., 2015)

In Table 2.2, τ_{max} represents the maximum bond stress, L is the effective bond length, t_f is the thickness of FRP sheet, f_{cu} is the cubic compressive strength, f_{co} or f_c' represents the cylindrical axial compressive strength of concrete. The axial tensile strength is represented by f_t, n_f is the number of layers of FRP sheet and E_f is the elastic modulus of FRP sheet. Comparing the FRP bond stress obtained from the experiment (3.27 MPa) carried out by Shen et al. (2015) and the average theoretical FRP bond stress (3.22 MPa) from all the models calculated, it is observed that both results are almost the same. However, if each model is evaluated individually, it is observed that some models overestimated the FRP bond stress while others underestimated the bond stress as seen in their IAE values. This discrepancy is partially attributed to the difference in test methods (Shen et al., 2015).

Results of test carried out by Shen et al. (2015) on BFRP sheets showed that maximum bond stress has no significant relationship with the stiffness of FRP sheet but is related to

the strength of concrete. Peak bond stress moves along the length of FRP sheet as loading increases, indicating the propagation of cracks due to debonding.

2.6.1.2 Bond Length and Development Length of FRP Sheets Bonded to Concrete

In FRP-to-concrete bond, there is a measurable bond length beyond which an increase in the bond length of the FRP sheet will not result in any further increase in transfer load resistance. This phenomenon is known as “development length”, “effective transfer length”, or “effective length” (Shadravan, 2009, Bizindavyi and Neale, 1999, Li et al., 2015). Strain distributions influence the development length of FRP bonded RC structures, and development length is measured from the point where the strain is maximum (at maximum moment location for beams and slabs) to a point where the strain value is about 5 percent the peak strain (Huo et al., 2006).

Li et al. (2015), attempting to determine the effect of bond length on the bond behaviour of FRP-to-concrete interface, carried out tests on specimens with four varying bond lengths. Two of the bond lengths were less than the effective bond length while the other two exceeded the effective bond length. It was discovered that two-way debonding (debonding at both the loaded and free end of the FRP sheet) occurred for specimens with the lesser bond length, while one-way debonding (debonding at the free end of the FRP sheet) took place in the higher bond lengths. Strain values were seen to be higher at the loaded end of the FRP sheet compared to the free end of the FRP sheet. Figure 2.10 shows the strain distribution along the FRP-to-concrete interface of one specimen at different locations along the FRP sheet under different load levels.

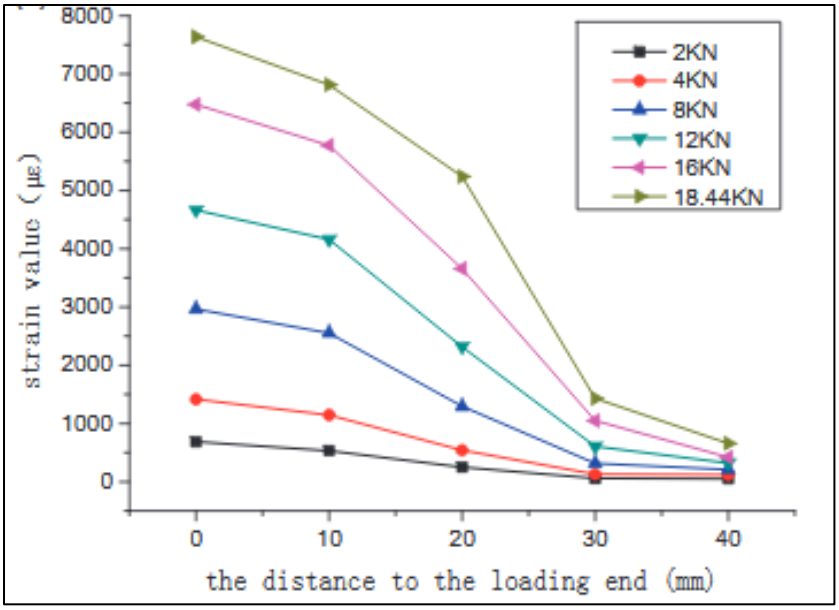

Figure 2.10: Typical FRP Strain Distribution along the FRP-Concrete Interface under Different Concrete Strengths and FRP Bonding Lengths (Li et al., 2015)

The effect of varying strain rates on the development length of BFRP sheet was studied by Shen et al. (2015); it was observed that the stiffness of the FRP sheet and concrete strength significantly affect the dynamic effective bond length of externally reinforced beams. As shown in Figure 2.11, the double lap shear test carried out in this investigation using a servo-hydraulic testing machine showed that there is a linear relationship between the ratio of dynamic to static development length and the logarithm of the ratio of dynamic to static strain and that the ultimate capacity of the FRP sheet does not increase for bond lengths larger than the development length. It was also observed that the development length of the BFRP sheet decreased as the strain rate is increased. Based on experimental results, a new model for the calculation of effective bond length was established and a comparison of previously developed models with theoretical results including those in the standard

codes was carried out in the literature using IAE. Details of the comparison are shown in Table 2.3. Due to the inaccuracy in the models, there is a large scatter in results obtained from the models some of which underestimated while others overestimated the development length values.

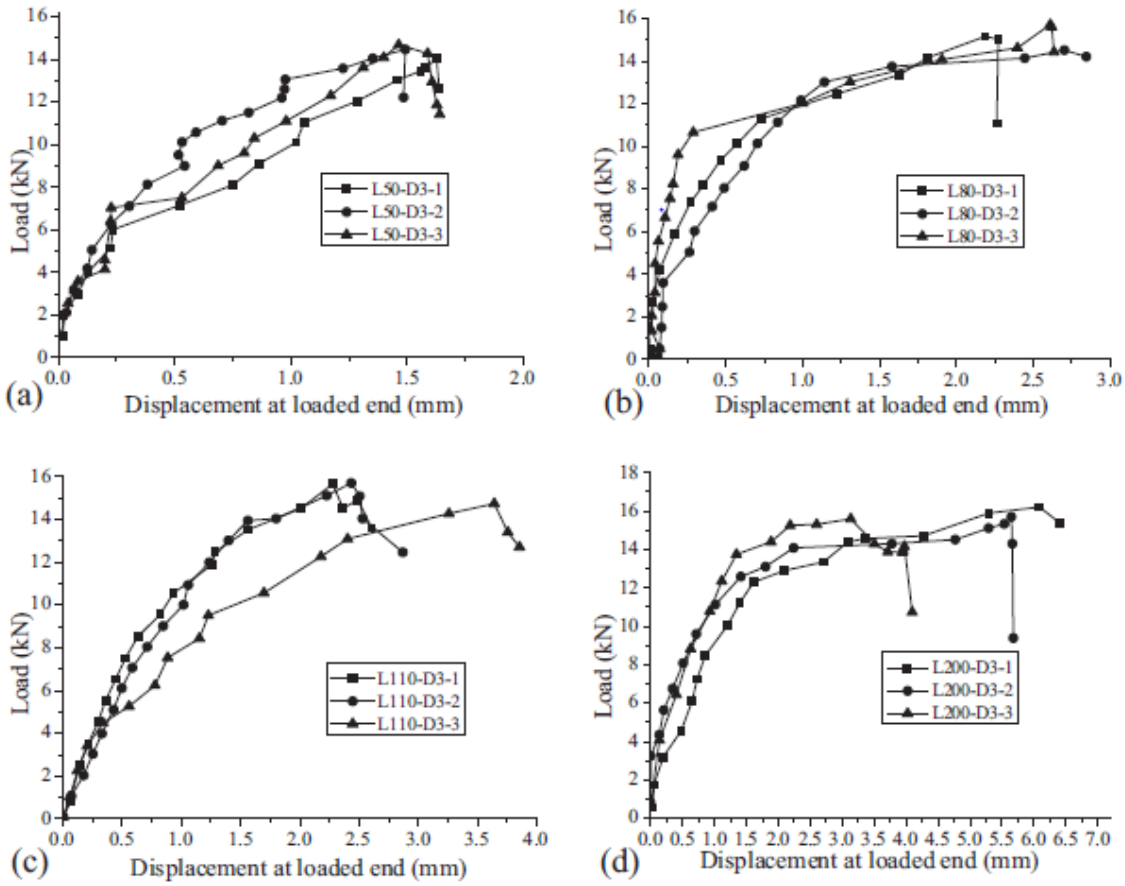

Figure 2.11: Load versus Displacement Curves of BFRP-Concrete Interface for Different Development Lengths

(Shen et al., 2015)

Table 2.3: Performance of Effective Bond Length Models

References	Equation	Consideration factors	Theoretical result (mm)	IAE (%)
Wu et al.	$L_e = 0.395\frac{(E_f t_f)^{0.54}}{f_{co}^{0.08}}$	E_f, t_f, f_{co}	47.9	33.3
Neubauer and Rostasy	$L_e = \sqrt{\frac{E_f t_f}{2f_t}}$	E_f, t_f, f_t	49.2	31.5
Khalifa	$L_e = e^{6.13-0.580\ln(E_f t_f)}$	E_f, t_f	105.2	46.5
Chen and Teng	$L_e = \sqrt{\frac{E_f t_f}{\sqrt{f_c'}}}$	E_f, t_f, f_c'	48.3	32.7
CNR-DT 200/04	$L_e = \sqrt{\frac{E_f t_f}{2f_{ctm}}}$	E_f, t_f, f_{ctm}	47.0	34.5
Lu	$L_e = 1.33\frac{\sqrt{E_f t_f}}{f_t}$	E_f, t_f, f_t	57.2	20.3
Yang et al.	$L_e = 100$ mm	-	100.0	39.3
ACI 440.2R-08	$L_e = \frac{23,300}{(nE_f t_f)^{0.58}}$	E_f, t_f	97.1	35.2
ISIS CSA S806-02	$L_e = \frac{25,350}{(E_f t_f)^{0.58}}$	E_f, t_f	105.6	47.1
Niedermeier	$L_e = \sqrt{\frac{E_f t_f}{4f_t}}$	E_f, t_f, f_t	34.8	51.5
Average value			69.2	37.2

Shen et al. (2015)

Huo et al. (2016) compared the effective bond length of the Eurocode model [EN 1998-3 (CEN 2005)], the model of CNR-DT 200 (CNR 2004), Cheng and Teng's model (2001) and the ACI Committee 440.2R-08 model (ACI 2008) with static and dynamic effective bond length experimental results. All the models except the ACI model showed that development length increases with the associated increase in FRP properties. The ACI model indicates that the development length is inversely proportional to the FRP stiffness. Figure 2.12 shows the relationship between the effective bond length of FRP sheet and its stiffness, comparing existing models with results obtained from experiment. $n_f t_f E_f$ represent the stiffness of the FRP sheet.

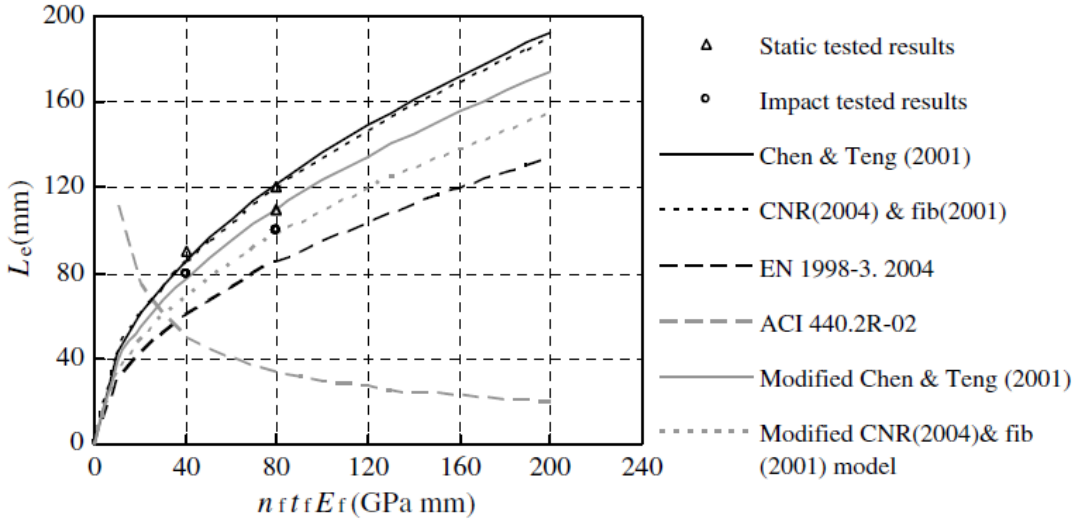

Figure 2.12: Effective Bond Length versus FRP Sheet Stiffness (Comparing existing curves with experimental results)

(Huo et al., 2016)

For specimens with bond length less than the effective bond length, rapid failure occurs prematurely because as debonding initiates, the part of FRP sheet still bonded to concrete is not long enough to transfer shear stresses to the concrete. A longer bond length however gives room for development even after the initial propagation of debonding (Ghorbani et al., 2016).

2.6.1.3 Effect of Strain Rate on Bond Strength of FRP Sheets Bonded to Concrete

Bond strength is an important factor that influences the efficiency of the method of rehabilitating RC structures using FRP sheets (Huo et al., 2016). Bond strength of the FRP-to-concrete interface and how it is affected by strain rate has been studied in the past (Shi et al, 2002, Shadravan, 2009, Alzubaidy, 2012), and these studies have shown that most FRP bonded RC elements undergo bond failure that occurs at the concrete to adhesive interface even before the full capacity of the FRP laminate is utilized. Hence, the reason

fracture mechanics and rupture energy are considered in most analytical studies and bond models developed for FRP bonded RC elements (Shadravan, 2009).

Huo et al. (2016), in their test to determine the dynamic behaviour of CFRP-to-concrete interface discovered that the loading rate greatly affects the bond strength of the FRP bonded RC member. Three-point bending tests at different loading rates and concrete strengths were carried out in this investigation and dynamic results were compared to that obtained from static tests. Results show that as the loading rate increased, there is a significant increase in the bond strength of the FRP strengthened RC element which further increased its loading capacity. This is as shown in Figure 2.13 (a) and (b).

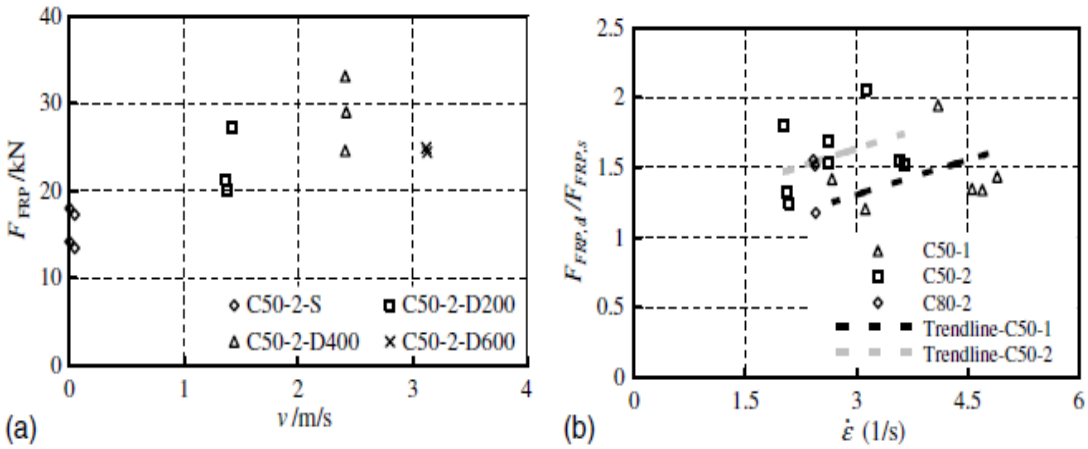

Figure 2.13: Effect of Impact Loading on Ultimate Loads: (a) Impact Velocity (b) Strain rate

(Huo et al., 2016)

$F_{FRP,d}$ and $F_{FRP,s}$ are the ultimate load under dynamic and static strain rates respectively, while $\dot{\varepsilon}$ represents strain rate. As seen in the graph presented in Figure 2.13 (b), the ultimate load increases with strain rate indicating that the bond capacity increases as the strain rate increased; thereby making it possible for the element to accommodate higher loads.

Bond strength is also sensitive to the FRP sheet-to-concrete width ratio, bond length as well as the angle in which the FRP sheet is loaded. Ghorbani et al. (2016) in a single lap shear test discovered that the bond strength increased with a negative increase in loading angle by about 37 percent over the control specimen under high strain rates. Results also showed that the increase in bond length improves the bond strength under high strain rates. This is because of the larger distribution of the effect of the peeling force on the FRP sheet in the un-debonded area. Figure 2.14 shows the influence of loading angle on the bond strength of FRP-to-concrete interface. Here, EBR means externally bonded reinforcement.

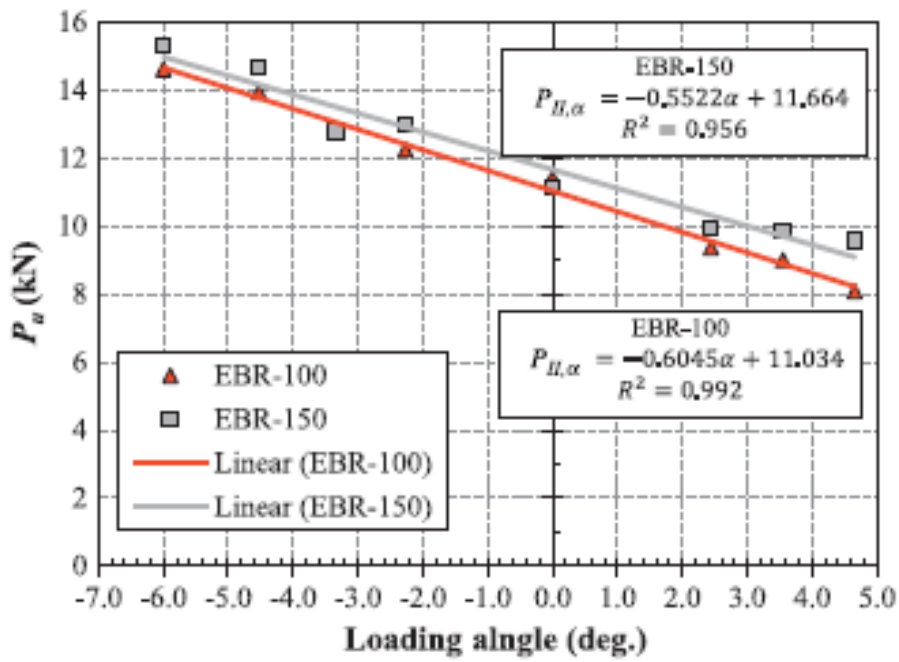

Figure 2.14: Effect of Loading angle on Bond Strength of FRP-to-Concrete (Ghorbani et al., 2016)

An incorrect recording of bond capacity is possible during a bond test if the ultimate load is used to determine the average shear strength between the FRP sheet and the concrete substrate. This will infer that an increase in bond will cause an increase in load resistance thereby leading to a deduction that the tensile strength of FRP sheet can be increased by an increase in bond length (Shadravan, 2009).

2.6.1.4 Effect of Strain Rate on Mechanical Properties of FRP Sheets Bonded to Concrete

High strain rate loading can cause mechanical properties of the structural materials (of which FRP is one) to sometimes perform poorly. Therefore, to ensure a durable and long-lasting structure, it is important to study the mechanical response of FRP sheets externally bonded to reinforced concrete members (beams) under various strain rates. Some of the mechanical properties include tensile, shear, and flexural properties of FRP sheets bonded to RC members (Jacob et al., 2004). As with many other properties of static and dynamic loads, previous investigations have been carried out on the tensile, shear and flexural strength of the FRP sheets bonded to RC members but results show inconsistencies and discrepancies as seen in some literature.

Tests carried out by Bizindavyi and Neale (1999) indicate that FRP sheet is likely to attain its full tensile strength when bonded to concrete irrespective of the number of layers of the FRP sheet if the right bond length is considered. Tensile properties of FRP sheets are generally known to increase when the loading rate increases. This has been demonstrated in most studies (Rodriguez et al. (1996), Barre et al. (1996), Daniel and Liber (1976) and so on) except for those carried out by Hayes and Adams (1982) and Daniel et al. (1981) where it was observed that the tensile strength decreases as strain rate increases. This

different finding might be due to an imperfect test or as a result of premature debonding failure (Pham and Hao, 2016).

Jacob et al. (2004) carried out a detailed review of the effect of loading rate on the mechanical properties of FRP sheets. He studied numerous work that involved determining the effect of strain rate on the flexural, tensile and shear properties of FRP sheets bonded to concrete. In this study, it was stated that Sims et al. (1998), Rotem and Lifshitz (1076) and Okoli and Smith (1999) all concluded that the tensile strength, shear and modulus of FRP sheets saturated with epoxy increase as the strain rate is increased. Melin and Asp (1995) concluded that these mechanical properties of saturated FRP sheets are insensitive to strain rates.

Esfahani et al. (2007), in their study carried out tests to determine the flexural behaviour of RC beams strengthened with FRP sheets. The flexural strength of FRP bonded beams was compared with control specimens that were not bonded with FRP sheets. Results show that FRP sheets improved the flexural strength and stiffness of the RC beam. Although they tested at static load only, they observed that the models specified in the ACI 440.2R-08 (2008) design code and that specified in the ISIS Canada (2008) document are overestimated for beams with low reinforcing bar ratio when compared to experimental results. The models are however suitable for beams with high reinforcing bar ratio.

2.6.1.5 Bond Stress-slip Relationships of FRP sheets Bonded to Concrete

The bond stress-slip relationship helps in determining the tensile strength of FRP sheets based on the strain distribution, bond stress, and fracture energy parameters (Shen et al., 2015 and Shi et al., 2012). In this section, strain rates and how it affects the relationship

between bond stress and slip based on experimental data and analytical models proposed in previous investigations is discussed.

Shadravan (2009) pointed out that pull tests are the most commonly used tests to derive a complete bond slip model. One way in which to define the bond-slip curves from pull tests is by first finding the bond stress at a section along the FRP-to-concrete interface using strain values obtained from strain gauges at the said section. The FRP strain values are then numerically integrated to get the corresponding slip (relative displacement between the FRP-to-concrete interface) values. This method is simple but can be inaccurate due to the discrepancies in the strain values. The differences in strain is as a result of crack propagation and debonding failure that may occur on the test specimen. Another way in which the stress-slip relationship can be determined is from the load-slip curve. Even though it has its own disadvantages, it is an easier approach because local bond-slip curves are likely to yield similar response as load-displacement curves (Lu et al., 2005).

In the model proposed by Shen et al. (2015) in determining the bond-slip relationship of FRP sheets bonded to concrete, it was assumed that: (1) the relative displacement between the concrete and sheet at the free end of the sheet is zero; (2) the displacement of the concrete specimen far away from the concrete cover is negligible; (3) a linear variation of strains exists in the FRP sheet between two subsequent strain gauges. The bond-slip curve was obtained by determining the average slip between two strain gauges and their corresponding stresses under different strain rates. It was finally concluded that the relationship between bond stress and slip under different strain rates are analogous. The model was proposed based on Popovic's (1973) findings as stated in Equation 2.2:

[2.2] $$\tau = \tau_{max} \left[\frac{s}{s_0} \frac{n}{(n-1)+(s/s_0)^n} \right]$$

Where τ is the local bond stress (MPa), s is the local slip (mm), τ_{max} is the maximum local bond stress (MPa), s_0 is the slip corresponding to τ_{max} and n is a constant.

Jacques (2016), using flexural beam-end tests studied the characteristics of the bond between FRP bars and concrete at high strain rate. Fourteen beam specimens were tested at high strain rates ranging from 5×10^{-6} to $1.2\ s^{-1}$. Although the beams tested in this research where not externally bonded with FRP sheets, it was discovered that high strain rates significantly affected the bond strength of the beams tested but had little to no effect on the bond stress-slip curve relationship. It was also indicated in this work that the flexural beam test method is the most appropriate type of test for dynamic loading and was recommended for future studies.

Wu et al. (2002), Yuan et al. (2001), Bronsens and Van Gemert (1998) and Nakaba et al. (2001) all used models based on fracture mechanics to compare bond-slip relationships in their experiments. New models were proposed based on their findings and results. It is stated by Wu et al (2002) and Yuan et al. (2001) that models based on fracture mechanics yield very simple equations for the determination of the ultimate bond strength. The only parameters used in these expressions are the FRP stiffness and interfacial fracture energy.

Examples of simplified bond-slip curves at different strain rates as obtained by Shen et al (2015) are as shown in Figure 2.15. As seen in the figure, the dynamic maximum bond stress increases with strain rate. All the curves follow a similar pattern which indicates similar behaviour at varying strain rates.

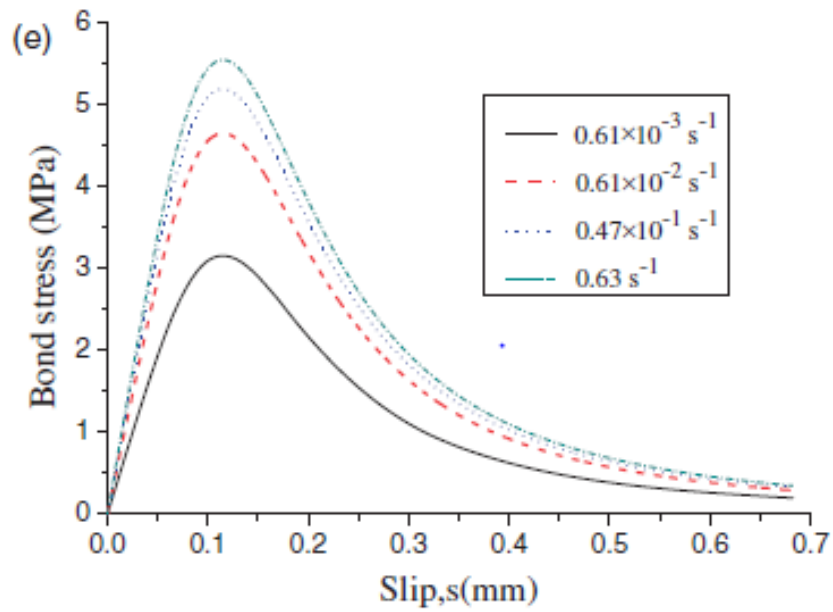

Figure 2.15: Relationship between Dynamic Bond Stress and Slip under Different Strain rates (Shen et al., 2015)

2.6.2 Studies involving Computational Techniques

The bond strength and behaviour of an FRP strengthened beam mainly depends on the interaction between the substrate and FRP interface. Since more studies have been carried out for beams subjected to static loads, many models have been suggested based on experimental data and theories in fracture mechanics to predict the bond behaviour of FRP-to-concrete interface under static loads rather than dynamic loads. Although there is need to study and develop analytical and numerical models for FRP strengthened members under dynamic loads, it is also important to access those models proposed for strengthened members under static loads.

An FRP reinforced concrete structure can be modelled using the beam, plate or shell theory based on the type of structural element being considered. The response of the structural element is based on the geometry and boundary conditions of the structural system and this

response is determined using analytical or numerical models, closed-form solutions or by using a finite element approach (Ruiters, 2014). Past analytical and numerical models for both static and dynamic loadings will be discussed in this section.

2.6.2.1 Analytical and Numerical Studies

Smith and Teng (2001) carried out an in-depth review of twelve previously developed analytical static models. Results from these models were compared with data obtained from fifty-nine experimental beam test specimens. It was observed that of all the twelve models, those developed for steel-plated beams were more accurate than those developed for FRP strengthened RC beams. A new model was proposed in the literature by modifying the model developed by Oehlers (2004) for steel-plated beams. The new model which is based on the relationship between the shear forces of the FRP sheet and the concrete substrate is as indicated in Equation 3.2 below;

[2.3] $$V_{db,end} = \eta V_c$$

where $V_{db,end}$ in kN is the sheet end shear force and V_c is the shear force of the concrete. η is a factor that varies depending on the failure mode being designed against. The aim of the above model is to design against various modes of failure that may affect the strength capacity of the FRP strengthened beam.

Shi et al. (2015) suggested a linear relationship between ultimate load and interfacial fracture energy after tests carried out on fifty-seven specimens at varying strain rates up to 1 s^{-1}. Fracture energy is the energy value that causes crack in a unit surface area and it is a significant factor when determining the bond-slip relationship in an FRP-to-concrete

interface. As the strain rate increases, the fracture energy increases logarithmically. The model is as indicated in Equation 2.4 below;

[2.4] $$G_f = \frac{P_u^2}{2{b_f}^2 E_f t_f}$$

where G_f (N/mm) is the interfacial energy and is calculated from the data obtained from tests, P_u is the ultimate load of the specimen, E_f, t_f, and b_f are the modulus of elasticity, the thickness, and the width of the FRP sheet, respectively. The equation of interfacial shear stress, $\tau(x)$ in MPa is given in Equation 2.5 as;

[2.5] $$\tau(x) = \left| E_f t_f \frac{d\varepsilon(x)}{dx} \right| = \frac{a}{b^2} \times \frac{E_f t_f e^{\frac{x-x_0}{b}}}{\left(1+e^{\frac{x-x_0}{b}}\right)^2}$$

where $\varepsilon(x)$ is the strain distribution on the FRP sheet, E_f and t_f are the modulus and thickness of FRP sheet, a, b, and x_0 are fitting parameters and x is the distance away from the loaded end. The values of the strain distribution are deduced from the equation taken from the bond-slip model by Dai et al. (2005).

It was pointed out by Shen et al. (2015) that Lu's (2004) model to determine effective bond length is one of the most precise amongst the existing models. An equation to determine the effective bond length under static load proposed by Lu et al. (2004) is as indicated in Equation 2.6:

[2.6] $$L_e = \alpha \frac{\sqrt{E_f t_f}}{f_t}$$

where E_f and t_f are the Elastic modulus and thickness of the FRP sheet, f_t is the tensile strength of concrete, L_e is the development length of FRP sheet in mm while α is a constant

obtained from test results. The equation shows that the effective bond length is directly proportional to the square root of the FRP stiffness and inversely proportional to the tensile strength of the FRP sheet. The effective bond length of FRP under dynamic high strain rates can be determined based on the Dynamic Increase Factor. That is, the ratio of dynamic effective bond length to the static bond length as indicated in Equation 2.7;

[2.7] $$\frac{L_e^d}{L_e^s} = \frac{\sqrt{E_f^d / E_f^s}}{f_f^d / f_f^s}$$

Where E_f^d and E_f^s are the static and dynamic modulus of elasticity of the FRP sheet respectively and f_f^d and f_f^s are the static and dynamic tensile strength of the FRP sheet respectively. The elastic modulus and concrete tensile strength are affected by strain rate, therefore the ratio of the static to the dynamic modulus and tensile strength can be written in terms of strain rate as shown in Equations 2.8 and 2.9;

[2.8] $$\frac{E_f^d}{E_f^s} = 1 + \gamma log_{10}\left(\frac{\dot{\varepsilon}_d}{\dot{\varepsilon}_s}\right)$$

[2.9] $$\frac{f_f^d}{f_f^s} = 1 + \gamma log_{10}\left(\frac{\dot{\varepsilon}_d}{\dot{\varepsilon}_s}\right)$$

The coefficient γ can be established through regression analysis (r^2 $value$=0.972) with the values of the coefficient for the modulus and tensile equations being equal to 0.0625 and 0.173, respectively.

Shen et al. (2015) presented their own FRP bond stress versus strain rate relationship model after studying and comparing previous models developed by other researchers. Based on the study carried out in this literature, it was concluded that bond stress increases as strain

rate increases. Various models were used to calculate the stress increase as the strain rate was increased from static $(1 \times 10^{-3}\ to\ 1.0 \times 10^{-1})s^{-1}$ to dynamic strain $(1 \times 10^{-1}\ to\ 6.3\ \times 10^{-1})s^{-1}$. Equation 2.10 was chosen to be the most accurate model to determine dynamic bond stress increase as the strain rate increases.

[2.10] $$\frac{\tau_{max}^{d}}{\tau_{max}^{s}} = 1 + \alpha\left(log_{10}\left(\frac{\dot{\varepsilon}_d}{\dot{\varepsilon}_s}\right)\right)^{\beta}$$

Where τ_{max}^{d} and τ_{max}^{s} are the dynamic and static maximum bond stresses, respectively, $\dot{\varepsilon}_d$ and $\dot{\varepsilon}_s$ are the dynamic and static strain rates respectively. α and β are coefficients determined from regression analysis. The above equation was chosen as the most accurate because the results of the deviations of the equation from the experimental test carried out are minimal.

The Chen and Teng (2001) effective length static model was modified by Huo et al. (2016) for it to be suitable for dynamic calculations as shown in Equation 2.11 The dynamic effective bond length ($L_{e,d}$) is estimated by substituting the static compressive strength (f_{cm}) with its dynamic counterpart as indicated in Equation 2.12.

[2.11] $$L_{e,d} = \left[{E_f t_f}\Big/{(DIF \cdot f_{cm})^{0.5}}\right]^{0.5}$$

[2.12] $$\left(f_{cm,d} = DIF \cdot f_{cm}\right)$$

where DIF is the Dynamic Increase Factor. The FIB model (2001) as well as the CNR-DT 200 (2004) model were also modified using the DIF. Results showed that the modified formulas were very much accurate. The same can also be done when determining the ultimate bond force under dynamic loading. The ultimate static bond force models by Chen and Teng (2001) and CNR (2004) were multiplied by the DIF as indicated in Equation 2.13:

[2.13] $$P_{u,d} = \begin{cases} DIF \cdot b_f \sqrt{0.06 E_f t_f k_b \sqrt{f_{ck} \cdot f_{ctm}}} \\ DIF \cdot 0.427 \cdot \beta_p \beta_L \sqrt{f_c'} b_f L_e \end{cases}$$

where f_{ck} is the characteristic strength of concrete, f_c' is the cylinder compressive strength of concrete, b_f is the width of FRP sheet, k_b is the geometric coefficient, β_p is the coefficient of width ratio, and β_L is the FRP coefficient which is mostly equal to 1.

Maeda et al. (1997) presented an equation for the surface bond stress τ and the effective bond length L_e as shown in Equation 2.14 and 2.15. The ultimate bond force is then determined by multiplying the bond stress by the effective bond area.

[2.14] $$\tau = 110.2 \times 10^{-6} E_f t_f$$

[2.15] $$L_e = \exp\left(6.134 - 0.58 \ln(E_f t_f)\right)$$

Recently developed models for determining the development length of FRP sheets bonded to concrete use similar variables ($E_f, t_f, n, b_{f,}$ etc) and most of these variables appear in the numerator. That is, the variables are directly proportional as opposed to older models where the variables appear in the denominator. Irrespective of these discrepancies, several guidelines have approved these proposed old models for use in the design of FRP bonded RC structures (Shadravan, 2009). The effective length equation recommended in the ACI 440.2R-08 (2008) is as shown in Equation 2.16:

[2.16] $$L_e = \frac{23300}{(nE_f t_f)^{0.58}}$$

Quantrill et al. (1996) in their model, used the principle of strain compatibility and equilibrium to determine the behaviour of FRP strengthened beams under impact. Stresses in the concrete, steel reinforcement and FRP sheet were then calculated using material property relations (modulus of elasticity, strain value, material area and thickness). Results

of the analysis showed that reducing the FRP sheet area may lead to a reduction in stiffness and improvement of ductility. It also causes an increase in FRP strain and subsequently a reduction in the general strength of the beam.

2.6.2.2 Finite Element Models

Finite element analysis (FEA) can be used to determine the behaviour of FRP bonded reinforced concrete structures under varying strain rates. The closed-form solutions as previously described are generally used for linear elastic simulations where stress and strain can be calculated globally, but when the geometric and material properties of the structure is nonlinear, FE analysis can be used to predict the behaviour and progressive failure of such elements (Rahimi et al., 2001). When the propagation of crack is well understood, the numerical analysis of debonding failures is well predicted. There are two major methods of analysis when it comes to crack propagation; 'the discrete crack method' and 'the smeared crack method' (Yang et al., 2002).

Nam et al., (2009) carried out a numerical evaluation of the retrofit effectiveness for GFRP strengthened slabs under blast loads. The behaviour of a reinforced concrete slab bonded with GFRP sheet was analyzed and the results compared with past experimental results. The analysis was carried out using three LS DYNA material models; concrete damage model, piecewise linear plasticity model and the orthotropic elastic model for concrete, steel reinforcement, and FRP reinforcement, respectively. These basic codes model the resistance of GFRP or other types of fibers considering the effect of strain rate and debonding failure.

2.7 Conclusion Based on Literature Review

From the research carried out in this chapter, it can be concluded that there is an effective bond length beyond which there is no further increase in the transfer load resistance of the FRP sheet. Various experimental tests and analytical research have been carried out to determine the authenticity of the previous statement. The most common failure method of FRP is by debonding which occurs before the ultimate strength of the material is effectively utilized. Hence the need to improve the bond strength of FRP sheets bonded to concrete. Previous studies have shown that various properties affect the bond strength of FRP sheets bonded to reinforced concrete structures and they include the stress-strain properties of the FRP sheet, development or effective length of the FRP sheet, mechanical properties (tensile, shear, compressive and flexural) of both the FRP sheet and the concrete substrate. Effective bond length is a major parameter to consider when trying to improve the bond strength of the FRP-to-concrete interface.

Strain rate affects the behaviour of FRP sheets bonded to reinforced concrete. Most of the past studies carried out concluded that FRP strengthened reinforced concrete generally have higher bond capacity under high strain rate compared to those subjected to static load. Effective bond length also increases as the strain rate increases. In terms of how strain rate affects the mechanical properties of the FRP sheet, some researchers concluded that as strain rate is increased, the tensile strength, modulus and shear properties are improved. Some have concluded that these properties are not affected by strain rate, while others have observed that the properties decrease as the strain rate is increased. Bond stress-slip relationship is also important to consider when determining the bond strength of FRP sheets. Strain rates had little to no effect on the bond stress- slip relationship.

Many analytical expressions for effective bond length in relation to other properties of the FRP sheet and concrete substrate have been formulated but there have been different opinions as to how these parameters are to be incorporated into an expression for determining effective bond length. The expressions adopted by the CSA S806-12 standard is being challenged by researchers in recent years (Chen and Teng, 2001, Yuan et al., 2001, Shen et al., 2015, Shi et al., 2015) because of how the FRP sheet and concrete properties are incorporated in these models. In the new models or expressions, FRP sheet properties appear in the numerator as opposed to previous models where they are inversely proportional to the effective bond length. Some have also introduced the concrete properties such as compressive and tensile strength as well as concrete modulus of elasticity into the expressions to determine development length and ultimate capacity of FRP sheets bonded to concrete.

There are various test setups (direct shear test methods) that have been used to determine the effective bond length and bond strength of FRP-to-concrete interface which do not accurately determine many important parameters. The difference in setups also significantly affects the results obtained in these tests. There is therefore a need to reconsider these test setups and make appropriate adjustments such that more reliable results are obtained from these experiments.

3.0 EXPERIMENTAL INVESTIGATION

An experimental study was designed and carried out to determine the bond behaviour of externally bonded CFRP sheets on reinforced concrete under static loading. Twelve specimens were tested in tension using the double lap pull test method. Each specimen consisted of a pair of concrete prisms bonded together with one layer of CFRP sheet at varying bond lengths. Details of the test specimens, test set-up, test procedure, instrumentation and data acquisition procedures are presented in this section of the study. Table 3.1 gives a summary of the test program carried out in this study, with the ratio of the bond length tested to the calculated development length $\left({}^{L}/_{L_e}\right)$.

Three bond lengths were to be tested of which one bond length was supposed to be under developed, one equal to the development length and the last being over developed; but due to an error in the design calculations, all the bond lengths tested were larger than the development length (effective bond length). This did not affect the purpose of the study as the value of the development length is not affected by variations in bond length.

Three groups of specimens were tested with each group of four having the same bond length. Each specimen is identified with a label “LX-S-n” where the letter L indicates bond length, X gives the value of the bond length that changes for each group, S refers to static load, and n is the progressive test number.

Table 3.1: Summary of CFRP Sheet Properties Bonded to Concrete Prisms

Identification of Specimen	Bond Length (L) (mm)	L/L_e	Bond Width (mm)	Number of Layers of CFRP
L160-S-1	160	2.8	100	1
L160-S-2				
L160-S-3				
L160-S-4				
L240-S-1	240	4.2	100	1
L240-S-2				
L240-S-3				
L240-S-4				
L350-S-1	350	6.2	100	1
L350-S-2				
L350-S-3				
L350-S-4				

*L_e is the calculated effective bond length

3.1 Properties of Test Specimens

The specimen geometry was based on the recommendations in Annex N of the CSA S806-12 standard. Ready mix concrete with a 28-day average compressive strength of 34.3 MPa was used to cast the prisms with a 20-mm reinforcing bar embedded in the middle of each prism. The concrete was cast in plywood formwork constructed specifically for this test program. The formwork, as illustrated in Figure 3.1, was designed to accommodate two prims used to construct a double lap specimen. The size of the rebar was chosen such that it would remain elastic until the CFRP sheet reached rupture stress. The compressive strength (f_c') of the concrete was measured from tests on 100 mm by 200 mm cylinders.

The cast prisms were demolded after 48 hours and were moist cured for seven days before being subjected to the laboratory's temperature. The CFRP sheets were installed on the prisms at 51 days of age. The double lap tests were carried out 87 days after the CFRP sheets were installed. Compressive strength of the concrete equaled 32.3 MPa after 279 days. It is observed that there is a slight decrease in the compressive strength of the concrete

after 279 days. The decrease in compressive strength may have due to errors either during the casting of one or more of the cylinders or during their testing.

Figure 3.1: Formwork of Specimen with Rebars Placed at the Center of each Box

Figure 3.2 shows some cast concrete prisms with rebars protruding at each end. The concrete prisms had cross-sectional dimensions of 150 by 150 by 500 mm each.

(a)

(b)

Figure 3.2: (a) Reinforced Concrete Prisms Immediately after Casting (b) Prisms after Curing for 7 days

A commercial CFRP product (MasterBrace FIB 300-50CFS) was used in this investigation because these kinds of FRP sheets are commonly used in retrofitting actual beams in the industry. The material is a dry unidirectional carbon fiber sheet with a nominal unsaturated thickness of 0.165 mm. An adhesive that consists of three composite strengthening systems from Master Brace was the bonding epoxy used in this study. The three bonding systems include a primer, a putty and a saturant.

CFRP coupon tensile tests were carried out according to Annex F of the CSA S806-12 standard to measure the mechanical properties of the saturated fibers. A CFRP sheet of gauge length 340 mm and width 38 mm was coated with saturant on a smooth flat horizontal surface and a roller was used to work out trapped air. Aluminum tabs of length 76.5 mm and width corresponding to that of the CFRP sheet were bonded on both ends of the CFRP sheet using the saturant. The tabs served as grips for installing and pulling the coupons in the testing machine. Figure 3.3 shows a schematic diagram of the CFRP coupon specimen. Five coupons were tested in tension using a 250 kN capacity Instron testing machine and the force and machine displacement values were recorded by the inbuilt data acquisition system in the Instron. The strain values were recorded using a Digital Image Correlation (DIC) system. Figure 3.4 shows one of the coupons installed in the Instron before and after testing.

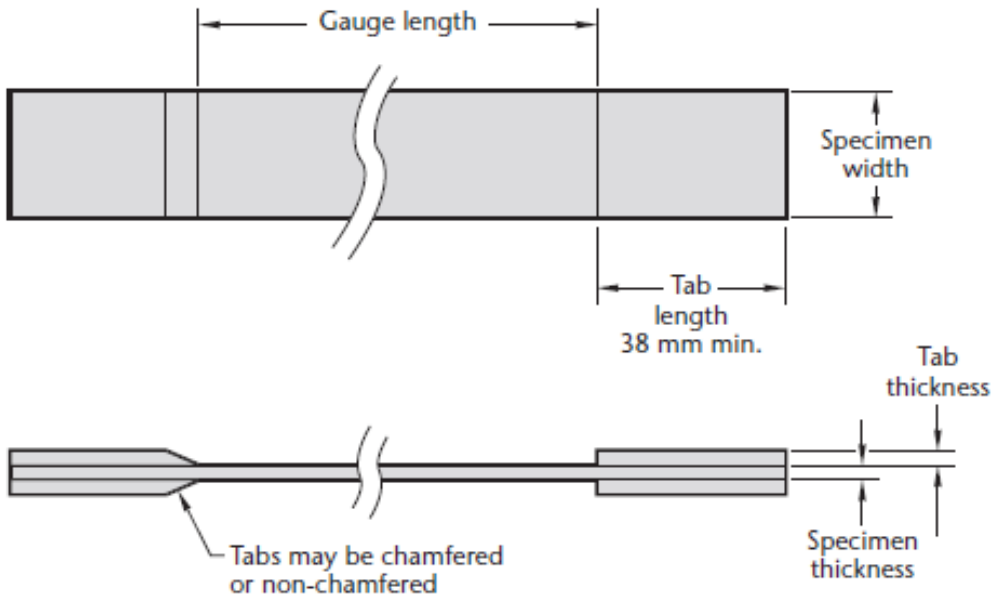

Figure 3.3: Schematic Diagram of FRP Coupon Test Specimen

(CSA S806, 2012)

Figure 3.4: CFRP Coupon Specimen in the Instron before and after Testing

Details of the tensile strength, ultimate strain, ultimate load and elastic modulus with corresponding average values of the coupons are summarized in Table 3.2. The stress-strain plots for all the specimens are shown in Figure 3.5. Stress is obtained by dividing the applied force by the product of the width of the CFRP sheet and an assumed thickness of 1 mm. The elastic modulus is obtained from the slope of the stress-strain curve. Based on the analysis of the coupon data, the tensile strength, elastic tensile modulus, and ultimate strain of the CFRP sheet were computed as 642 MPa, 37.8 GPa, and 1.9 percent respectively using the equations provided in Annex F of the CSA S806 (2012) standard.

Table 3.2: CFRP Coupon Test Results

Specimen	Ultimate Load (kN)		Ultimate Strain (%)		Tensile Strength (MPa)		Modulus of Elasticity (GPa)	
	Individual	Average	Individual	Average	Individual	Average	Individual	Average
Coupon 1	23.3	24.4	0.019	0.019	613.7	641.6	38.42	37.84
Coupon 2	24.2		0.018		636.1		35.66	
Coupon 3	24.0		0.020		632.4		37.94	
Coupon 4	26.2		0.018		689.5		38.39	
Coupon 5	24.2		0.019		636.1		38.81	

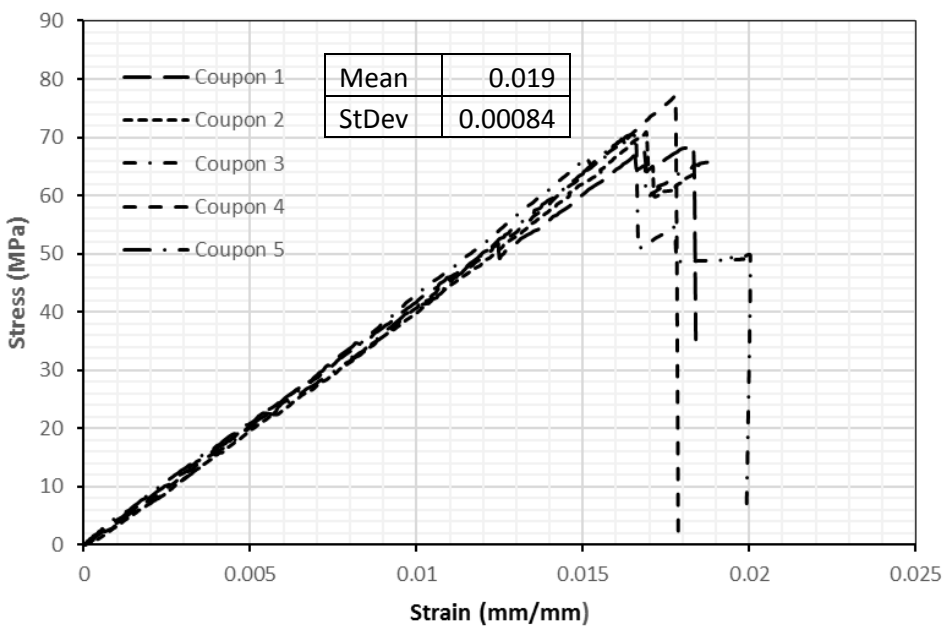

Figure 3.5: Stress-Strain Behaviours of the CFRP Coupons

3.2 Specimen Preparation

The bond behaviour between the FRP sheet and the concrete substrate can be determined using various methods such as the flexural beam test (bending test), the double lap pull-out test, and the push-out test (direct shear tests) as previously stated. The shear tests have been employed in the past by many researchers (Shadravan, 2009, Bizindavyi and Neale 1997, Chajes et al 1996 and Yao et al 2005). They are easy to perform and although real life beams are not subjected to that kind of loading, they produce similar stresses on the specimen as those that are encountered in the real beams (Shadravan, 2009). The double lap pull-out shear test method as recommended in Annex N of the Canadian Standard Association's CSA S806 (2012) was used in this research to investigate the bond behaviour of FRP-to-concrete interface.

Figure 3.6 shows schematic details of a pair of reinforced concrete prisms with CFRP sheets applied on opposite sides of the specimen acting as a joining material for the two prisms. The prisms each have one steel reinforcing bar embedded in the middle. The bar protrudes on one end of each specimen, so it can later be used to grip during the tests. The gap between the two prisms was set to approximately 3 mm and was maintained during the CFRP sheet installation by using a plaster material (durabond) after plastic was placed in between the prisms to eliminate any form of bond connection between the end surfaces. Initially, for all the specimens, one side of the specimen was bonded along its full length with a CFRP sheet 1000 mm long and 100 mm wide to serve as an anchorage during the test. On the opposite side of the specimen, the full length of one prism was covered with CFRP sheet while the other prism had varying bond lengths of 160 mm, 240 mm and 350 mm. The specimens that had the longest CFRP bond length (350) was further anchored at

one end by wrapping a 150 mm width of CFRP sheet around the cross-section to prevent debonding failure from taking place at that end. The specimens were prepared in this manner so that failure was most likely to occur on the side that had the shorter bond length which would be the focus of the study. However, after testing 4 of the 12 specimens (3 with bond lengths of 160 mm and 1 with a bond length of 240 mm), it was observed that 2 out of the 4 specimens failed on the side that was not being monitored (the longer side of the FRP sheet). This may have been due to the shorter length of the FRP sheet being relieved of stresses after concrete tension crack at the termination of the FRP sheet took place. Stresses were then transferred to the longer end until it failed. Hence, the remaining specimens were altered by cutting off the longer side to be the same as the corresponding bond lengths to be monitored so that failure is likely to occur on either sides bonded with FRP sheet. This is as shown in Figure 3.7.

The FRP sheet lengths were taken as KL_e, where L_e is the development length calculated using Equation 3.1 from CSA S806 (2012. The CSA S806 (2012) standard also specifies that K may be taken in increments of 0.2 from 0.6 to 1.6. However, in this study, K was taken as 2.8, 4.2 and 6.2 to give bond lengths of 160 mm, 240 mm and 360 mm respectively since the bond lengths tested were generally larger than the calculated development length (57 mm).

[3.1] $$L_{ea} = \frac{25350}{(t_f \times E_f)^{0.58}}$$

where t_f and E_f are the thickness and elastic modulus of the CFRP sheet respectively. Photographs of some specimens with CFRP sheets bonded on opposite sides are illustrated in Figure 3.8.

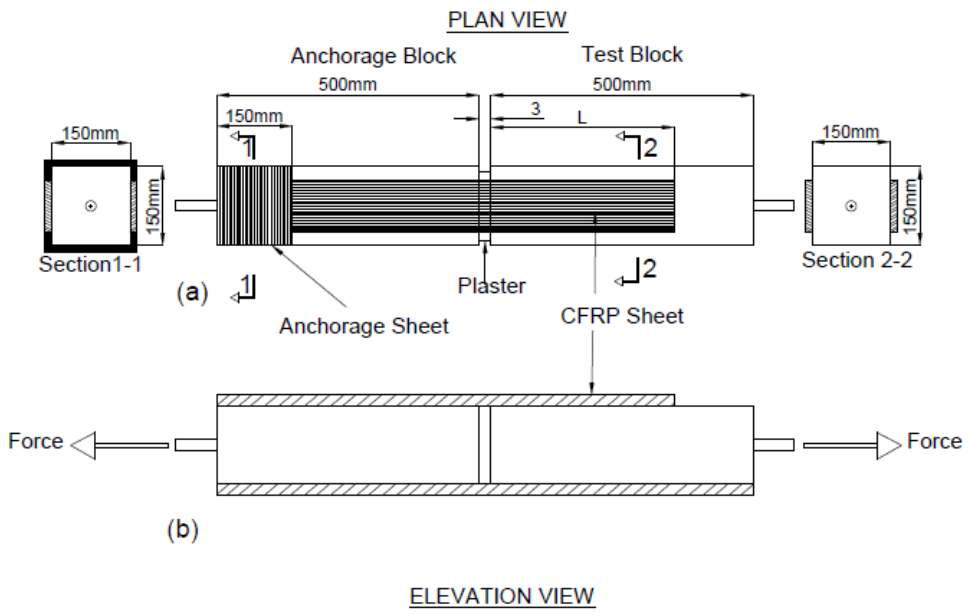

Figure 3.6: Schematic Diagram of Test Specimen before the Modification (L represents the varying bond length of CFRP)

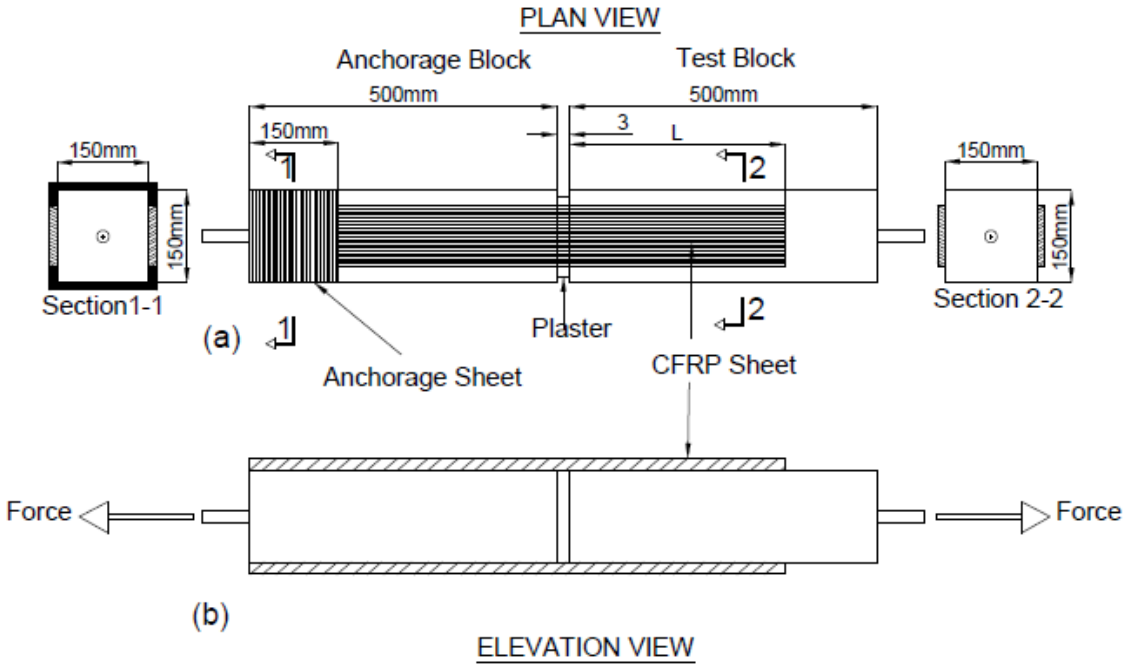

Figure 3.7: Modified Schematic Diagram of Test Specimen (L represents the varying bond length of CFRP)

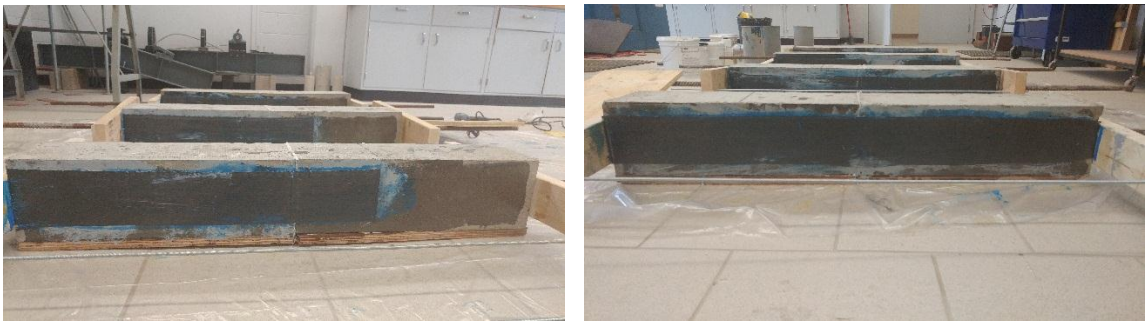

(a) Shorter Length of CFRP **(b) Longer Length of CFRP**

Figure 3.8: Specimens with CFRP Sheet Bonded on Opposite Sides

Before the sheets were applied on the concrete prisms, the surfaces were first thoroughly cleaned to remove dust, lose debris and moisture. A plaster like material (durabond) was applied in between the two halves of the specimen to fill the 3 mm gap between them as stated earlier. Plastic was placed on both end faces prior to the application of the plaster to eliminate any form of bond connection between the prisms. Both halves were clamped together for 24 hours until the plaster was cured. This allowed for easy maneuvering and proper alignment of the RC prisms during the FRP sheet installation. The primer was applied first using a nap roller followed by the putty to cover up pores and level uneven surfaces. The dry CFRP fabric was cut into the required width and length, permeated with saturant, and then pressed onto the surface of the concrete using a nap roller. A layer of saturant was then applied to fully encapsulate the fibers and was allowed to cure before testing (87 days after). Figure 3.9 shows the steps on how the CFRP-to-concrete specimen was prepared.

The twelve specimens were tested at a loading rate of 0.5 mm/min. The DIC software used to record strain values during the test was set to capture images every 0.4 s except for the first specimen whose images were captured every 0.5 s. Table 3.3 summarizes the

properties of the test specimens and test variables. It also indicates the specimens that had equal and unequal CFRP lengths installed on the sides of the prisms.

(a) Specimen before applying plaster

(b) Specimen after applying plaster

(c) Primer applied on Specimens

(d) Putty applied on specimen

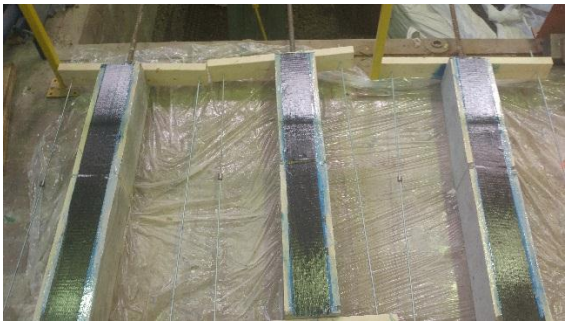

(e) CFRP Sheet Laid on Concrete prisms

(f) Close-up view of Finished Specimen

Figure 3.9: Steps in the Specimen Preparation Process

Table 3.3: Summary of Specimen and Test Properties

Identification of Specimen	Bond Length (L) (mm)	Modified or Unmodified Specimen	L/L_e	Concrete Strength (MPa)	Loading rate (mm/min)	DIC Image Time Interval (ms)
L160-S-1	160	unmodified	2.8	34.3	0.5	500
L160-S-2						400
L160-S-3						
L160-S-4		modified				
L240-S-1	240	unmodified	4.2	34.3	0.5	400
L240-S-2		modified				
L240-S-3						
L240-S-4						
L350-S-1	350	modified	6.2	34.3	0.5	400
L350-S-2						
L350-S-3						
L350-S-4						

*L_e is the calculated effective bond length

3.3 Test Set-up

The specimens were subjected to static loading using a Universal testing machine in the Structures Laboratory of the University of New Brunswick. The length of the specimen was governed by the development length of the rebar embedded in the concrete and load was applied under tension through the reinforcing bars protruding from either end of the specimen. Prior to the test, the ultimate capacity of the FRP sheet was conservatively calculated using the material specifications provided by the manufacturer. The specimen was put in place in the machine using two couplers each at the top and bottom cross heads of the machine to hold the specimen. Steel plates with holes were placed before the couplers were installed as shown in Figure 3.10 so that the specimen is well centered on the machine. Load was applied at a displacement control rate of 0.5 mm/min until failure of the specimen.

Figure 3.11 shows a specimen comprised of two prisms installed on the Universal testing machine. Values of load were recorded by the data acquisition system inbuilt into the testing machine. As stated earlier, the test specimen had to be modified after it was

observed that two of the twelve specimens failed on the longer side of the FRP sheet directly opposite the bond length being tested. The new set up brought about the possibility of failure taking place on either side of the specimen even though only one side was monitored by the DIC system.

Figure 3.10: Steel Plates and Coupler used to Install, Align and Hold the Specimen

Figure 3.11: Specimen Installed on the Universal Testing Machine

3.4 Instrumentation

Strain and corresponding displacement values of the specimens were monitored and recorded using a Digital Image Correlation measurement system known as VIC 3D. This method was adopted in place of regular strain gauges because it is known to give strain values with a high degree of accuracy as validated by Bisby et al, 2007, Zhu et al., 2014 and Dutton, 2012. Another advantage of the DIC is that strain across the specimen can be determined at every point compared to strain gauges that only give localized strain values (Dutton, 2012). The DIC software obtains and analyses data using a digital image-based surface displacement technique. A pair of digital cameras is used to capture images of the specimen as the experiment proceeds at specified time intervals. An initial reference image is taken and then subsequently compared to a series of deformed images taken during the test. The reference image is subdivided into square patches of pixels which contain enough variation in intensity and colour for ease of tracking in subsequent images (Bibsy et al., 2007, Dutton, 2012). The difference, measured in pixels, between each patch of the reference image and the target image, gives the displacement vector that is used to compute the strain of the specimen using mathematical correlation algorithms.

Prior to their installation on the machine, the face of the specimen being monitored was painted with black speckles on a white background as shown in Figure 3.12 to convey a high contrast image for the DIC to capture. A pair of Sony Pregius IMX250 digital cameras with 5 Megapixel resolution was vertically fixed on a tripod in front of the specimen such that the angle between them is within a range of 15 to 23 degrees to yield optimum results. The distance between the camera system and the specimen is set such that the specimen roughly fills the field of view with the area of interest being visible in both cameras. The

area of interest being the area on the specimen covered by the CFRP sheet. Figure 3.13 shows the cameras mounted on tripods and placed in front of the machine at an appropriate distance.

Figure 3.12: Specimen Speckled with Black Dots on a White Background

Figure 3.13: Camera Installed on a Tripod Stand and Positioned infront of the Universal Testing Machine

The focus on both cameras was adjusted such that a sharp focus is obtained on the entire specimen. The right amount of white light was introduced by adjusting the exposure time and aperture settings such that an appropriate specimen brightness is achieved. The cameras were then calibrated by positioning the correct size of grid in the intended plane of the specimen to ensure the accuracy of the camera images and data to be recorded. DIC images were recorded at a time interval of 0.4 second during the tests except for the first specimen whose images were recorded every 0.5 second. The DIC computing software (VIC 3D) (correlated Solutions, 2010) was used for the processing and analysis of data obtained from the captured images. The values recorded by the DIC software include strain values in the x, y and z directions at every point on the specimen and the corresponding time and displacement in all three directions.

Strain results from the DIC software were correlated with the load data from the testing machine by aligning plots based on times when important events took place during the test (a decrease in force with a corresponding drop in strain). Since load was recorded every 0.1 second and strain values recorded every 0.4 second, values were correlated by taking every fourth load value recorded to correspond to the values recorded by the DIC system after their plots have been matched based on key times.

3.4.1 DIC Analysis Procedures

The analysis procedure for data obtained from the DIC to determine the bond behaviour of FRP-to-concrete interface is to some degree different from the analysis procedure of data obtained from traditional strain gauges. Speckled images captured during the test were first analyzed using the VIC 3D software. The area of interest (AOI) which is the area covered by the CFRP sheet with the bond length being monitored is as shown in Figure 3.14. The

AOI was specified on the specimen using the mask tools which are of different shapes as provided in the DIC software system. Appropriate subset and step sizes were selected after the AOI was selected. Subset size controls the area of the image that is used to track the displacement between images. The analyses were then run on the software for the computation of strain values at every point in the AOI indicated. Figure 3.15 illustrates a specimen with a specified subset size. Results were then exported into excel for plotting of graphs and comparison with force values obtained from the universal testing machine data acquisition system which was recorded 0.1 second intervals.

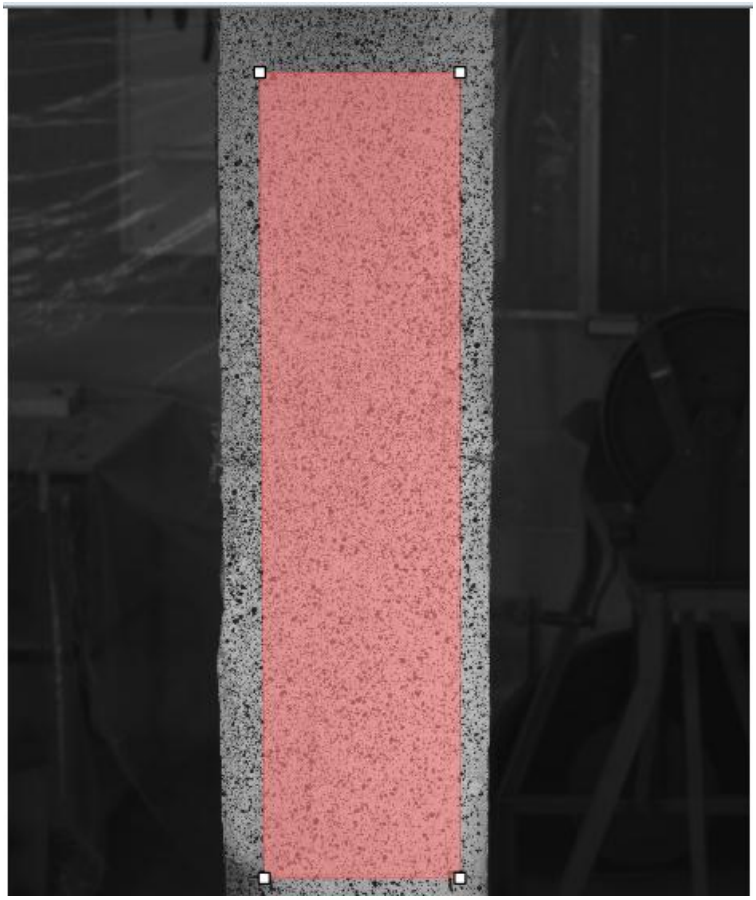

Figure 3.14: Specified Area of Interest on Specimen using the Rectangular Mask Tool

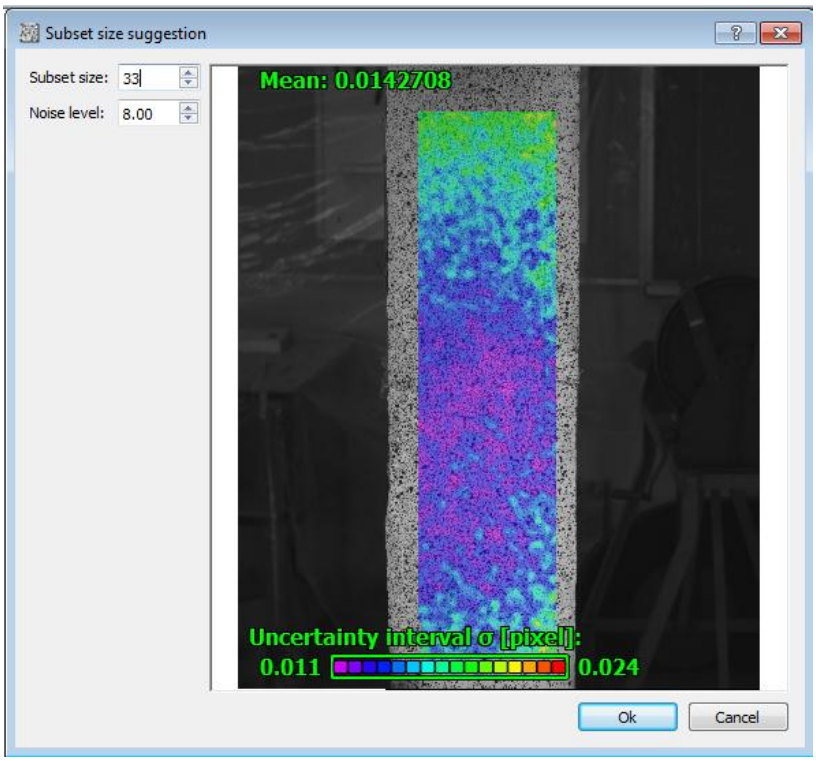

Figure 3.15: Choosing a Subset Size and Noise Level for a Specimen

3.5 Summary of Experimental Investigation

Twelve specimens were tested on a Universal testing machine. Each specimen was prepared by first casting the concrete prisms. CFRP sheets were then installed on opposite sides of a pair of prisms. After curing, the FRP sheets installed on the prisms were speckled with black dots on a white background. Specimens were tested on a Universal Testing Machine. Load values were recorded at an interval of 0.1 seconds while strain values were recorded using a DIC technique at a time interval of 0.4 seconds. All specimens except specimens L160-S-1, L160-S-2, L160-S-3 and L240-S-1 had the bond length of the FRP sheets installed on both sides of the specimens being equal. The others had one bond length longer than the other.

4.0 EXPERIMENTAL RESULTS

The results for all specimens with the three different bond lengths tested under static load are presented in this section of the report. Four specimens of each group of development length were tested. A detailed report of one specimen from each group is presented while the details of the other specimens are presented in Appendix A of this thesis. Data from all specimens is compared with each other based on some key parameters such as development length, bond stress, ultimate bond capacity, and slip. Generally, all specimens failed by debonding at the concrete to adhesive interface irrespective of their bond length. Test results are summarized in terms of force-time curves, plus stress and strain data for the FRP sheet relative to time along the bond length of the CFRP sheet.

Table 4.1 gives a summary of the ultimate loads of all specimens. From the results, it can be observed that an increase in bond length of the CFRP sheet did not cause a significant increase in its failure load of the CFRP-to concrete interface. This hypothesis was confirmed by carrying out a statistical analysis comparing results obtained from all the groups of specimens using the Analysis of Variance (ANOVA) tool. A graph showing the summary of failure load results with error bars are indicated in Figure 4.1.

Table 4.1: Summary of Failure Load Results

Identification of Specimen	Bond Length (L) (mm)	P_u (N)		
		Individual	Average	Variance
L160-S-1	160	39104	38667	4.7
L160-S-2		36690		
L160-S-3		37324		
L160-S-4		41548		
L240-S-1	240	48792	43382	20.9
L240-S-2		38547		
L240-S-3		40874		
L240-S-4		45315		
L350-S-1	350	43967	40111	21.9
L350-S-2		38528		
L350-S-3		34195		
L350-S-4		43755		

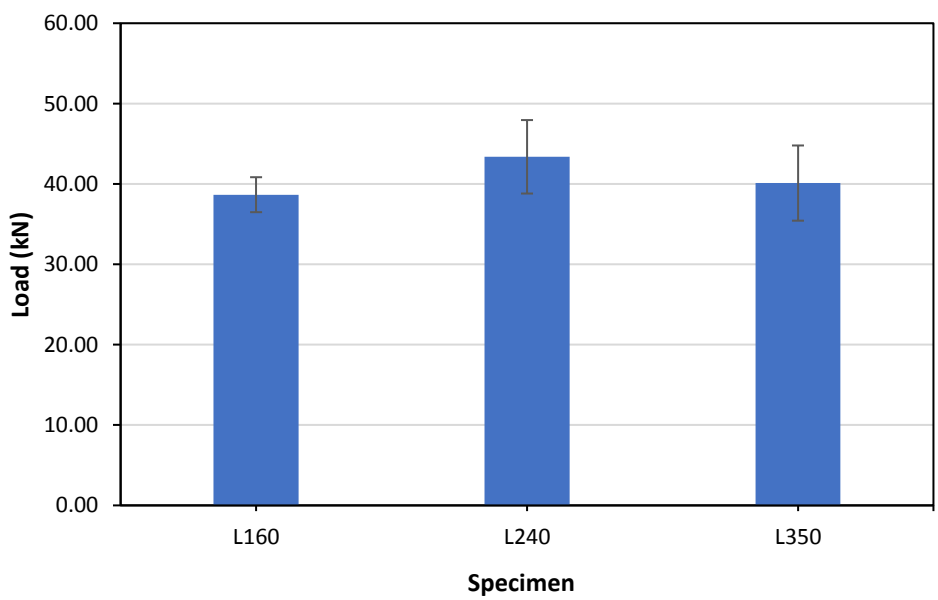

Figure 4.1: Summary of Failure Load Results

4.1 Specimen L160-S-4 ($L_e = 160\ mm$)

Figure 4.2 shows pictures of the specimen installed on the Universal testing machine speckled only on one side. The specimen was properly installed in the machine and was held in place using couplers on the rebars at the top and bottom of the specimen. The FRP sheets on either side of the specimen were of the same bond length of 160 mm measured from the loaded end of the specimen.

(a) Front of Specimen (b) Back of Specimen (c) Side of Specimen

Figure 4.2: Views of Specimen L160-S-4 Installed in the Machine before Testing

The specimen experienced a brittle failure with a loud noise at the time of failure when it was tested. Pictures taken immediately after the test was completed are presented in Figure 4.3. From Figure 4.3(a), it is seen that failure took place on the speckled side with no rupture of the FRP sheet. Figures 4.3(b) and 4.3(c) show a crack that developed on both the left and right sides of the specimen normal to the force applied on the FRP sheet indicating tension failure. The crack developed at the location where the CFRP sheet terminated. A concrete wedge failure also developed at the loaded end of the specimen as seen in Figure 4.3(d) while Figure 4.3(e) shows a close-up view of the debonded region in which debonding failure was initiated by the wedge crack that developed at the loaded end

of the FRP sheet. It was observed that the CFRP sheet was well bonded to the concrete because debonding occured by shearing of concrete below the bonded surface. The back side of the specimen failed due to buckling of the FRP sheet immediately after the debonding failure on the front side took place as shown in Figure 4.3(f). The buckling of the FRP sheet installed on the back side of the specimen was caused by rotation of the prism after debonding of the FRP sheet on the front face took place.

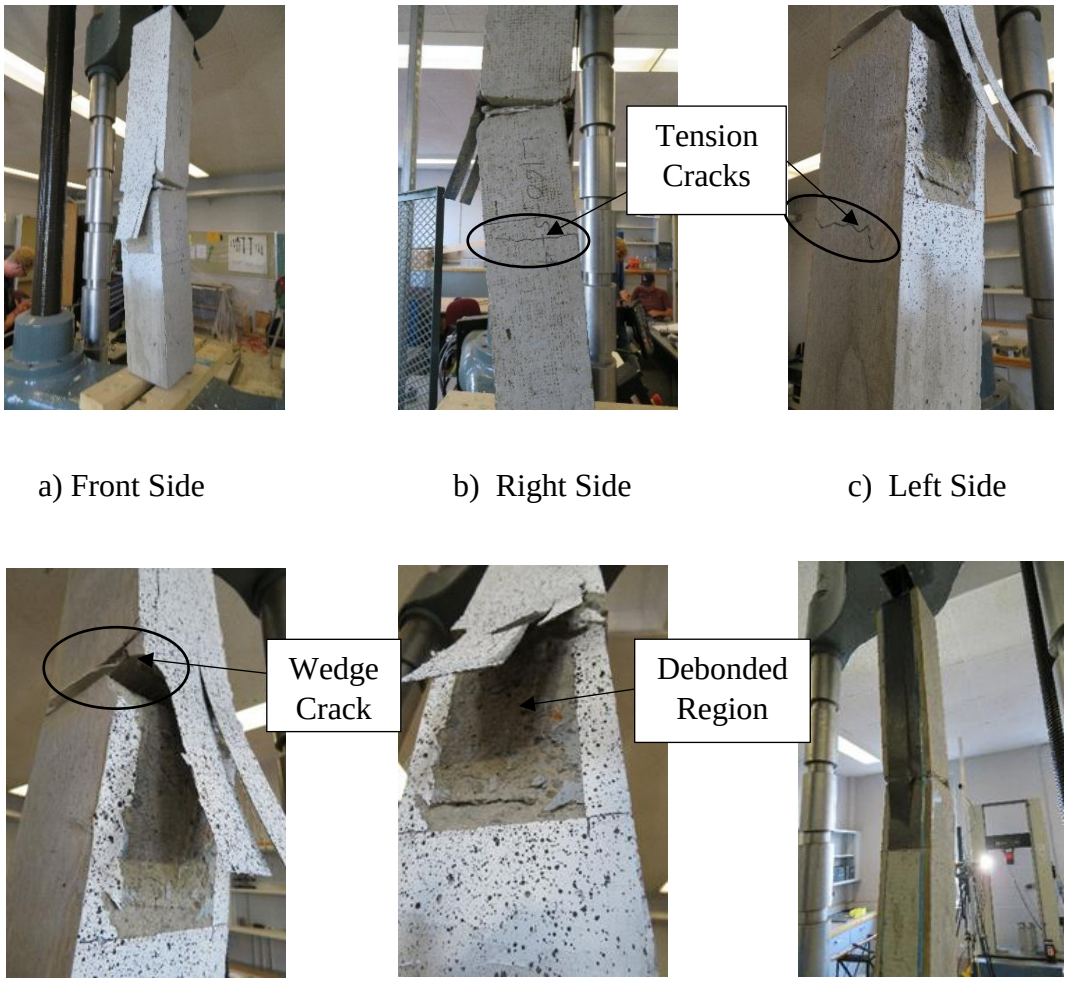

a) Front Side b) Right Side c) Left Side

d) Concrete Wedge Crack e) Debonded Region f) Back Side

Figure 4.3: Views of Specimen L160-S-4 after Failure

Figure 4.4 gives a sketch of the general failure pattern and formation of cracks for all the specimens tested in this study. All the specimens failed by debonding due to the initiation of wedge cracks at the loaded end of the FRP sheet. Tension cracks were observed only on specimens with 160 and 240 mm bond lengths but were not observed on the specimens with 350 mm bond length. These tension cracks extended towards the face of the prisms bonded with the FRP sheet in some specimens while some of them did not.

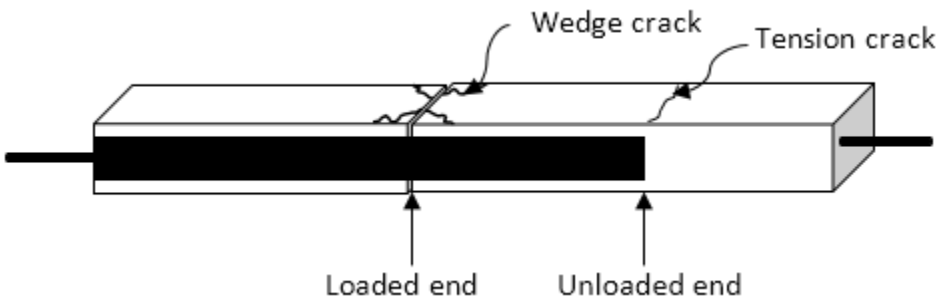

Figure 4.4: Close-up View of the Crack Pattern after Specimens Failure

Numerical data obtained from the Universal testing machine and the DIC software were analyzed and presented using graphs and contour diagrams. Figure 4.5 shows the experimental load versus time curve of the CFRP-to-concrete interface with points indicating significant occurrences at varying times for specimen L160-S-4. Points (a), (b) and (c) on the graph represent the elastic behaviour of the specimen. The applied load gradually increased as time increased until point (d) when the concrete wedge crack (as shown in Figure 4.3(d)) occurred causing a decrease in force to point (e). The wedge crack caused the stresses in the specimen to redistribute after which the specimen started to gain more load up to point (g). Point (f) on the graph is a random position between the point where the minimum force occurred, and the ultimate load of the specimen was recorded. At point (g), the tension cracks along the sides of the specimen began to propagate causing

a decrease in force to point (h) (27.7KN). After the redistribution of stresses, the load started to increase up to point (i) at which the FRP-to-concrete interface failed suddenly. The table on the graph shows the forces and corresponding times at which significant occurrences took place during the test.

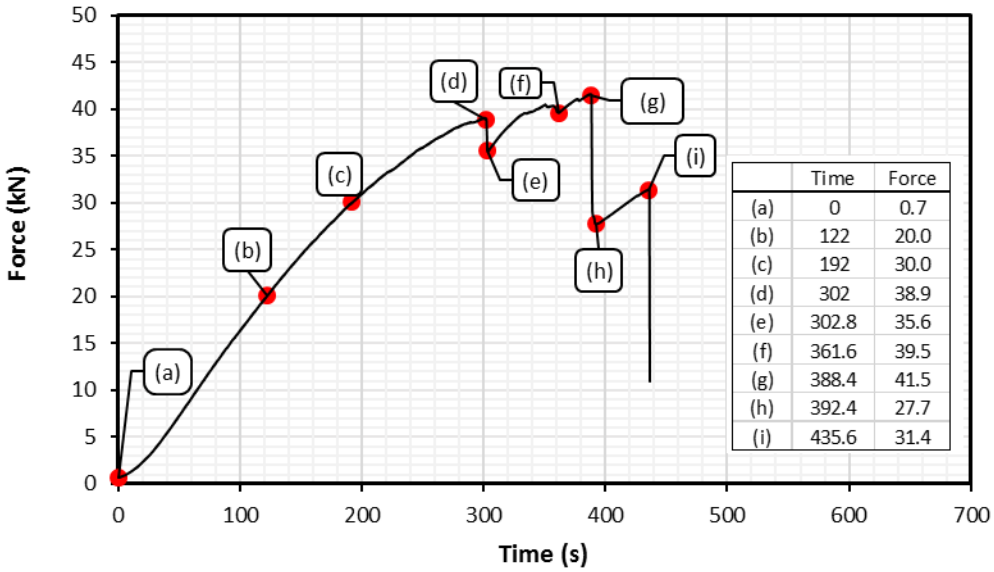

Figure 4.5: Force versus Time curve for Specimen L160-S-4 Showing Key Points During the Test

Figure 4.6(a) shows the contour diagram of the FRP sheet indicating the position of a strain inspector line at the middle of the CFRP sheet along its bond length while Figure 4.6(b) shows the graph of longitudinal strain against distance along the bond length of the FRP sheet at the key times previously highlighted in Figure 4.5. As the load increased, the strain curve began to shift upwards indicating an increase in strain over time. Curves labelled (a), (b) and (c) are the lowest and have similar shape, indicating elastic behaviour of the specimen. However, over time and increasing load, the curve began to shift upwards with the slope shifting towards the end of the FRP sheet. The flat segment of the curves indicates

the initiation of cracks and subsequent debonding, propagating from the loaded end of the FRP bonded specimen to its unloaded end. The elastic region of the curve known as the active bond zone indicates the part of the CFRP sheet still well bonded to the concrete where most of the interfacial stresses are transferred from the CFRP sheet into the concrete. This zone shifts towards the unloaded end of the FRP sheet as it debonds. This elastic zone is the effective bond length beyond which there is no further increase in load the FRP sheet can carry. The strain continues to increase with time until (f) when there was a decrease in strain from 0.55 percent to 0.39 percent and then remaining fairly constant (but increases slightly) until (i) with 0.45 percent strain before failure. The effective bond length for this specimen is 40 mm.

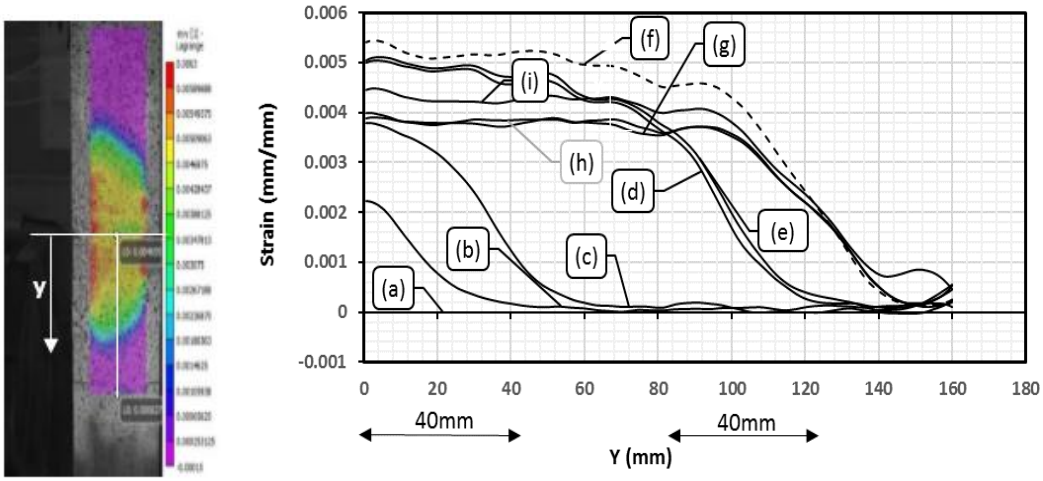

(a) (b)

Figure 4.6: (a) Contour Diagram Showing Position of Strain Inspector Line along the Bond Length of FRP Sheet (b) Strain versus Distance along the Bond Length of FRP Sheet at Times shown in Figure 4.5

Figure 4.6(c) shows a clearer illustration as to how the effective length was determined from the graph. The effective length values were determined by direct measurement of the elastic region of the curves which is fairly constant over the test duration of each specimen. The average value obtained from the development length or effective length measured for this specimen (L160-S-4) is 40 mm.

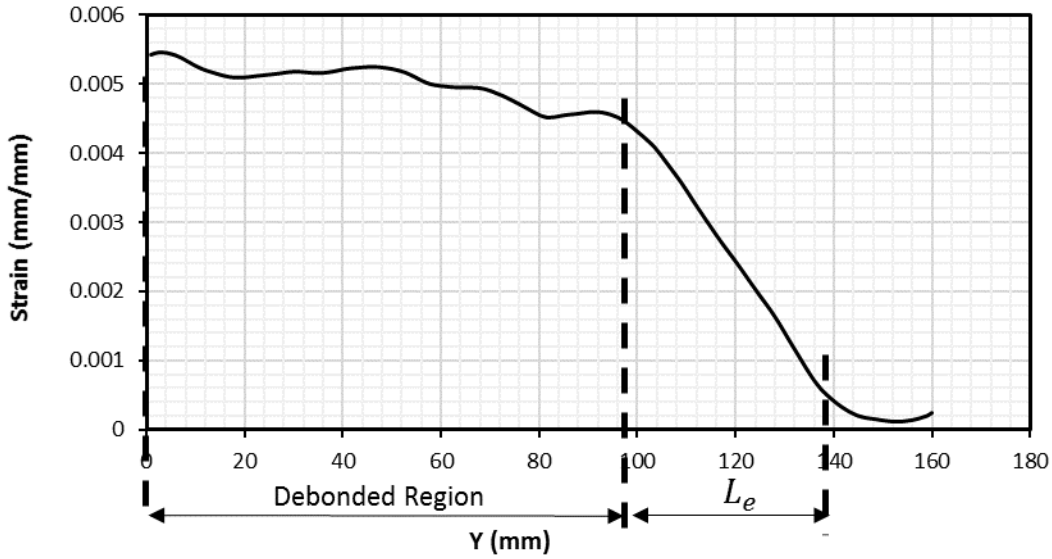

Figure 4.6(c): Strain versus Distance along the Bond Length of FRP Sheet showing Development Length.

Contour diagrams of longitudinal strain fields obtained from the DIC software at key times indicated in Figure 4.5 are presented in Figure 4.7. Figures 4.7(a), (b), (c) and (d) show a gradual increase in longitudinal strains originating from the loaded end of the FRP sheet until the occurrence of the wedge crack. After the wedge failure took place at time (d), there was a slight increase in strain as seen in (e) which further increased in (f). A decrease

in strain can however be noticed between times (f) and (g) from their corresponding contour diagrams.

It can also be observed from the contour diagrams that strain distribution gives a curve shape across the FRP width that gradually propagates towards the unloaded end of the FRP sheet as the load increased. The uneven distribution of stresses along the width of the specimen is known as the shear lag effect. It is also observed that there is an asymmetry in the strain fields across the width of the FRP sheet. This may be due to force being transferred from the machine to the specimen at an eccentricity. Force being transferred at an eccentricity may be caused by not placing the specimen at the exact center of the machine during installation or not placing the FRP sheet to align accurately to the center of the concrete prism during the preparation of the specimen. The load eccentricity effect can be avoided by properly aligning the sheet on the concrete surface when the specimen is being prepared and properly aligning the specimen as a whole to the exact center of the testing machine. Figure 4.7 shows various strain fields showing the distribution of longitudinal strains on the FRP sheet until failure.

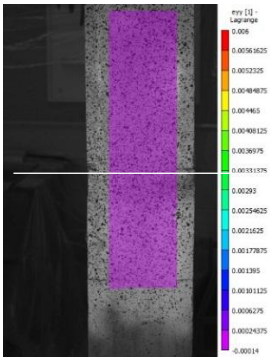

(a) ε_{yy} Dist. at T= 0 s

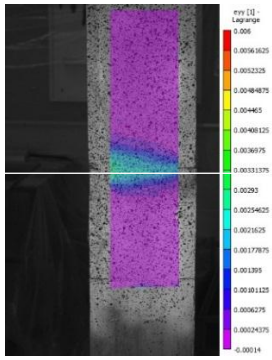

(b) ε_{yy} Dist. at T=122 s

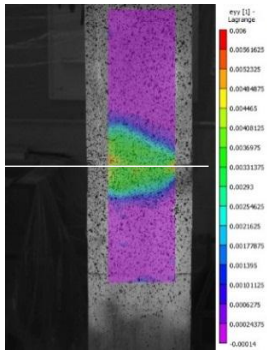

(c) ε_{yy} Dist. at T=192 s

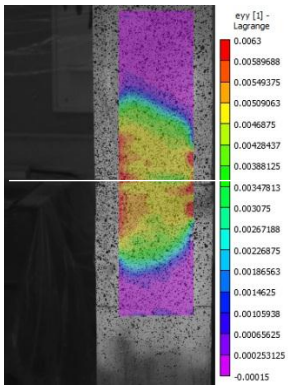

(d) ε_{yy} Dist. at T=302 s

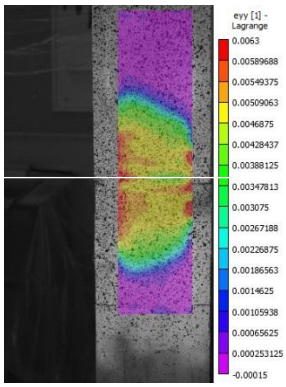

(e) ε_{yy} Dist. at T=302.8 s

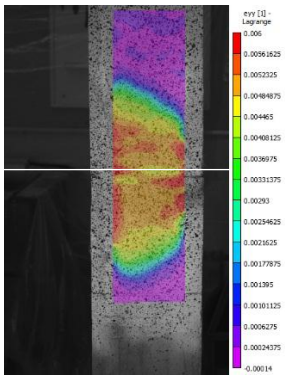

(f) ε_{yy} Dist. at T=361.6 s

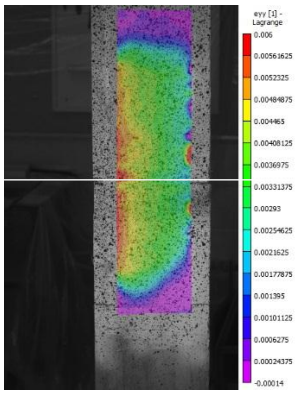

(g) ε_{yy} Dist. at T=388.4 s

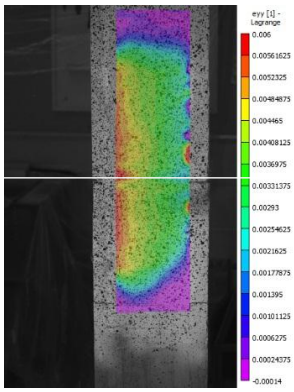

(h) ε_{yy} Dist. at T=392.4 s

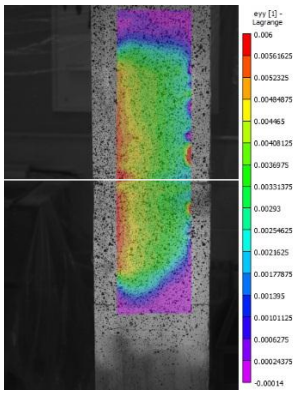

(i) ε_{yy} Dist. at T=435.6 s

Figure 4.7: Strain Fields showing the Distribution of Longitudinal Strains (ε_{yy}) on FRP Sheet at Different Times as Test Progressed to Failure for Specimen L160-S-4

Figure 4.8 shows the longitudinal strain contour diagram with 8 strain gauge locations positioned at the quarter and half width of the CFRP sheet. A pair is aligned at approximately the same level on the FRP sheet as shown in Figure 4.8(a). From the graph, it can be deduced that gauges (g5), (g6), (g7) and (g8) recorded higher strain values compared to gauges (g1), (g2), (g3) and (g4) due to the shear lag and load eccentricity effect as previously discussed. It is observed that the strain values of gauges g3 and g7 did not start to increase until the initiation of the wedge crack and subsequent propagation of debonding that caused the redistribution of stresses. Just before failure, all gauges indicated a sudden drop in strain right before the instantaneous redistribution of stresses.

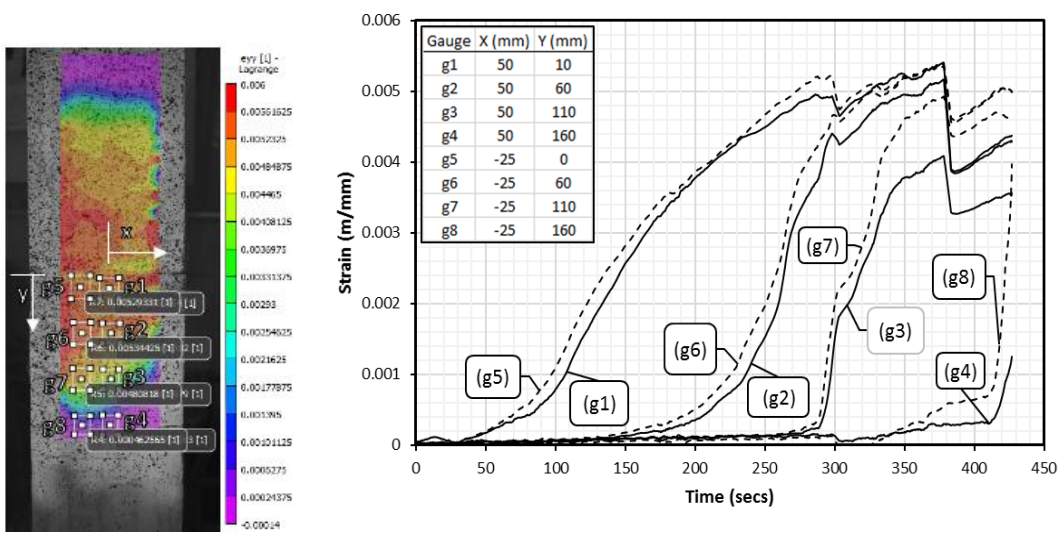

(a) (b)

Figure 4.8:(a) Contour Diagram Showing Position of 8 Gauges on FRP Sheet (b) Strain versus Time Curves of Specimen L160-S-4 at Locations of Gauges as Indicated in the Contour Diagram in (a)

The force versus strain curves for gauges g1, g2, g3 and g4 are shown in Figure 4.9. This strain data is useful in assessing the bond-slip relationship of the FRP sheet. The highest strain values were recorded by gauge g1 which is located at the critical end of the FRP sheet. The relation between these two variables as seen in the graph is bi-linear and the maximum strain varied between 0.4 and 0.5 percent.

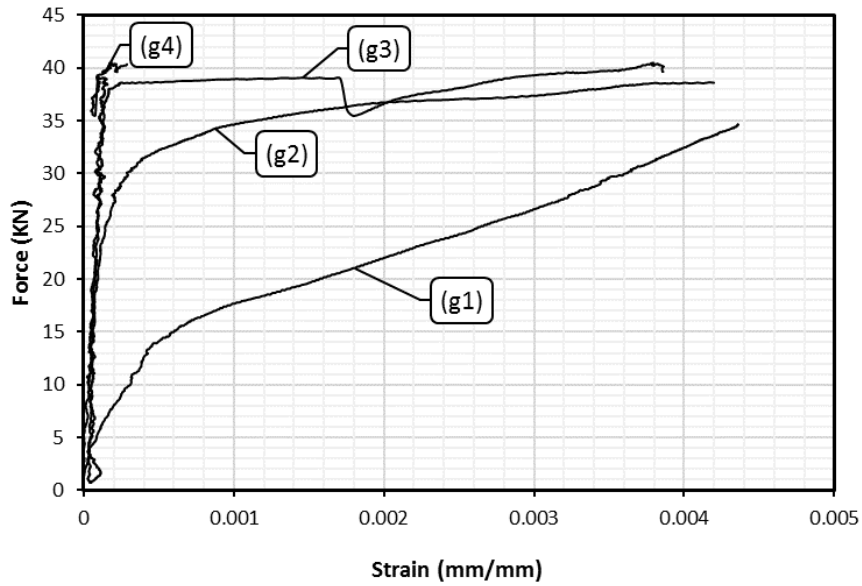

Figure 4.9: Force versus Strain Curves for Strain Gauges g1, g2, g3 and g4 in Figure 4.8(a) on Specimen L160-S-4

4.2 Specimen L240-S-4 ($L_e = 240\ mm$)

Figure 4.10 shows the pictures of the speckled specimen after it was installed in the testing machine with the FRP sheet on both sides being of equal length (240mm bond length). Only one side of the specimen was speckled while the other side had the original colour of the FRP sheet (black). The specimen was held firmly on the machine with couplers at the top and bottom as stated previously.

(a) Front of Specimen (b) Back of Specimen (c) Side of Specimen

Figure 4.10: Views of Specimen L240-S-4 Installed in the Machine Prior to Testing

Failure of this specimen was also brittle accompanied by a loud noise. Figure 4.11 shows the pictures taken after the experiment. There was good bonding as failure was by concrete cover debonding on the speckled side with no rupture as shown in Figure 4.11(a). Tension cracks developed on the left and right sides which proceeded to the back of the specimen as seen in Figures 4.11 (b) and 4.11 (c). A clearer view of the crack and failure pattern is like what is represented in Figure 4.4 of this thesis. The back side of specimen failed due to buckling of the FRP sheet immediately after the speckled side failed.

a) Front Side

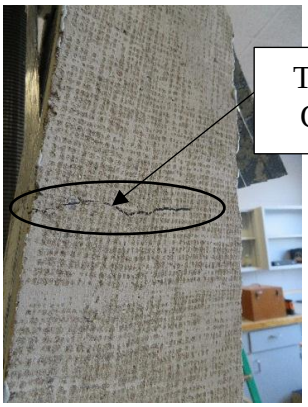

b) Right Side

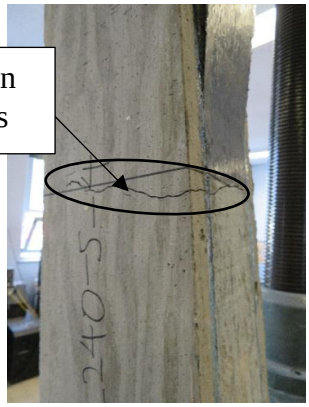

c) Left Side

d) Wedge Crack Failure

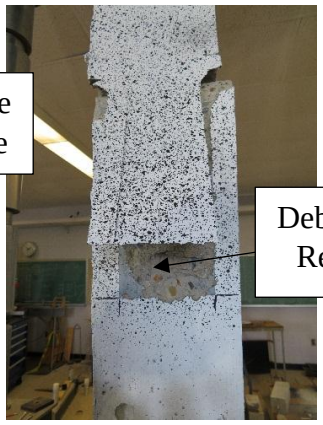

e) Debonded Region

f) Back Side

Figure 4.11: Views of Specimen L240-S-4 after Failure

Analysis of the force versus time data obtained from the testing machine indicates a decrease in force at two different times during the test before failure as shown in Figure 4.12. Points (a), (b) and (c) show the elastic behavior of the specimen. The applied load gradually increased as time increased until point (d) when the concrete wedge failure (as shown in Figure 4.11(d)) occurred causing a decrease in force to (e). The wedge failure caused the stresses in the FRP sheet to redistribute after which the specimen started to gain more load up to point (f). At point (f), the tension cracks along the sides of the specimen

began to propagate causing a decrease in force to point (g) (39.5KN). After the redistribution of stresses, the load started to increase up to maximum at point (i) (45KN) before debonding failure took place suddenly. The table on the graph shows the forces and corresponding times at which key occurrences took place during the test.

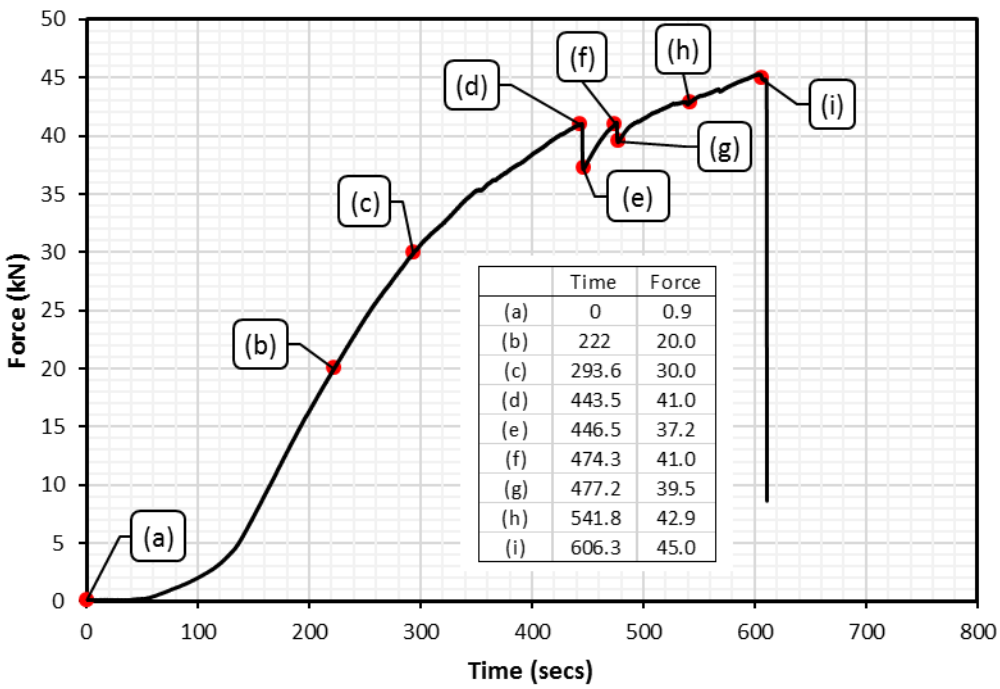

Figure 4.12: Force versus Time curve for Specimen L240-S-4 showing Key Points During the Test

The position of a strain inspector line and a graph corresponding to the strain recorded over length of the FRP sheet by the inspector line is as indicated in Figure 4.13. Similar behaviour as in specimen L160-S-4 was also observed in this specimen. The effective bond length shifted along the FRP sheet length as the load and strain increased correspondingly. The flat segment of the curve represents the region that has debonded due to the wedge cracks that developed at the loaded end of the FRP sheet. The strain increased until time

(d) where there was a drop in strain from 0.47 percent to 0.43 percent. A peak strain of 0.57 percent was recorded before failure by debonding of the FRP sheet took place. The effective bond length of the FRP sheet in this specimen was measured to be 50 mm.

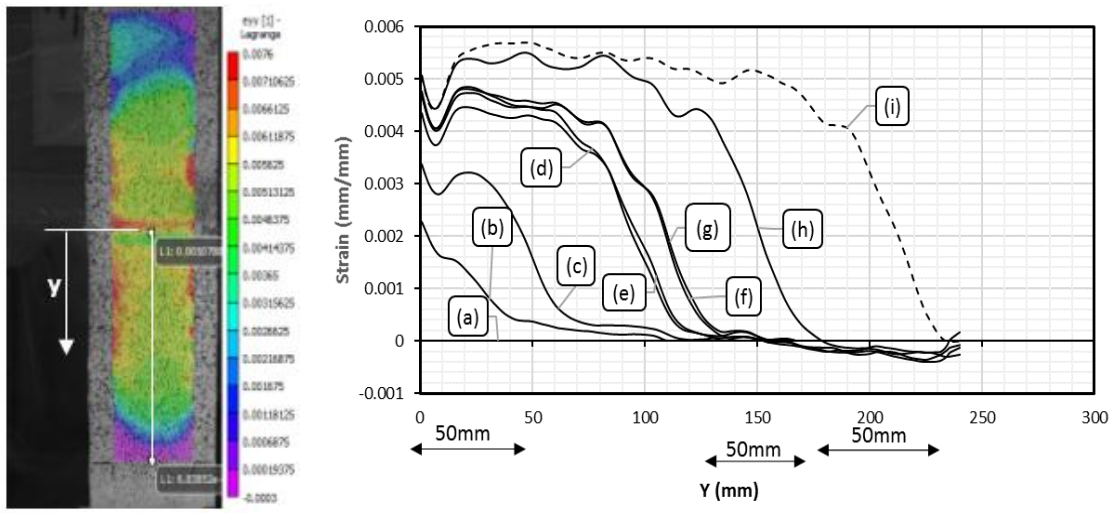

(a) **(b)**

Figure 4.13: (a) Contour Diagram showing Position of a Strain Inspector Line along the Bond Length of FRP Sheet (b) Strain versus Distance along the Bond Length of FRP Sheet at Times shown in Figure 4.12 for Specimen L240-S-4

Figure 4.14 shows contour diagrams at times indicated in Figure 4.12. It can be observed that the maximum strain was at the loaded end of the FRP sheet which is at the joint between the two prisms. There was a gradual increase in strain as seen in pictures 4.14(a) to 4.14(d). Although not very evident in the contour diagram in Figure 4.14(e), the strain dropped slightly due to the wedge crack at the loaded end of the FRP sheet and then gradually increased from (f) to (g) before attaining its maximum strain at (i) as seen in Figure 4.14(i). Shear lag was also observed in the contour diagrams as strain distribution

gave a curved contour shape as seen in the figures, but the effect of load eccentricity was not significant in this specimen.

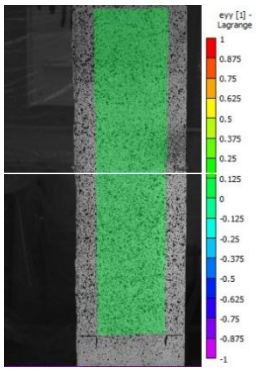

(a) ε_{yy} Dist. at T= 0 s

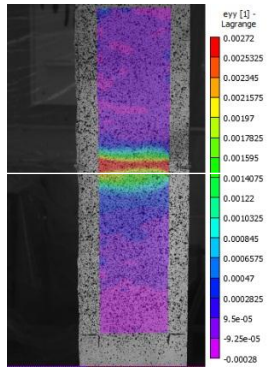

(b) ε_{yy} Dist. at T= 222 s

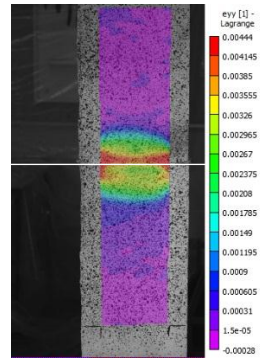

(c) ε_{yy} Dist. at T= 293 s

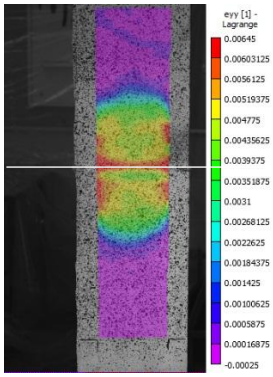

(d) ε_{yy} Dist. at T= 444 s

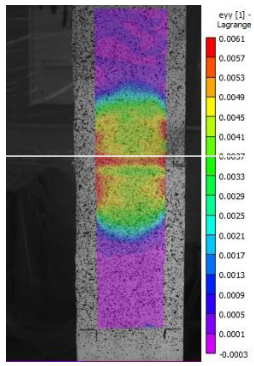

(e) ε_{yy} Dist. at T= 447 s

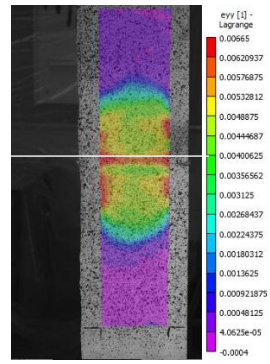

(e) ε_{yy} Dist. at T= 447 s

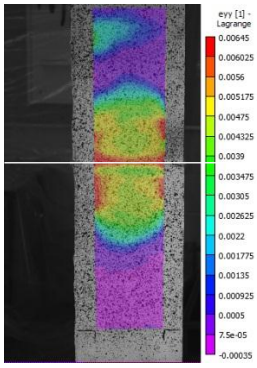

(g) ε_{yy} Dist. at T= 477 s

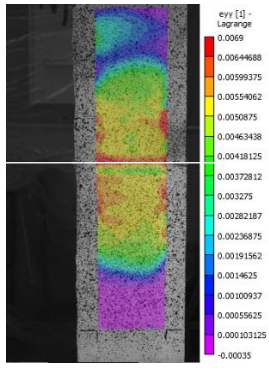

(h) ε_{yy} Dist. at T= 541 s

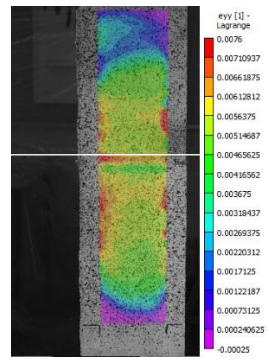

(i) ε_{yy} Dist. at T= 606 s

Figure 4.14: Strain Fields Showing distribution of longitudinal Strains (ε_{yy}) on FRP Sheet at Different Times as Test Progressed to Failure for Specimen L240-S-4

The longitudinal strain contour diagram with 8 strain gauge locations positioned at quarter and half the width of the FRP sheet are shown in Figure 4.15. Unlike specimen L160-S-4, gauges at the middle recorded higher strain values except for gauge (g5) which recorded higher values than (g1). Strain values at gauge locations (g4) and (g8) only started to increase just when the specimen was about to reach failure due to the instantaneous redistribution of stresses.

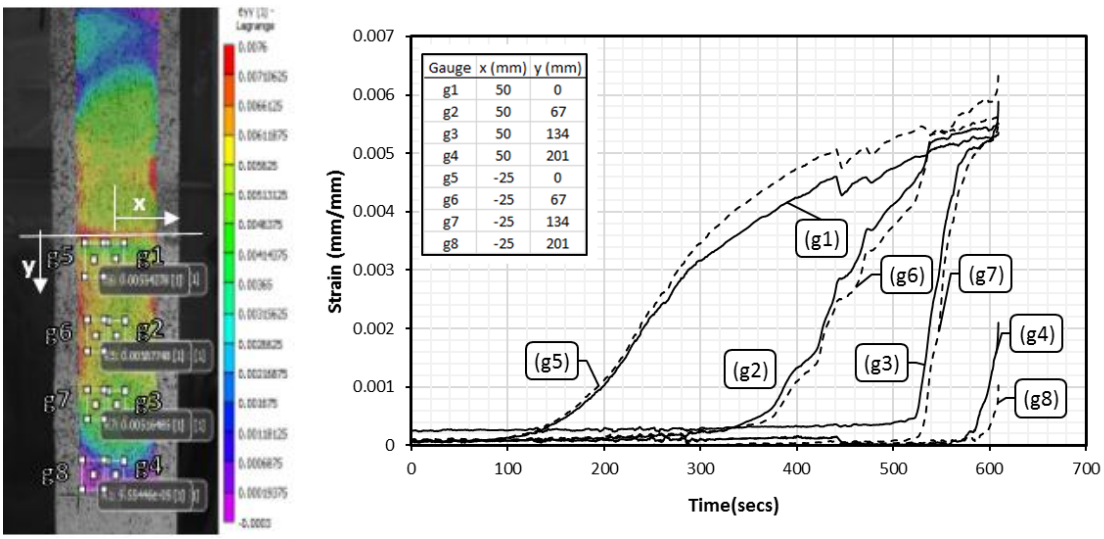

(a) **(b)**

Figure 4.15:(a) Contour Diagram showing 8 Gauge Locations (b) Strain versus Time Curves of Specimen at Locations of Gauges as Indicated in the Contour Diagram in 4.15(a)

The force versus strain curves for gauges g1, g2, g3 and g4 are shown in Figure 4.16. Similar results were observed in this specimen when compared to specimen L160-S-4. The relationship between these two variables as seen in the graph is bi-linear.

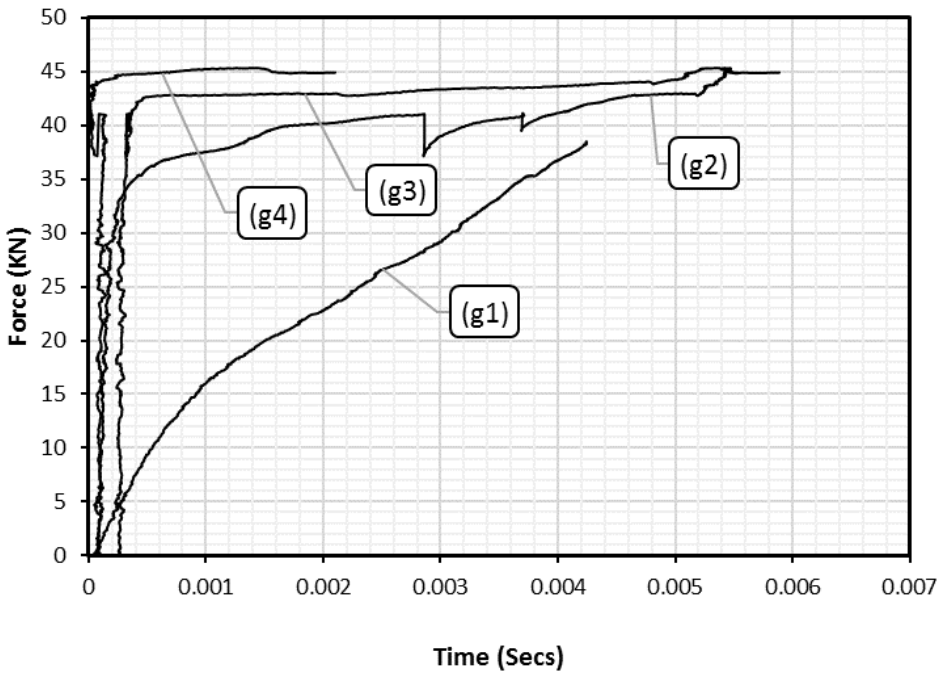

Figure 4.16: Force versus Strain Curves for Strain Gauge Locations g1, g2, g3 and g4 in Figure 4.14(a) on the Specimen

4.3 Specimen L350-S-1 ($L_e = 350\ mm$)

Figure 4.17 shows the speckled images of the specimen properly installed in the machine with both sides having a bond length of 350 mm. The end of the FRP sheet at the top of specimen was anchored by wrapping a 150 mm width FRP sheet around it to prevent it from failing before the bottom end. One side was speckled while the other side had the original colour of the FRP sheet.

(a) Front of Specimen (b) Back of Specimen (c) Side of Specimen

Figure 4.17: Views of Specimen L350-S-1 Installed in the Testing Machine Prior to Testing

The test was carried out and failure was as observed in specimens L160-S-4 and L240-S-4. Figure 4.18 shows the views of the specimen after failure. Failure was by debonding of the FRP sheet as seen in Figure 4.18(e). Wedge crack failure as shown in Figure 4.18(d) was observed in this specimen but no visible tension cracks were seen on the sides of the specimen as observed in the previous tests. The back of specimen also failed by debonding as seen in Figure 4.18(f). The wedge crack that caused the progressive debonding to develop at the loaded end of the FRP sheet is similar to what was illustrated earlier in Figure 4.4

a) Front Side

b) Right Side

c) Left Side

d) Wedge Failure

e) Debonded Region

f) Back Side

Figure 4.18: Views of Specimen L350-S-1 after Failure

The force versus time graph for specimen L350-S-1 shows elastic behaviour from (a) to (b) as seen in Figure 4.19. It is observed that there was a decrease in force from (b) to (c) and then slightly from (d) to (e) due to the wedge crack that developed as the experiment proceeded. The force started to increase after stress redistribution but then dropped again from (g) to (h). The force then began to increase with time after that up until failure at (i).

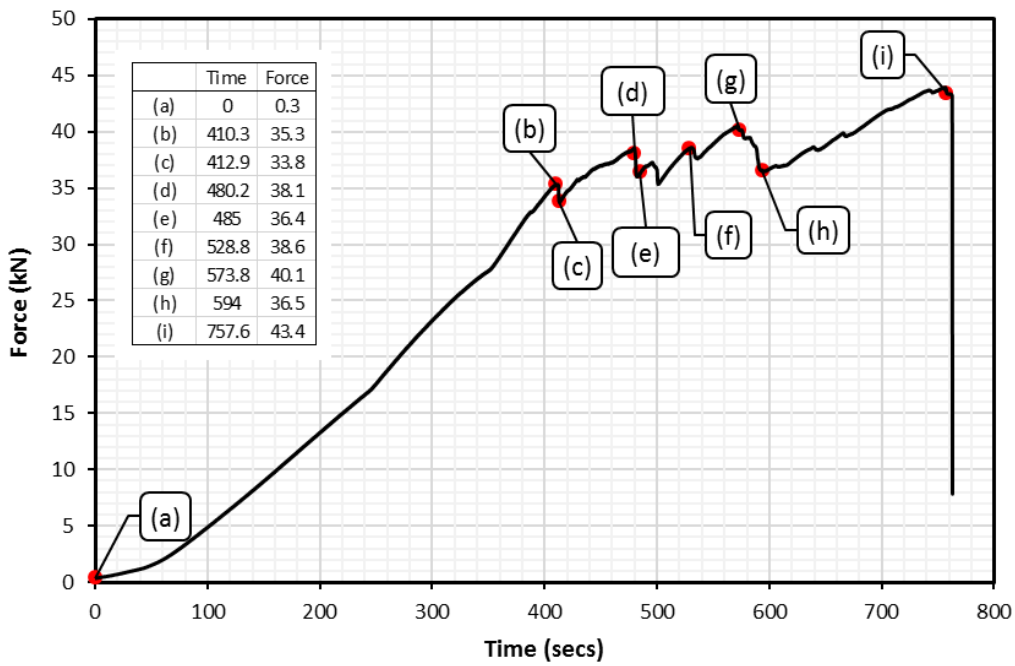

Figure 4.19: Force versus Time curve for Specimen L350-S-1 Showing Key Points During the Test

Figure 4.20 shows the contour diagram with a strain inspector line along the mid width of the FRP sheet with a corresponding strain versus time graph for key points indicated in Figure 4.19. Similar observation is noticed in this specimen compared to the other two previously analyzed specimens. As the load increased, the strain values also increased. Curves (a), (b) and (c) have the lowest strain values with linear curves. Over time, as load increased, the slope of the curve began to shift towards the unloaded end of the FRP sheet from its loaded end. A decrease in strain is observed from (g) to (h) as seen in Figure 4.19 when the force dropped significantly. A maximum strain of 0.57 percent was recorded just before failure as seen in the curve labelled (i). The active bond zone (development length) ranged from 50 to 70 mm throughout the test.

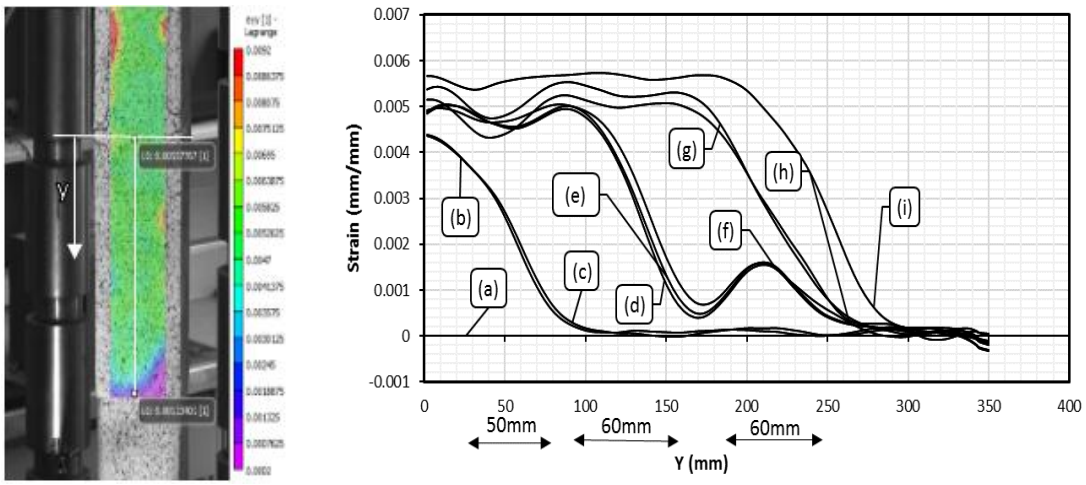

(a) **(b)**

Figure 4.20: (a) Contour Diagram Showing Position of Strain Inspector Line along the Bond Length of FRP Sheet (b) Strain versus Distance along the Bond Length of the FRP Sheet at Times shown in Figure 4.19 for Specimen L350-S-1

Figure 4.21 shows contour diagrams at times indicated in Figure 4.19. It can be observed that the maximum strain was at the loaded end of the FRP sheet. There was a gradual increase in strain as seen in pictures 4.21(a) to 4.21(f). Although not very evident, at 4.21(g), the strain dropped slightly due to the wedge crack at the loaded end of the FRP sheet and then gradually increased from (h) to (i). Shear lag and the effect of load eccentricity on the FRP sheet was also observed in the contour diagrams as higher strains are observed on the left half of the FRP sheet compared to the strains on the right side.

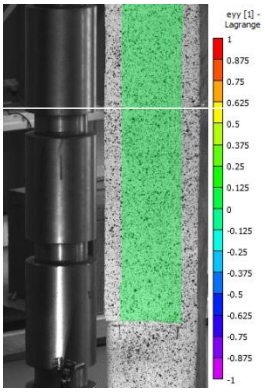

(a) ε_{yy} Dist. at T= 0 s

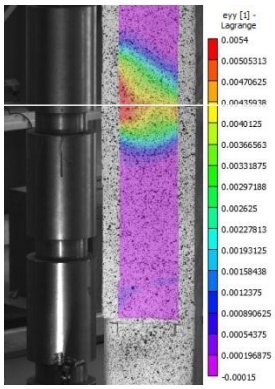

(b) ε_{yy} Dist. at T= 410 s

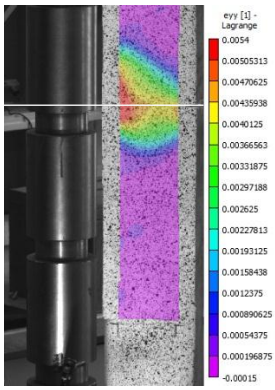

(c) ε_{yy} Dist. at T= 412 s

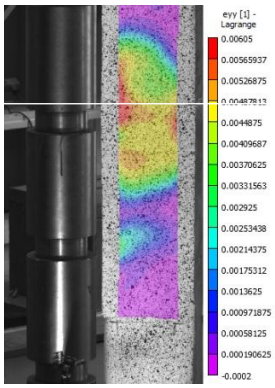

(d) ε_{yy} Dist. at T= 480 s

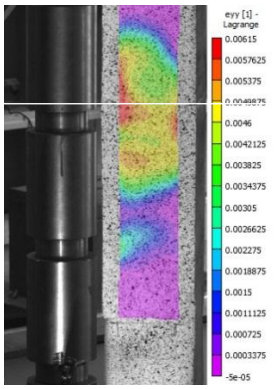

(e) ε_{yy} Dist. at T= 485 s

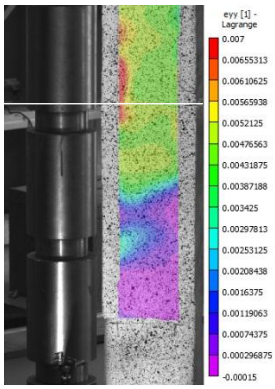

(f) ε_{yy} Dist. at T= 529 s

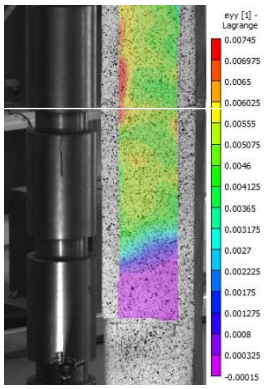

(g) ε_{yy} Dist. at T= 574 s

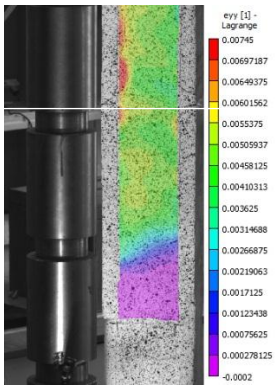

(h) ε_{yy} Dist. at T= 594 s

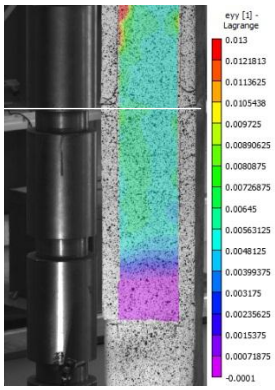

(i) ε_{yy} Dist. at T= 758 s

Figure 4.21: Strain Fields Showing Distribution of Longitudinal Strains (ε_{yy}) on FRP Sheet at Different Times as Test Progressed to Failure for Specimen L350-S-1

Eight strain gauges were positioned as shown in Figure 4.22. Gauges located at quarter the width of the FRP sheet recorded slightly higher strain values because of shear lag and load eccentricity effect on the FRP sheet. The strain values at locations (g2), (g6), (g3) and (g7) did not start to increase until after the first drop in force while the strains at locations (g8) and (g4) only started to increase just when the FRP sheet was about to fail by debonding. It is observed that at (g7) and (g3) there was a local strain anomaly that caused the strain values at those locations to be constant for some time before increasing during the test. This may have been caused by non-uniformities in the concrete at that location. This anomaly can also be observed in the contour diagrams in Figure 4.21.

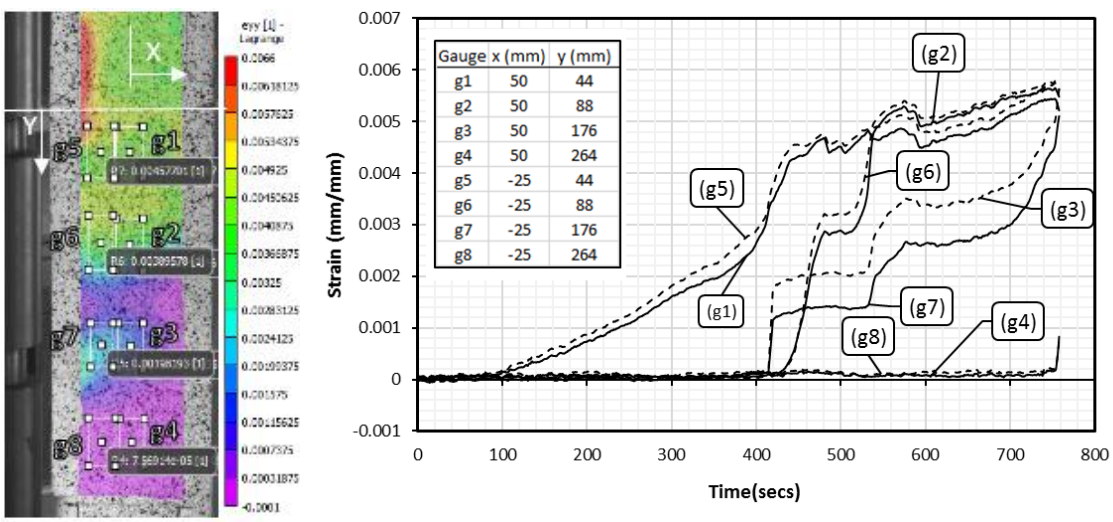

(a) **(b)**

Figure 4.22: (a) Contour Diagram Showing Position of 8 Gauges (b) Strain versus Time Curves of Specimen at Locations of Gauges as Indicated in the Contour Diagram in (a) for Specimen L350-S-1

The force versus strain curves for gauges g1, g2, g3 and g4 are shown in Figure 4.23. Similar results were observed in this specimen when compared to specimens L160-S-4 and L240-S-4. The relation between these two variables as seen in the graph is bi-linear.

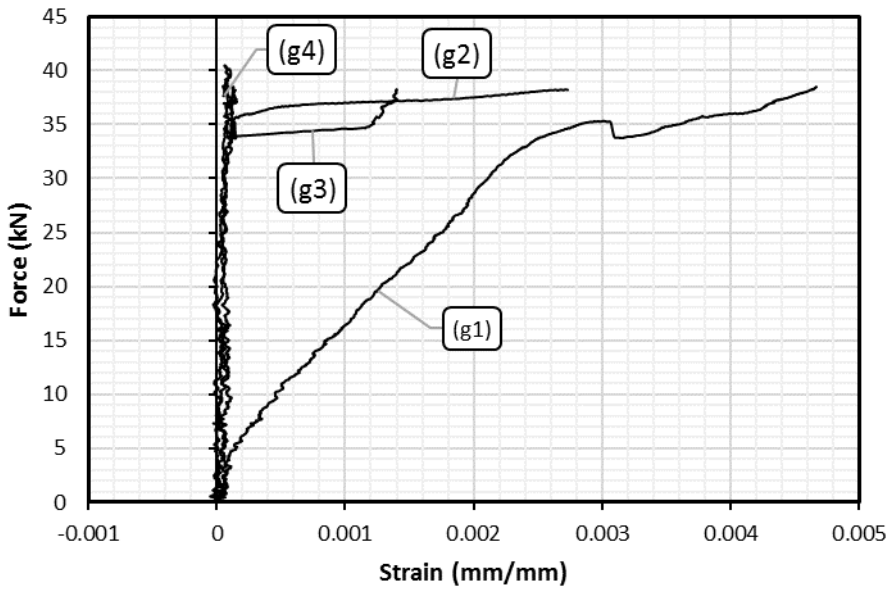

Figure 4.23: Force versus Strain Curves for Strain Gauges g1, g2, g3 and g4 in Figure 4.22(a) for Specimen L350-S-1

4.4 Summary of Experimental Results

Table 4.2 provides a summary of the ultimate loads, longitudinal strains and effective (development) length at ultimate load for all the twelve specimens tested in this program. The development length of the FRP sheet was theoretically calculated using Equation 3.1 as provided in this document. The theoretical calculation gave the development length of the FRP sheet to be 57 mm. Results obtained from the experimental results were similar to what was obtained theoretically thereby validating the experimental test set-up and instrumentation used in this research. From the ultimate load values obtained, it is observed

that there is no significant increase in load when the bond length was increased from the statistical analysis carried out. Load increased by 12 percent when bond length was increased from 160 mm to 240 mm but decreased by 7 percent when the FRP bond length was increased to 350 mm. Further work needs to be carried out to determine why the failure load decreased when bond length was increased from 240 mm to 350 mm. A similar trend was observed for the longitudinal strain values obtained from the tests.

Table 4.2: Results of Ultimate Load with their corresponding Strain and Development Length

Identification of Specimen	Loading Rate (mm/min)	DIC Time Interval (s)	P_u (N)			Longitudinal Strain (%)			Effective Bond Length (mm)		
			Individual	Average	Variance	Individual	Average	Variance	Individual	Average	Variance
L160-S-1	0.5	0.5	39104	38667	4.7	0.52	0.54	0.0062	50.0	50.0	66.7
L160-S-2		0.4	36690			0.64			60.0		
L160-S-3			37324			0.55			50.0		
L160-S-4			41548			0.45			40.0		
L240-S-1	0.5	0.4	48792	43382	20.9	0.70	0.64	0.0029	70.0	55	100
L240-S-2			38547			0.65			50.0		
L240-S-3			40874			0.65			50.0		
L240-S-4			45315			0.57			50.0		
L350-S-1	0.5	0.4	43967	40111	21.9	0.57	0.57	0.0023	60.0	57.5	25.0
L350-S-2			38528			0.54			60.0		
L350-S-3			34195			0.52			50.0		
L350-S-4			43755			0.63			60.0		

Based on what was observed from the test results, it can be concluded that all specimens failed due to progressive debonding which was caused by the initiation of a wedge crack at the loaded end of the FRP sheet. A shear lag effect on the FRP sheet was observed in most of the specimens as the distribution of stresses along the width gave a curve or parabolic shape. This may be due to the FRP sheet being stressed more at its middle because of the transfer of stresses by the reinforcing bar at the middle of the specimen. Load eccentricity on the FRP sheet caused by an asymmetry in the strain fields was also observed in some of the specimens.

5.0 Experimental Study on Effective Bond Length and Bond Behaviour of CFRP Sheets Externally Bonded to Concrete

Abstract

Fiber reinforced polymer (FRP) sheets have become widely used in retrofitting existing reinforced concrete (RC) structures because of their high strength and stiffness-to-weight ratio. An important aspect in the design of this composite element is determining the bond behaviour between the reinforced concrete and the FRP sheet. Previous studies have involved the use of conventional instrumentation (typically strain gauges) that provide limited data to work with. This paper presents an experimental investigation to determine the effect of bond length on the bond behaviour of FRP sheet-to-concrete interface under static loads using a digital image correlation (DIC) technique. Twelve double lap shear specimens bonded with carbon fiber reinforced polymer (CFRP) sheets were tested with varying bond lengths at the same loading rate. Development length, longitudinal strains and corresponding bond stress and slip relationships were obtained and compared with values computed from existing models. Comprehensive and well detailed results were obtained from the DIC technique which allowed for proper monitoring of the progression of failure and the effect of shear lag on the distribution of stresses in the FRP sheet.

5.1 Introduction

The use of FRP sheets in recent times has gradually replaced the application of steel plates in the rehabilitation and strengthening of reinforced concrete (RC) structures (Huo et al., 2016). The use of this material in improving RC structures tends to increase the service life and subsequently reduce the frequency of demolition and reconstruction of RC structures (Shen et al., 2015). FRP is made up of strands of fibers which can be carbon, glass, aramid

or basalt bonded together by a polymer matrix which is usually an epoxy resin. The composite materials formed from the combination of these fibers and epoxy are called carbon fiber reinforced polymer (CFRP), glass fiber reinforced polymer (GFRP), aramid fiber reinforced polymer (AFRP) and basalt fiber reinforced polymer (BFRP) respectively (Goldston et al.,2016). Although brittle when saturated, FRP sheets are used in rehabilitation because they are not expensive to install and maintain, and have a high strength-to-weight ratio and are corrosion resistant. (Meier, 1997, Maalej and Leong, 2005).

The most common method of failure for FRP in tension bonded to concrete is debonding which is caused by high stress concentrations at the interface between the FRP and the concrete substrate. It is therefore important to consider the bond interface when studying the debonding failure of these kinds of structures (Shen et al., 2015 and Karbhari et al 2006). Debonding occurs prematurely before the ultimate capacity of the FRP sheet is fully utilized. Hence, the need to understand the bond behaviour and properly design the FRP-to-concrete composite member to improve its bond strength. The type of loading on the structure including certain characteristics of the FRP sheet and concrete substrate affect the bond capacity of the structure's interface (Shadravan, 2009). The thickness, stiffness, bond length of FRP sheet, and other mechanical and physical properties of the FRP sheet as well as the concrete substrate material properties such as tensile strength and elastic modulus also affect the bond behaviour of the retrofitted element (Shen et al., 2015 and Shadravan et al., 2009).

Although, a significant amount of research has been carried out on determining the bond behaviour of FRP sheets externally bonded to reinforced concrete subjected to static load

(with various analytical models being formed based on research results), there is still a need to revisit this research area. This is because varying test setups and specimen parameters have been employed in the experimental and analytical programs which in turn have yielded discrepancies in the experimental results and analytical models so far developed. Many of these models were developed based on data constrained from experiments due to the instruments available for testing. Specifically, strain gauges used in strain measurement only give the strain values for specific areas where the strain gauges are installed. It is therefore imperative that an extensive experimental research be carried out using an appropriate test method and instrumentation technology to determine the much-needed data that gives the bond properties at every point along the length of the FRP sheet. An experimental program for determining the bond behaviour of CFRP sheets using the double lap pull-out test method is the focus of this study. A digital image correlation (DIC) technique was used to determine the strain values along the length of the CFRP sheet to get accurate values at every point of the specimen.

5.2 Background

Interfacial shear stresses at the bond interface between the FRP sheet and the concrete substrate facilitate the transfer of forces induced in the FRP sheet to the concrete. This transfer of forces is possible over a small length along the FRP sheet near the applied load and is called the effective bond length (Huo et al., 2016, Shen et al., 2015, Li et al.,2015). The effective bond length, also known as development length, is the length beyond which an increase in the length of the FRP sheet will cause no further increase in the load resistance of the structure (Bizindavyi and Neale, 1999, Shadravan,2009). The effective bond length is an important parameter when studying the bond behaviour and load capacity

of FRP sheets. Hence, most bond strength models are developed based on the concept of an effective bond length (Shen et al.,2015) even though bond stress, ultimate bond force and bond-slip models are also considered (Lu et al., 2007).

Past experimental work and subsequent effective bond length equations, stress models, and bond-slip relationships suggested by researchers (Maeda et al., 1997, 1997, Oehlers, 1992) have been contested and modified in recent studies (Wu and Niu, 2000, Shi et al.,2015, Shen et al., 2015, Lu et al., 2004, Smith and Teng, 2001). Earlier models focused on the main variables (modulus and thickness of the FRP sheet) affecting the effective bond length of FRP sheets as being inversely proportional to the bond length, while the more recent models use these variables as multipliers in the numerator indicating that they are directly proportional to the effective bond length. Other expressions from recent work show the effective bond length being dependent on both the concrete and FRP sheet properties such as compressive and tensile strength, bond stress, concrete elastic modulus and rupture energy (Shadravan, 2009).

The Canadian Standard for the Design and Construction of Structures with FRPs (CSA S806-12) still adopt the equations suggested by Maeda et al. (1997). Since these equations are being contested in recent times (Smith and Teng, 2001, Lu et al., 2004) as not being adequate, there is therefore a need to conduct more studies to investigate the bond behaviour of FRP sheet bonded to concrete considering as many properties of the FRP sheet and concrete substrate as possible in determining the effective length, bond stress and bond-slip relationship.

5.3 Experimental Program

An experimental study was designed and carried out to determine the bond behaviour of externally bonded CFRP sheets on reinforced concrete. Details of the test specimens, test set up, test procedure, instrumentation and data acquisition procedure are presented in this section of the paper.

5.3.1 Test Program

The double lap pull-out shear test was used to test the specimens in this study. A modified test procedure was used based on the method recommended in Annex N of the CSA S806 (2012) standard. Table 5.1 summarizes the experimental program with details of the bond length, concrete strength, and number of layers. Specimens not cut off at the longer end are also indicated in the table.

Table 5.1: Summary of Experimental Program

Identification of Specimen	Bond Length (L) (mm)	L/L_e **	Concrete Strength (MPa)	DIC Image Time Interval (s)	Number of CFRP Layers
L160-S-1*				0.5	
L160-S-2*					
L160-S-3*	160	2.8	34.3	0.4	1
L160-S-4					
L240-S-1*					
L240-S-2					
L240-S-3	240	4.2	34.3	0.4	1
L240-S-4					
L350-S-1					
L350-S-2					
L350-S-3	350	6.2	34.3	0.4	1
L350-S-4					

**L_e is the calculated development length
* Specimens with FRP sheets not cut off at the anchorage face

Figure 5.1 shows a schematic diagram of the test specimen. Each specimen consisted of two prisms of length 500 mm and 150 mm by 150 mm in cross-section. The prisms each had a 20M (300 mm^2 area) steel reinforcing bar embedded in the middle for tension application. The bar protrudes on one end of each prism, so it can later be used to grip the specimen during the test. The gap between the two prisms was set to approximately 3 mm and was maintained during the CFRP sheet installation by using a plaster material (durabond, Rona, 2017) after plastic was placed in between the prisms to eliminate any form of bond connection between the end surfaces. Initially, for all the specimens, one side of the specimen was bonded along its full length with a CFRP sheet 1000 mm long to serve as an anchorage during the test. On the opposite side of the specimen, the full length of one prism was covered with a CFRP sheet while the other prism had varying bond lengths of 160 mm, 240 mm and 350 mm. The width of the FRP sheets were 100 mm for all the specimens. The specimens that had the longest CFRP bond length (350 mm) was further anchored at one end by wrapping a 150 mm width of CFRP sheet around the cross-section to prevent debonding failure from taking place at that end. The specimens were prepared in this manner so that failure was most likely to occur on the side that had the shorter bond length which would be the focus of the study. However, after testing 4 of the specimens (3 with bond lengths of 160 mm and 1 with a bond length of 240 mm), it was observed that 2 out of the 4 specimens failed on the anchored face that was not being monitored. This may have been due to stresses in the shorter FRP length being relieved after a tension crack in the concrete developed. These stresses were then transferred to the FRP laid on the opposite side until failure occurred on that side. Hence, the remaining specimens were modified by

cutting off the longer side to be the same as their corresponding bond lengths so that failure is likely to occur on either side of the test block.

A total of twelve specimens were tested in three groups with each group having the same bond length. Each specimen is identified with a label "LX-S-n" where the letter L indicates bond length, X gives the value of the bond length that changes for each group, S refers to static load, and n is the progressive test number. The FRP sheet lengths were taken as KL_e, where L_e is the development length calculated using Equation 3.1 from CSA S806 (2012. The CSA S806 (2012) standard also specifies that K may be taken in increments of 0.2 from 0.6 to 1.6. However, in this study, K was taken as 2.8, 4.2 and 6.2 to give bond lengths of 160 mm, 240 mm and 360 mm respectively. This was due to an error in the initial experimental design calculations. However, the error did not affect the purpose of the study as the value of the development length is not affected by variations in bond length.

[5.1] $$L_e = \frac{25350}{(t_f E_f)^{0.58}}$$

Where t_f and E_f are the thickness and modulus of elasticity of the FRP sheet. All the specimens were subjected to a static load rate equal to 5 mm/min.

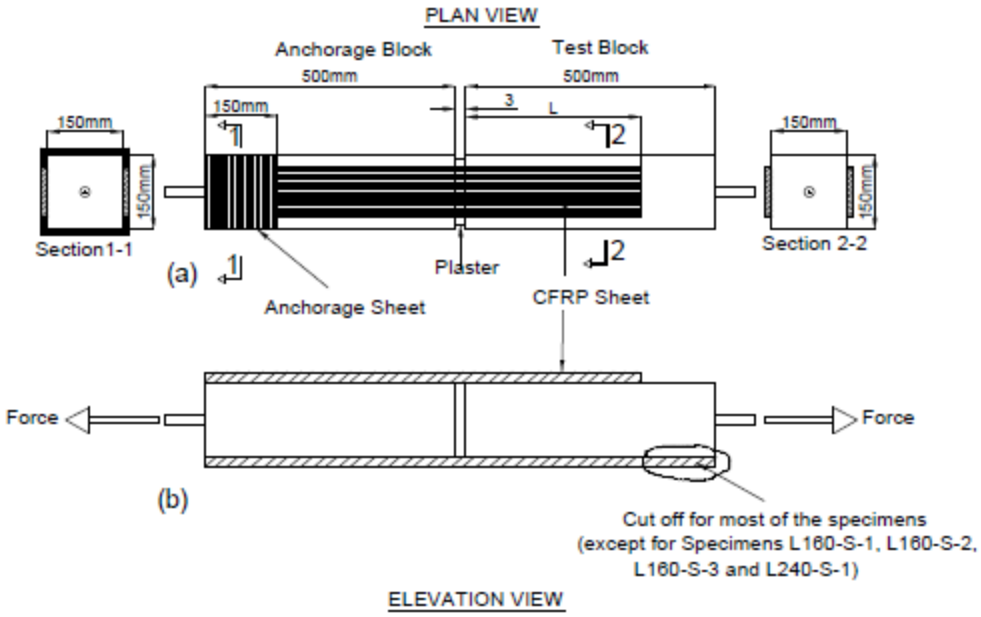

Figure 5.1: Schematic Diagram of Test Specimen (L represents the varying bond length of CFRP)

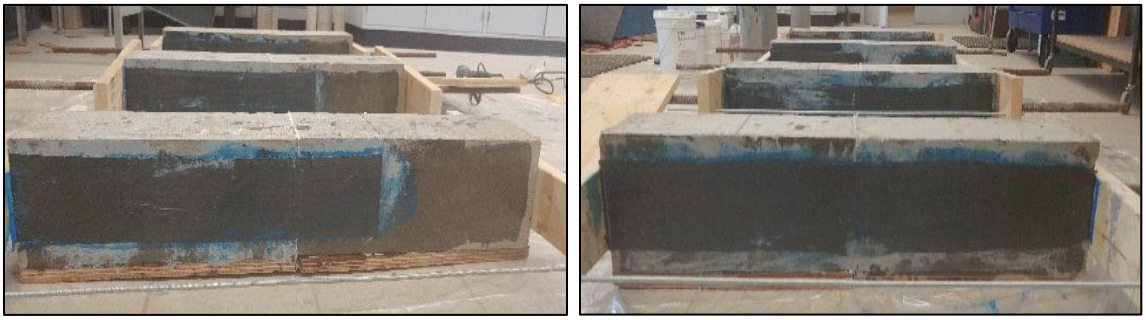

(a) Shorter Length of CFRP (b) Longer Length of CFRP

Figure 5.2: Specimens with CFRP Sheet Bonded on Opposite Sides of Concrete Prisms

5.3.2 Properties of Test Specimens

Ready mix concrete was used to cast the prisms for the experimental program. The specimens were cast in wooden molds specially constructed for this purpose. The specimens were demolded after forty-eight hours and moist cured for seven days under wet

burlap and a plastic sheet while being exposed to the laboratory's temperature. Cylinders with sizes 100 mm by 200 mm were tested and the compressive strength (f_c') of the concrete equaled 34.3 MPa at 28 days and 32.3 MPa at 279 days. The cylinders were cured under the same conditions as the concrete specimens (prisms). Five CFRP coupons of gauge length 340 mm, width 38 mm and nominal thickness of 1 mm were used to test the mechanical properties of the CFRP sheet. The coupon test was carried out according to Annex F of the CSA S806 (2012) standard. The average value of the tensile strength, elastic modulus and ultimate strain were calculated as 642 MPa, 37.8 GPa, and 1.9 percent respectively. Table 5.1 shows the summary of the properties of the specimens tested in this study.

Table 5.1: Summary of the Test Specimens

Test Specimen	Loading Rate (mm/min)	Bond Length (mm)	Number of CFRP Layers	Bond Width (mm)	Concrete Strength (Mpa)
L160-S-1 L160-S-2 L160-S-3 L160-S-4	0.5	160	1	100	34
L240-S-1 L240-S-2 L240-S-3 L240-S-4	0.5	240	1	100	34
L350-S-1 L350-S-2 L350-S-3 L350-S-4	0.5	350	1	100	34

The CFRP sheets were applied on the concrete prisms after 51 days of curing. Before the CFRP sheet was applied, the concrete surface was first thoroughly cleaned to remove grit and debris. Primer was then applied on the surface followed by the application of a putty material to fill the pores and voids on the concrete surface. The CFRP sheet was cut to its

appropriate size and then impregnated with the resin saturant before it was laid carefully on the surface of the concrete. A second coat of the resin was then applied on the CFRP sheet already installed on the concrete. No strain gauges were installed on the CFRP sheets as the strains were measured using the digital image correlation (DIC) technique which is discussed in subsequent sections.

5.3.3 Test Set-up and DIC Measurements

The specimens were tested under axial tension 87 days after the CFRP sheets were installed with a Universal Testing Machine. The test configuration is shown in Figure 5.3(a). The specimen was held in place using couplers at the top and bottom of the machine cross heads. All the double lap shear specimens tested in this program were loaded in tension at a displacement rate of 0.5 mm/min up to failure. The applied tension load was recorded by a data acquisition system at a time interval of 0.1 second.

Prior to the installation of the specimens on the machine, the side of the specimen that would be monitored was painted with black speckles on a white background to enable strain measurements using the DIC technique. The DIC software uses a digital image-based technique to analyze data. Images of the specimen are captured as the experiment proceeds at specified intervals and are subsequently compared to an initial reference image of the specimen taken before the commencement of the test. In this experimental program, images were taken every 0.4 seconds except for the first specimen (specimen L160-S-1) whose images were taken every 0.5 seconds. The difference, measured in pixels, between each patch of the reference image and the target image is the displacement vector that is used to compute the strain of the specimen using mathematical correlation algorithms between images (Bibsy et al., 2007, Dutton, 2012, Zhu et al., 2014). The cameras as shown in Figure

5.3(b) were fixed on a tripod in front of the specimen at a distance that ensured the specimen filled the field of view with the area of interest (AOI) being visible in both cameras. The AOI is the area covered by the CFRP sheet with the bond length being monitored. VIC 3D (Correlated Solutions, 2010), a type of DIC software, was used to measure and analyze the strain fields on the CFRP sheet.

1. **(b)**

Figure 5.3: (a) Specimen Installed on the Universal Testing Machine (b) Cameras Installed on Tripods and Positioned at an Appropriate Distance

5.4 Test Results and Analysis Procedures

A typical failure mode of the FRP-to-concrete bonded specimen is illustrated in Figure 5.4. All specimens experienced a brittle failure accompanied by a loud noise. Failure was by debonding with part of the concrete cover being removed and no rupture of the FRP sheet indicating a good bond. Concrete wedge cracks (tension cracks that relieved stress at the

critical end of the FRP sheet) at the loaded end were observed in all the specimens. It was also observed that tension cracks developed on the left and right side of all specimens at the unloaded end of the bonded FRP sheet region. Tension cracks at the unloaded end of the FRP bond length was not observed on the specimens with bond length of 350 mm. A better illustration of the crack patterns observed and the location of the loaded and unloaded ends on the specimens are shown in Figure 5.5.

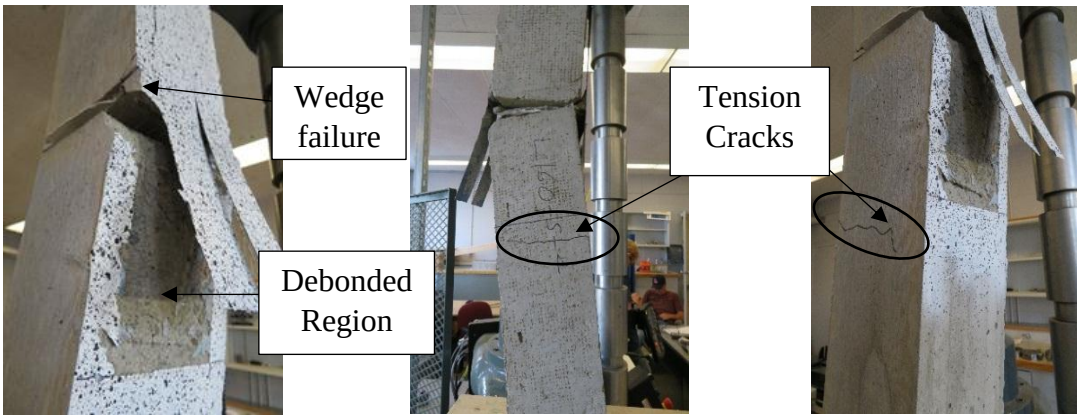

a) Front Face b) Left Face c) Right Face

Figure 5.4: Typical Failure Modes of the FRP Sheets

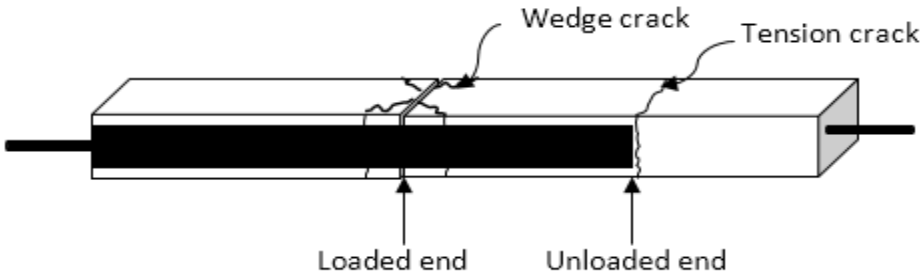

Figure 5.5: Close-up View of the Crack Patterns after Specimens Failure

Numerical data obtained from the universal testing machine and the DIC software were analyzed and presented using graphs and contour diagrams. To analyze image data using

the VIC 3D software, the area of interest (AOI) to be analyzed was specified as seen in Figure 5.6(a) using the mask tools of appropriate shape as provided in the software. After the appropriate subset and step size were selected, the analyses were run to compute the strain values on the FRP sheet in the AOI indicated.

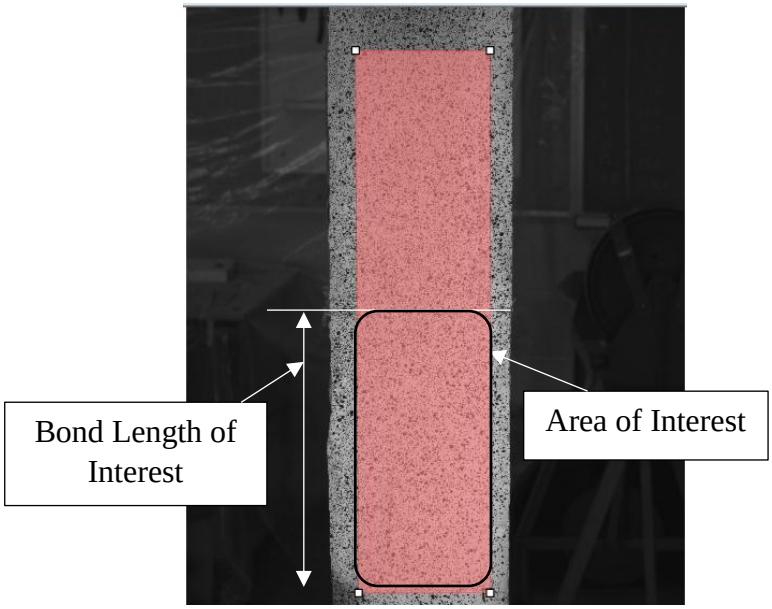

Figure 5.6: Specified Area of Interest on FRP Sheet using the Rectangular Mask Tool

Figure 5.7 shows the experimental load versus time graphs of three specimens each of different bond lengths (160, 240 and 350 mm respectively). This figure shows different points indicating significant occurrences at varying times. Points (a), (b) and (c) on Figure 5.7(a) correspond to the elastic behaviour of specimen L160-S-4. At point (d), there was a drop in force to point (e) due to the development of the concrete wedge crack at the loaded end of the FRP sheet. Point (f) is a random position between the time when the minimum and maximum loads occurred. The wedge crack initiated debonding and then subsequent redistribution of stresses after which there was an increase in load up to point (g). There

was a decrease in force to point (h) which is as a result of the tension cracks that surfaced on the sides of the concrete prism. The load then increased to (i) after the redistribution of stresses until the sudden failure of the FRP-to-concrete bond. The specimen attained an ultimate load of 41.5 kN.

Specimens L240-S-4 and L350-S-1 showed behaviour similar to specimen L160-S-4. Both specimens had an elastic phase until the wedge crack developed, causing a decrease in load and then a subsequent increase after the redistribution of stresses. Wedge and tension cracks were observed in the L240-S-4 specimen with force values dropping and subsequently increasing after stress redistribution to a maximum of 45 kN before failure. Specimen L350-S-1 behaved slightly different from the other two in that, there were no tension cracks developed on the side faces of the concrete prism. Even though there were no tension cracks observed, load values fluctuated until it reached the maximum (43.4 kN) before failure.

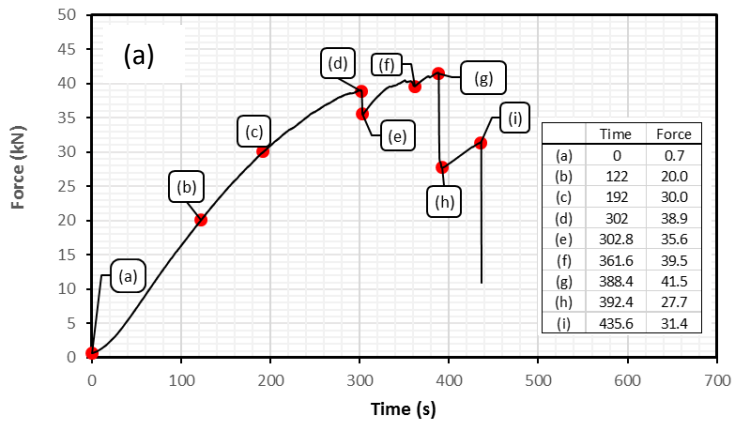

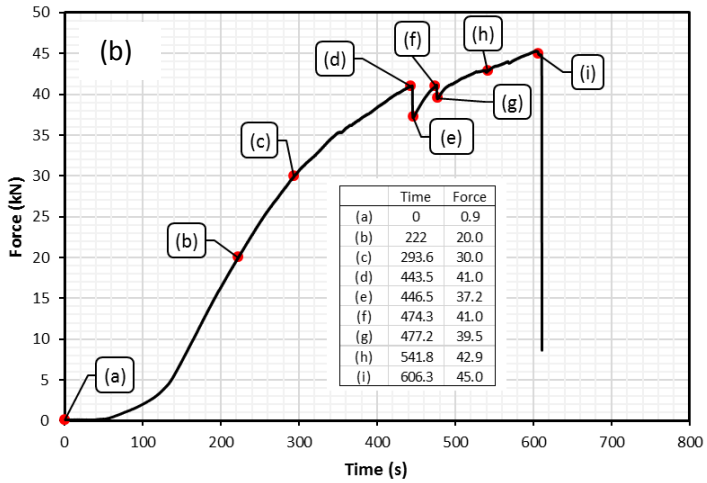

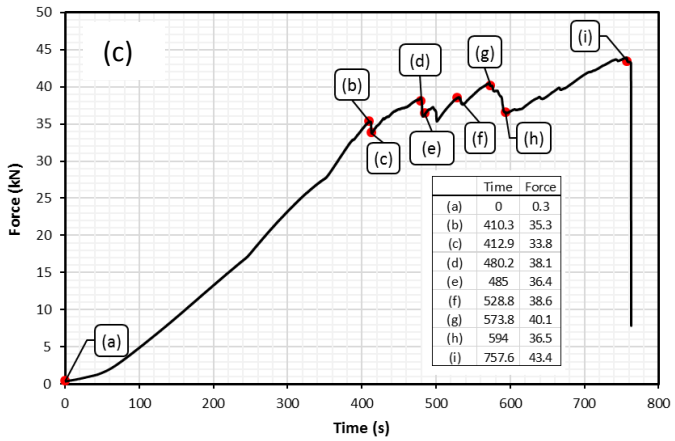

Figure 5.7: Force versus Time curve for Specimens (a) L160-S-4 (b) L240-S-4 (c) L350-S-1

Figure 5.8 shows the typical longitudinal contour strain fields for specimen L160-S-4 obtained from the DIC analysis. The load stages of Figure 5.8(a) to (d) are key points listed in the load-time curve as shown in Figure 5.7(a). The elastic behaviour of the specimen can be seen in Figures 5.8(a), 5.8(b), 5.8(c) and 5.8(d) as the strain gradually increased with time. After the wedge crack, there was a slight decrease in strain as seen in Figure 5.8(e) which then increased as seen in Figure 5.8 (f). There was however a subsequent decrease in strain from (f) to (g) as seen in the contour diagrams (Figure 5.8(f) and Figure 5.8(g)).

From the contour diagrams, the strain distribution gives a curve or parabolic shape along the FRP width that gradually propagates towards the unloaded end of the FRP sheet as the load increased. The uneven distribution of stresses across the width of the specimen is known as the shear lag effect. Strain gradually propagates towards the unloaded end of the FRP sheet indicating the propagation of debonding. It is also observed from the contour diagrams that there is an asymmetry in the strain fields which may be due to force being transferred from the machine to the specimen at an eccentricity. Force being transferred at an eccentricity may be caused by not placing the specimen at the exact center of the machine during installation or not placing the FRP sheet to align accurately with the center of the concrete prism during the preparation of the specimen.

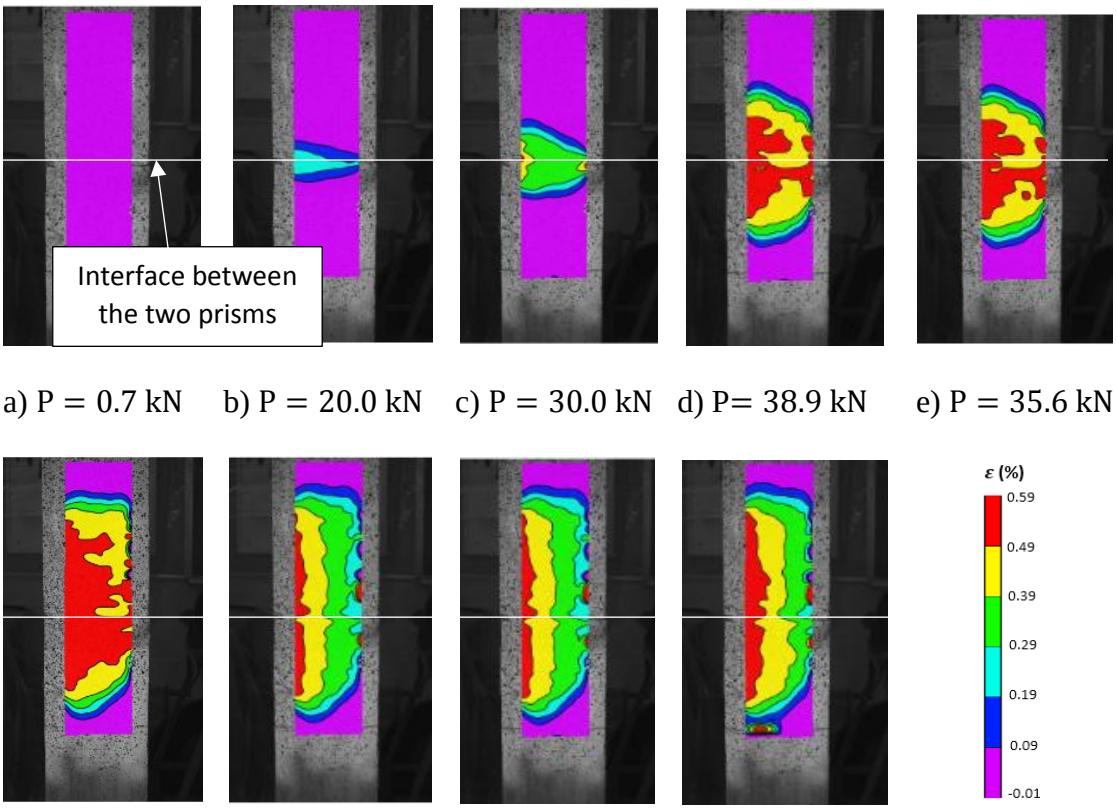

a) P = 0.7 kN b) P = 20.0 kN c) P = 30.0 kN d) P= 38.9 kN e) P = 35.6 kN

f) P = 39.5 kN g) P = 41.5 kN h) P = 27.7 kN i) P = 31.4 kN Scale

Figure 5.8: Strain Fields Showing Distribution of Longitudinal Strains on the FRP Sheet at Different Times as Test Progressed to Failure for Specimen L160-S-4

Figure 5.9 shows the contour diagrams with a strain inspector line along the middle of the FRP sheet and their corresponding graph of longitudinal strain versus distance along the length of the FRP sheet. Each curve represents strain values at key times as indicated in Figure 5.7. As seen in all three graphs, as the load increased, the curve began to shift upwards indicating an increase in strain over time. For specimen L160-S-4, curves (a), (b) and (c) have the lowest strain values and are of linear slope. The flat segment of the curves indicates the initiation of wedge cracks and subsequent debonding at the critical section (loaded end) and in some specimens, at the unloaded end of the FRP sheet. The elastic, linear region of the curves is known as the active bond zone which indicates the part of

CFRP sheet still bonded to the concrete surface where the majority of the interfacial stresses are transferred from the CFRP to the concrete. This zone is the effective bond length beyond which there is no further increase in the load the FRP sheet can carry. The maximum strain and effective bond length for specimens L160-S-4, L240-S-4 and L350-S-1 at ultimate load are 0.45% and 50mm, 0.57% and 50 mm and 0.57% and 60 mm respectively.

Table 5.2 shows details of the ultimate load, maximum strain and effective bond length values of all the specimens tested in this program. Results were analyzed statistically using the Analysis of Variance (ANOVA) tool. It is observed that the maximum load increased by 12 % as the bond length of the FRP sheet increased to L240-S but decreased slightly by 7 % when the bond length was increased to L350-S indicating no further increase in the maximum load even though the bond length of the specimen was increased. The same trend was also observed in the strain values recorded. The theoretical development length (57 mm) obtained from Equation 5.1 as specified in the Canadian CSA S806 (2012) standard also correlated with that obtained from the experimental results.

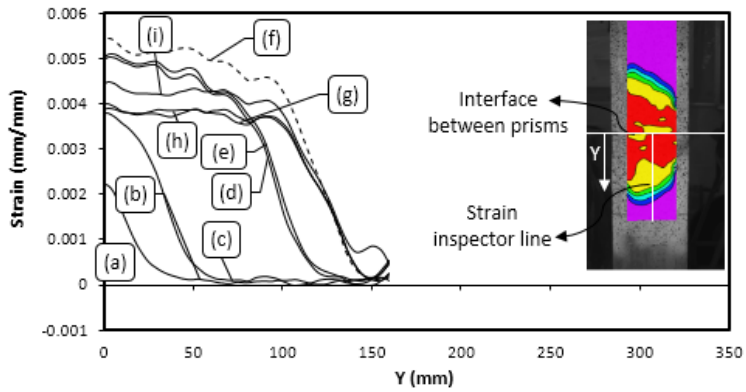

(a) Specimen L160-S-4

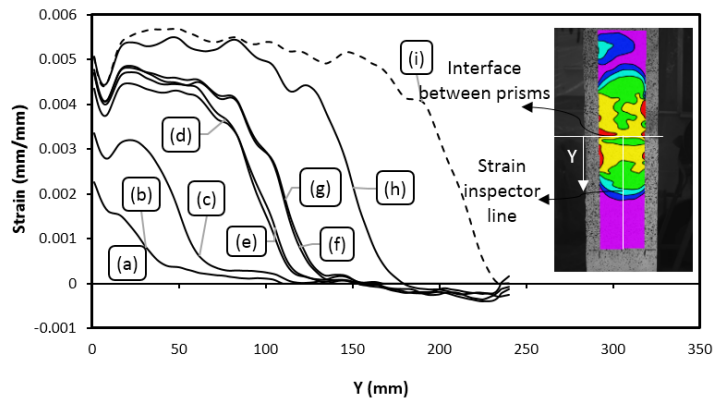

(b) Specimen L240-S-4

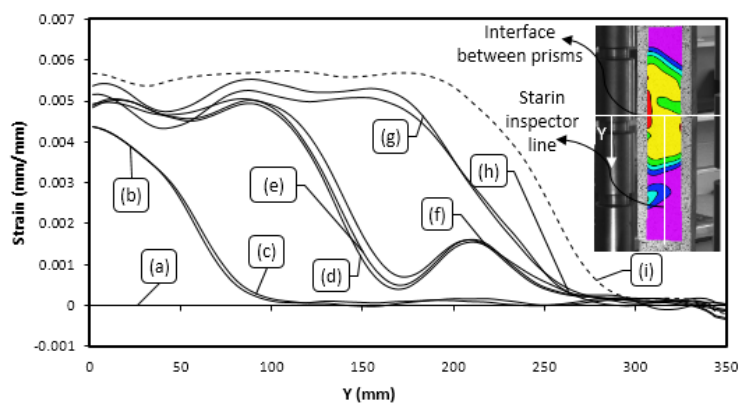

(c) Specimen L350-S-1

Figure 5.9: Strain versus Distance away from the Loaded end of FRP Sheet at Times Indicated in Figure 5.7 with Contour Diagram Showing Position of Strain Inspector Line along the Bond Length of FRP Sheet

Table 5.2: Results of Ultimate Load with Corresponding Strain and Development Length

Identification of Specimen	P (kN)			Longitudinal Strain (%)			Effective Bond Length (mm)		
	Ind.	Avg.	Var.	Ind.	Avg.	Var.	Ind.	Avg.	Var.
L160-S-1	39.1	39.0	4.7	0.52	0.54	0.0062	50.0	50.0	66.7
L160-S-2	36.7			0.64			60.0		
L160-S-3	37.3			0.55			50.0		
L160-S-4	41.6			0.45			40.0		
L240-S-1	48.8	43.4	20.9	0.70	0.64	0.0029	70.0	55	100
L240-S-2	38.6			0.65			50.0		
L240-S-3	40.9			0.65			50.0		
L240-S-4	45.3			0.57			50.0		
L350-S-1	44.0	40.0	21.9	0.57	0.57	0.0023	60.0	57.5	25.0
L350-S-2	38.6			0.54			60.0		
L350-S-3	34.2			0.52			50.0		
L350-S-4	43.8			0.63			60.0		

*Avg. = Average values, Ind. = Individual values, Var. = Variance

Graphs of longitudinal strain against time of the three specimens are as shown in Figure 5.10. Eight virtual strain gauges positioned at quarter and half the width of the CFRP sheet with a pair aligned at approximately the same level is as presented on the contour diagram in Figure 5.9(a). The table embedded in the graph indicates the position of each gauge location on the contour diagram. From the graph, it can be established that gauges (g5), (g6), (g7) and (g8) recorded higher strain values compare to gauges (g1), (g2), (g3) and (g4) due to the shear lag and load eccentricity effect as previously discussed. It can be observed that the strain at the level where gauges (g3) and (g7) are located only started to increase after the redistribution of stresses caused by the wedge crack. There was also stress redistribution as seen in all gauges right before failure. Similar occurrences took place for specimen L240-S-4, only that gauges at the middle recorded higher strain values except for gauge (g5) recording higher strain values than (g1). Strain at point (g4) only started to

increase just before debonding failure. In specimen L350-S-1, the strains at positions (g2), (g6), (g3), and (g7) did not start to increase until after the first drop in force while the strains at points (g4) and (g8) only started to increase just when the specimen was about to fail. It is observed that at (g3) and (g7) as previously seen in the contour diagram, there was a local strain anomaly on the FRP sheet.

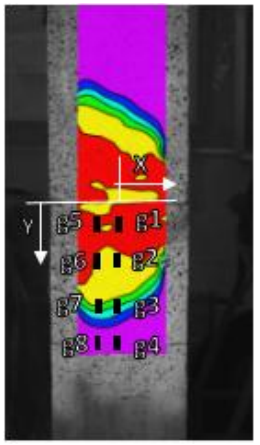

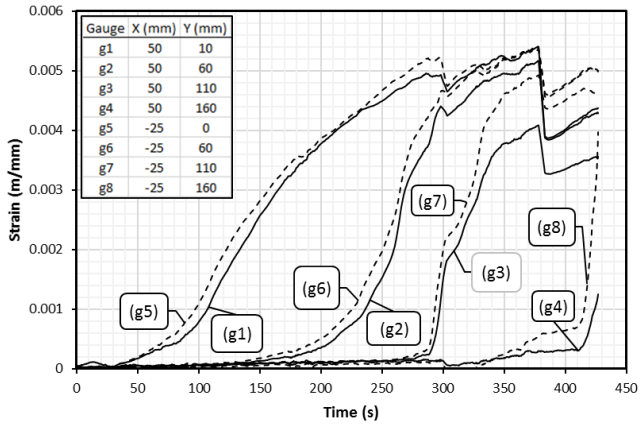

(a) (b) Specimen L160-S-4

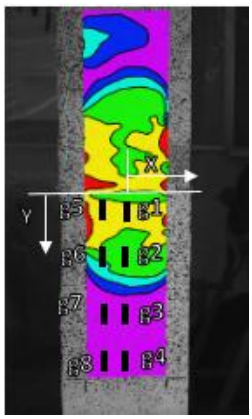

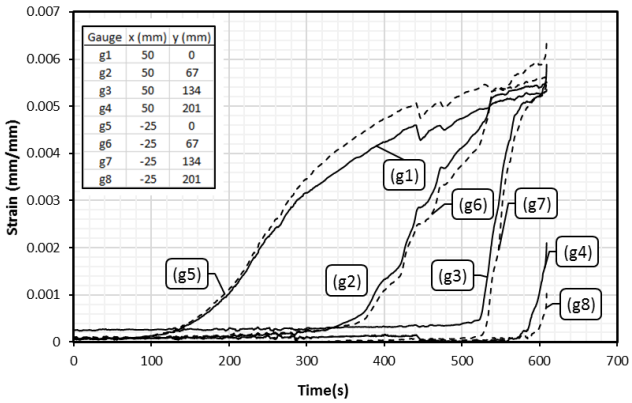

(a) (b) Specimen L240-S-4

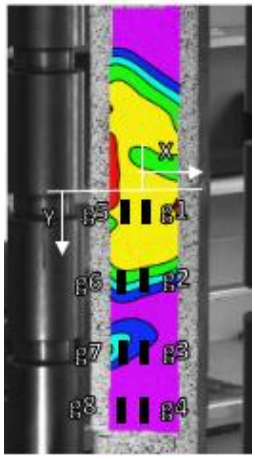

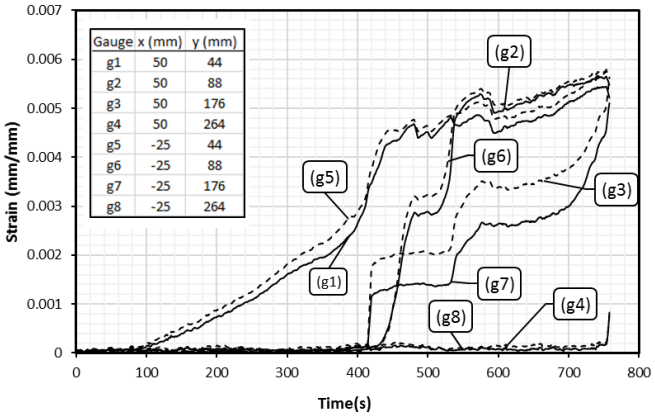

(a) (b) Specimen L350-S-1

Figure 5.10: (a) Contour Diagram Showing Position of 8 Gauge Locations (b) Strain versus Time Curves of the Specimens at Locations of Gauges Indicated in the Contour Diagram in 5.10(a)

5.5 Shear Stress Distribution along Bond Length of CFRP Sheet

Interface bond stress is computed using the relationship indicated in Equation 5.2 (Shi et al., 2015). The numerical derivative of the strain along the bond length of the FRP sheet is multiplied by the modulus of elasticity and assumed 1 mm thickness of the FRP sheet.

[5.2] $$\tau_i = E_f t_f \frac{d\varepsilon_i}{dx_i}$$

τ_i is the bond stress at a position along the bond length of FRP sheet, E_f and t_f are the elastic modulus and thickness of the FRP sheet respectively, and $d\varepsilon/_{dx}$ is the numerical derivative of the strain at each strain increment. As the load applied increased, the maximum bond stress moved along the length of the CFRP sheet away from the loaded end of the sheet. This also indicates the movement of the development length along the length of the CFRP sheet as seen in Figure 5.11.

Average bond stress between consecutive virtual gauge locations was also calculated using Equation 5.3 (Shen et al., 2015) with results compared to that obtained from Equation 5.2. The mean bond stress $\tau_{i+1/2}$ was calculated given two strain readings ε_i and ε_{i+1} at positions x_i and x_{i+1}, the elastic modulus E_f and the material thickness t_f. Positions x_i and x_{i+1} are points indicated on the tables embedded in Figure 5.10(b) for the specimens. This method has been used in the past when strain values were obtained from strain gauges positioned along the length of the FRP material (Bizindavyi and Neale, 1999, Huo et al., 2016).

[5.3] $$\tau_{i+1/2} = \frac{E_f t_f (\varepsilon_{i+1} - \varepsilon_i)}{(x_{i+1} - x_i)}$$

Figure 5.11 shows the typical bond stress distribution along the CFRP bond length based on results obtained from Equations 5.2 and 5.3. Some of the load stages of (a) to (d) as listed in Figure 5.7 are represented in the stress distribution curves. Generally, it is observed that both curves share the same variation trend in that, the maximum shear stress location moved towards the unloaded end of the specimen as the experiment progressed. The behaviour is the same as that observed from the corresponding strain profiles. The region to the right and left of the maximum bond stress indicates the region along the bond length where debonding has occurred. Y (in mm) on the graph indicates the distance away from the loaded end of the FRP sheet. Stress gradually decreases to zero towards the unloaded end indicating that the bond in that portion of the specimen cannot transfer load.

The stress values obtained from Equation 5.2 show many fluctuations in the CFRP bond stress which represents the actual conditions along the CFRP-to-concrete interface. In contrast, the stress curves obtained from Equation 5.3 are smoother and do not show fluctuations along the length of the specimen. This is because of the minimal number of longitudinal strain data points available based on the existing number of virtual strain gauges provided for the specimens as indicated in Figure 5.10(a). The stress values from the virtual strain gauges show how strain gauges could misrepresent bond stress values.

Annex N of the CSA S806 (2012) standard specifies an equation to determine the average bond stress of the FRP sheet. This expression as indicated in Equation 5.4 was also used to determine the bond stress of the specimens tested in this program.

[5.4] $$\tau = \frac{P}{WL}$$

where P, W and L are the ultimate load, width and bond length of the FRP sheet. Table 5.3 gives the results of stress values (τ_{max}) at maximum load for all three equations previously discussed.

As seen in Table 5.3, stress increased as the bond length increased from 160 to 240 mm but there was a decrease in stress due to the corresponding decrease in load when the bond length was increased to 350 mm. Comparing stress values obtained from all three methods for all specimens, it was observed that bond stress values at maximum load obtained from Equations 5.2 and 5.4 did not vary much (12.77%) but variations in values obtained from Equation 5.3 varied from Equations 5.2 and 5.4 by 69%. This therefore validates that strain gauges may not give accurate results when determining the strain distribution from which stresses are obtained along FRP sheets bonded to concrete.

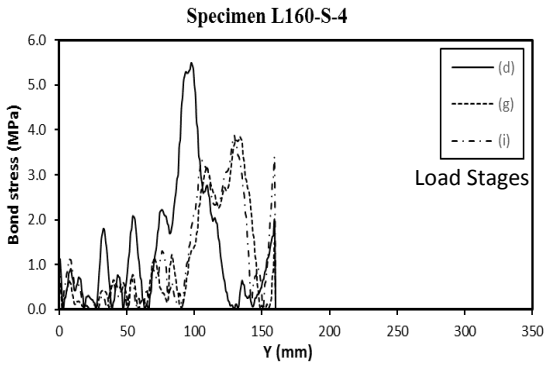

(a)

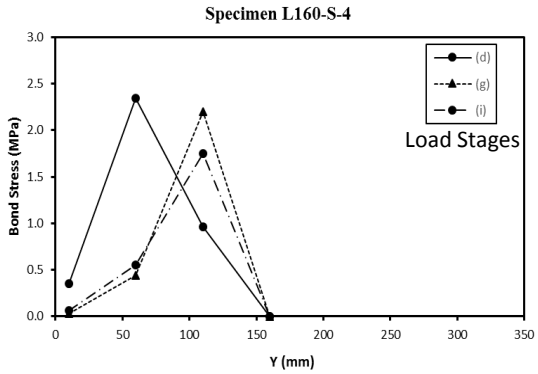

(b)

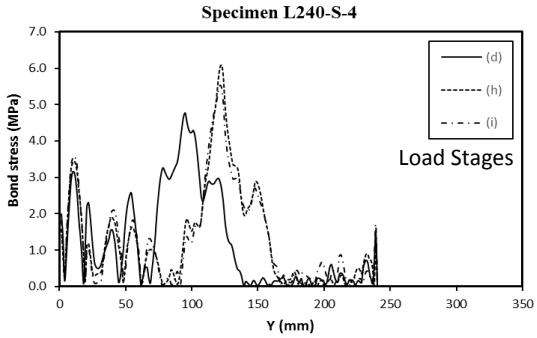

(c)

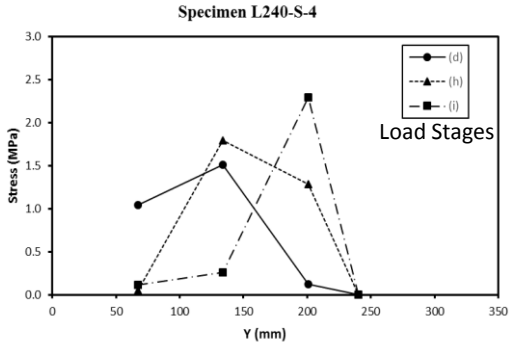

(d)

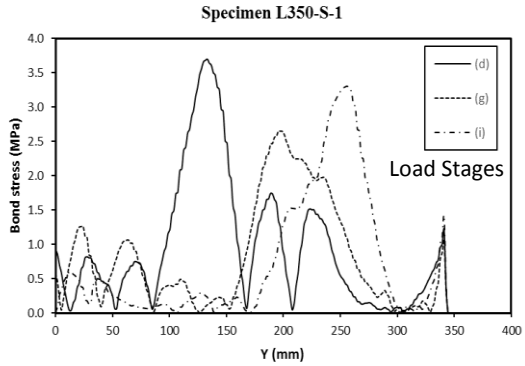

(e)

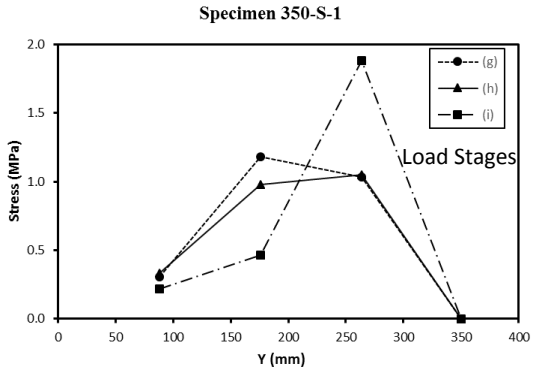

(f)

Figure 5.11: Graph of Bond Stress versus Distance away from FRP loaded End (Y): (a) Specimen L160-S-4 using Equation 5.2(b) Specimen L160-S-4 using Equation 5.3 (c) Specimen L240-S-4 using Equation 5.2 (d) Specimen L240-S-4 using Equation 5.3 (e) Specimen L350-S-1 using Equation 5.2 (f) Specimen L350-S-1 using Equation 5.3

Table 5.3: Computed Bond Stress Values at Ultimate Load

Specimen Number	$\frac{P}{WL}$ (MPa)		$E_f t_f \frac{d\varepsilon}{dx}$ (MPa)		$\frac{E_f t_f(\varepsilon_{i+1}-\varepsilon_i)}{x_{i+1}-x_i}$ (MPa)	
	Individual	Average	Individual	Average	Individual	Average
L160-S-1	7.62		5.23		2.21	
L160-S-2	8.26	7.13	10.21	6.67	2.76	2.36
L160-S-3	7.46		7.38		2.28	
L160-S-4	5.19		3.86		2.20	
L240-S-1	7.32		9.47		1.80	
L240-S-2	6.42	7.22	6.16	7.54	2.66	2.37
L240-S-3	6.81		7.58		2.71	
L240-S-4	8.31		6.96		2.29	
L350-S-1	4.71		3.30		1.88	
L350-S-2	6.42	5.79	6.17	4.20	1.03	1.56
L350-S-3	5.47		4.34		1.67	
L350-S-4	6.56		2.97		1.66	

5.6 Local Bond Stress-Slip Relationship of FRP Sheet Bonded to Concrete

Bond-slip relationship for FRP bonded to RC members is one of the important models used to determine their bond behaviour. To determine the slip along the CFRP sheet, it was assumed that the relative displacement between the FRP sheet and the concrete at the unloaded end is negligible (Guo et al., 2005). The slip is obtained by the numerical integration of the strain starting from the free end of the FRP sheet where initial slip is zero. Equation 5.5 (Guo et al., 2005, Shen et al., 2015) gives the expression for the slip used in this study.

[5.5] $$s(x_i) = s(x_{i+1}) - \frac{\Delta\varepsilon}{\Delta x} \cdot \frac{(\Delta x)^2}{2} + \varepsilon_i(x_{i+1} - x_i)$$

Where $\Delta\varepsilon/\Delta x$ is the numerical derivative of the strain at each increment, ε_i is the measured strain at a position x_i. The slip values were calculated at the different load levels indicated in Figure 5.7. Corresponding graphs of local bond stress versus slip for one specimen from

each bond length is presented in Figures 5.12(a), (b) and (c). As seen in the figures, there is a sharp increase in the curve at the initial stages of loading before descending after it has reached its peak stress. The descending region of the curve corresponds with the linear strain distribution and it moves along the bond length of the FRP sheet as the debonding crack propagates towards the unloaded end.

The Popovic's model (Popovic, 1973) as indicated in Equation 5.6, was used to fit the bond-slip curve. The fitting method is known to be adequate for investigating the bond-slip behaviour of FRP sheet bonded to concrete as well. Bond stress τ is calculated based on the maximum local bond stress (τ_{max}) at maximum load obtained directly from experimental results and its corresponding slip (s_0). A constant n is also included in the model and was calculated using the least square method from a normalized stress-slip relationship (Shen et al., 2015). This model was used in fitting the curves obtained from the experimental study. Results show that Popovic's model and the measured values show a high degree of correlation. This is as shown in Figure 5.12 where experimental results from specimen L160-S-4 was compared with results obtained from Popovic's model. Table 5.4 gives a summary of the maximum bond stress (τ_{max}) at maximum load, slip at τ_{max} and maximum slip s_{max} for all the specimens tested in this program.

[5.6] $$\tau = \tau_{max}\left[\frac{s}{s_0}\frac{n}{(n-1)+\left(s/s_0\right)^n}\right]$$

where, τ is the bond stress in MPa, τ_{max} is the ultimate bond stress at maximum load, s and s_0 are the slips at τ and τ_{max} respectively and n varies.

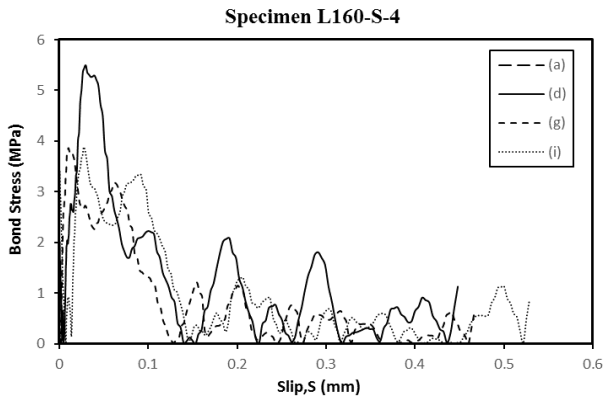

(a) Specimen L160-S-4

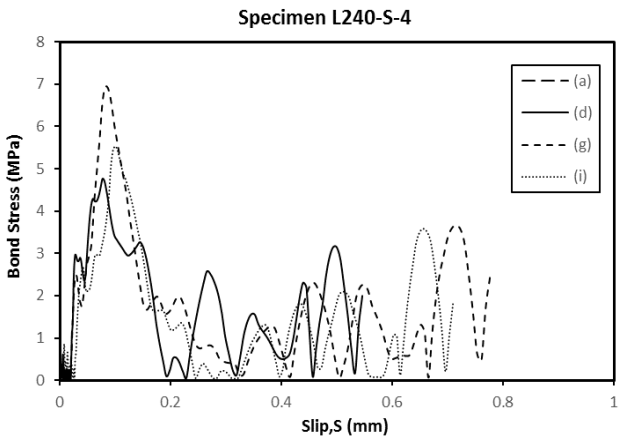

(b) Specimen L240-S-4

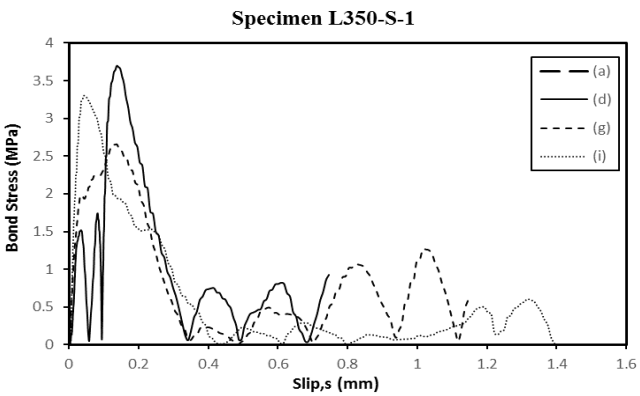

(c) Specimen L350-S-1

Figure 5.12: Relationship between Bond stress and Slip for Different Bond lengths at varying Load Levels

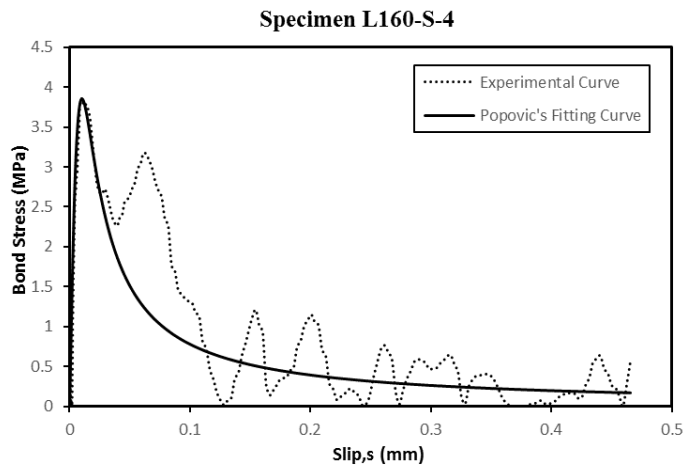

Figure 5.13: Comparison between Popovic's Model and Test Results for Specimen L160-S-4

Table 5.4: Test Results and Fitting Results of Bond-slip Relationship

Test Specimen	Ultimate Bond Stress (τ_{max}) (MPa)	Slip at τ_{max} (s_0) (mm)	Ultimate Slip (s_{max}) (mm)
L160-S-1	5.23	0.02	0.64
L160-S-2	10.21	0.48	0.48
L160-S-3	7.38	0.26	0.26
L160-S-4	3.86	0.01	0.47
L240-S-1	9.47	1.04	1.04
L240-S-2	6.16	0.10	0.70
L240-S-3	7.58	0.10	1.07
L240-S-4	6.96	0.08	0.78
L350-S-1	3.3	0.04	1.39
L350-S-2	6.17	0.01	0.07
L350-S-3	4.34	0.04	1.52
L350-S-4	2.97	0.15	1.01

Figure 5.14 shows the graphical comparison of the average ultimate load, longitudinal strain, development length and bond stress for all the groups of specimens tested. The error bars indicate the standard deviation of the measured and calculated results. Statistical

analysis generally indicated that there was no significant change in the values obtained even as length was increased. Hence, indicating that there is no increase in the FRP sheet capacity beyond its effective bond length.

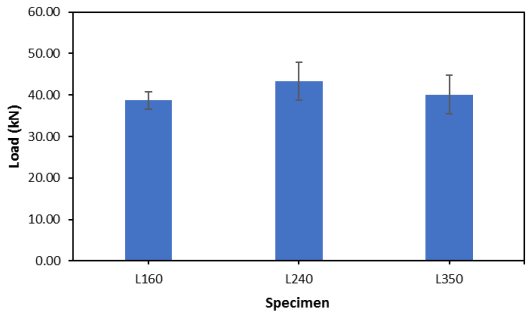

(a)

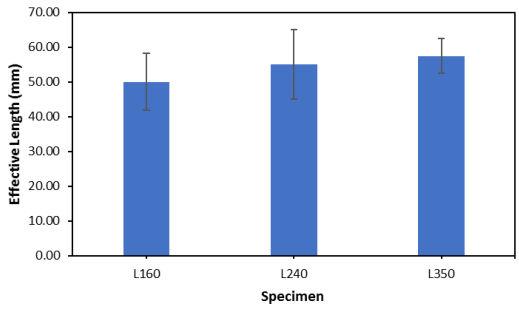

(b)

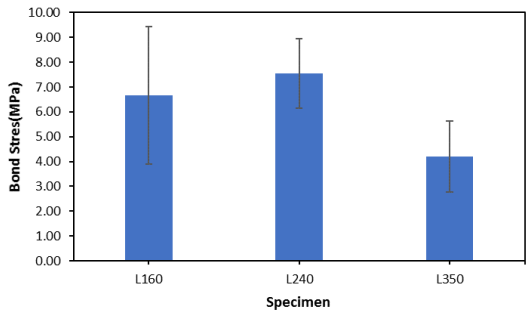

(c)

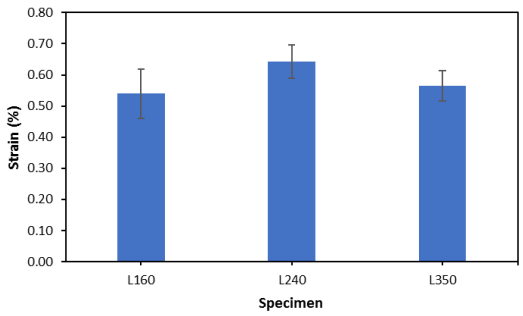

(d)

Figure 5.14: Summary of Statistical Comparison of (a) Ultimate Load (b) Effective Length (c) Bond Stress (d) Longitudinal Strain for all Groups of Specimen

5.7 Conclusions and Recommendations

This study presents the experimental investigation carried out to determine the bond behaviour of reinforced concrete bonded with CFRP sheets. A DIC technique was used to obtain and analyze strain data obtained from this program. Based on the results obtained, the following conclusions can be drawn:

1. Accurate and comprehensive results were obtained using the DIC technique when compared to the use of traditional strain gauges.
2. Strain results showed that beyond a certain bond length known as the effective bond length, there was no further increase in force which the CFRP sheet could resist. As debonding failure propagated from the loaded end along the CFRP bond length, there was a corresponding movement of the effective (development) length along the bond length over time.
3. An increase in bond length from 160 m to 240 mm did not cause a significant increase in ultimate load (12 % increase) and corresponding strain and bond stress values. Ultimate load and corresponding strain values decreased slightly (7%) when bond length was increased from 240 mm to 350 mm.
4. Although statistical analysis shows that the decrease in ultimate load when bond length was increased from 240 mm to 350 mm was not significant, it is recommended at further studies be carried out to ascertain why this occurred.
5. Bond stress values obtained from virtual strain gauges had a high discrepancy compared to the results obtained from the other two methods where local strains and maximum loads were used to determine the bond stress of the FRP sheet.

6. The bond-slip relationship curve from experimental results corresponded with the bond-slip relationship curve obtained using Popovic's 1973 model indicates a good amount of accuracy in the result obtained using the Popovic's model

It is recommended that more studies be carried out using the DIC technique for collecting and analyzing data to further validate the efficiency of this method. Future studies should also involve determining the effect of the properties of the concrete such as strength and those of the FRP sheet (width and layers) on how they affect the bond behaviour of the FRP sheets when bonded to reinforced concrete. The behaviour of surface bond characteristics of FRP strengthened reinforced concrete under high strain rates should also be studied. Other types of FRP materials such as glass, aramid and basalt fiber reinforced polymers should be considered in future experimental or analytical research. Finite element analysis would be a useful tool in determining the bond behaviour of FRP sheet bonded to reinforced concrete. Since the inadequacy of the bond strength between FRP-to-concrete interface has been identified, it is recommended that when FRP sheets are used to strengthen real life reinforced concrete members, physical anchorages may be installed to improve the interface bond strength of the retrofitted member.

REFERENCES

Bisby, L., Take W.A., Caspary, A. (2007). Quantifying Strain Variation in FRP Confined Concrete Using Digital Image Correlation: Proof-of-Concept and Initial Results. International Institute for FRP in Construction. Asia-Pacific Conference on FRP in Structures (APFIS 2007)

Bizindavyi, L. and Neale, K. (1999). Transfer lengths and bond strengths for composites bonded to concrete. Journal of Composite Construction, 10.1061/(ASCE)1090-0268(1999)3:4(153), 153–160.

Canadian Standard Association, (2012) S806-12 Design and construction of Building Components with Fibre-Reinforced Polymers, Toronto, ON, Canada, 2012.

Correlated Solutions (2010). The VIC 3D system. http://correlatedsolutions.com/vic-3d/

Dutton, M. (2012). Digital Image Correlation for Evaluating Structural Engineering Materials. MASc Thesis, Queen's University, Canada.

Goldston, M., Remennikov, S. and Sheikh, N.M. (2016). Experimental Investigation of the Behaviour of Concrete Beams Reinforced with GFRP bars under static and Impact Loading. Engineering Structures 113: 220–232.

Guo, Z. G., Cao, S. Y., Sun, W. M. And Lin, X. Y. (2005). Experimental Study on Bond Stress-Slip Behaviour Between FRP Sheets and Concrete. Proceedings of The International Symposium on Bond Behaviour of FRP in Structures. International Institute for FRP in Construction, 2005

Huo, J., Liu, J., Dai, X., Yang, J., Yuan Lu, Y., Xiao, Y., ASCE, F. and Monti, G. (2016). Experimental Study on Dynamic Behavior of CFRP-to-Concrete Interface. American Society of Civil Engineers, DOI: 10.1061/ (ASCE) CC.1943-5614.0000677.

Karbhari, V. M. and Gao, Y. (1997). Composite jacketed concrete under uniaxial compression—verification of simple design equations. J. Mater. Civ. Eng., 9(4), 185–193.

Lu, X. Z., Teng, J. G., Ye, L. P., and Jiang, J. J. (2005). Bond-slip models for FRP sheets/plates bonded to concrete. Engineering structures 27(6), 920–937.

Meier, U. (1997). Post-strengthening by continuous fiber laminates in Europe. Proa, 3rd Int. Symp., Non-Metallic (FRP) Reinforcement forConcrete Struct., Vol. 1, Japan Concrete Institute, Tokyo, 41-56.

Maeda, T., Asano, Y., Sato, Y., Ueda, T. and Kakuta, Y. (1997). A Study on Bond Mechanism of Carbon Fiber Sheet. Non-Metallic (FRP) Reinforcement for Concrete Structures, Vol. 1, Japan Concrete Institute, Japan, pp. 279-286.

Maalej M, Leong K.S (2005). Effect of Beam Size and FRP Thickness on Interfacial Shear Stress Concentration and Failure Mode of FRP-Strengthened Beams. Composites Science and Technology 65 (2005) 1148–1158.

Oehlers, D.J. and Seracino, R. (2004), Design of FRP and steel plated RC structures, Adelaide, Australia, 2004, Elsevier, 228p.

Popovics S. (1973). A numerical approach to the complete stress-strain relation for concrete. Cement Concrete Research 1973; 3:583–599.

Shadravan, B. (2009). Investigation of Surface Bond Behaviour of FRP Sheets on Concrete and Masonry Substrates. A thesis submitted to the department of Civil Engineering, University of Ottawa, Ottawa, Ontario, Canada. Heritage Branch, 978-0-494-69115-1.

Shen, D, Shi, X., Ji, Y. and Yin, F. (2015). Strain Rate Effect on Bond Stress–Slip Relationship between Basalt Fiber-Reinforced Polymer Sheet and Concrete. Journal of Reinforced Plastics and Composites. Sage, 2015, Vol. 34(7) 547–563.

Shi, J., Zhu, H., Wu, Z. and Diab, H. (2012). Strain Rate Effect on The Bond of FRP Laminate concrete Interface. Journal of Fiber Reinforced Polymer.

Smith, S. T and Teng, J. G (2001). FRP-strengthened RC beams I: review of debonding strength models. Engineering Structures, Elsevier 24 (2002) 385–395.

Wu, Z. S., and Niu, H. D (2000). Shear transfer along FRP-concrete interface in flexural members. J. Materials, Construction, Structures and Pavements, JSCE, 49 (662), 231-245.

Zhu, H., Wu, G., Shi, J., Liu C., And He, X. (2014). Digital Image Correlation Measurement of the Bond–Slip Relationship between Fiber-Reinforced Polymer Sheets and Concrete Substrate. Journal of Reinforced Plastics and Composites 2014, Vol. 33(17) 1590–1603

6.0 GENERAL DESIGN REQUIREMENTS FOR SURFACE BONDED FRP REINFORCING MATERIALS (CSA S806-12)

FRP sheet bonded to the surface of reinforced concrete shall conform to Clauses 7.2.2 and 7.2.3 of the CSA S806-12 standard for the design and construction of buildings using FRPs. Below is a summary of the step by step procedure in designing an FRP sheet used to strengthen or repair RC externally;

1. The type of FRP sheet and matrix to be used is selected and approved by the engineer based on the materials' impact to the environment and its resistance to various environmental conditions such as moisture, temperature, fire and so on.
2. Relevant physical (length, width and thickness) and mechanical (elastic modulus, flexural and tensile strength) properties of the FRP reinforcing system are determined by either testing according to procedures stated in the design standard (CSA S806-12) or directly referencing values from the manufacturers.
3. Bond length of the FRP sheet is selected such that it is not less than the development length (L_e) beyond which no strengthening is required. Development length (L_e) is calculated from Equation 6.1.

[6.1] $$L_e = \sqrt{\frac{n_f E_f t_f}{\sqrt{f_c'}}}$$

where n_f, E_f and t_f are the number of layers, elastic modulus and thickness of the FRP sheet and f_c' is the compressive strength of concrete. The development length of the CFRP sheet used in this study was theoretically calculated from Equation 6.1 to be 80 mm. In comparing the development length obtained experimentally (57

mm) to the theoretical development length, the design equation over estimates the development length which is the case generally for design models.

4. The maximum tensile strain (ε_{fmax}) in the FRP laminate shall be taken not greater than Equation 6.2.

[6.2] $$\varepsilon_{fmax} = 0.41\sqrt{\frac{f_c'}{n_f E_f t_f}} \leq 0.007$$

where n_f, E_f and t_f are the number of layers, elastic modulus and thickness of the FRP sheet and f_c' is the compressive strength of concrete. The theoretical maximum strain for the CFRP sheet used in this study exceeds 0.007, therefore, the theoretical maximum strain is taken as 0.007. Comparing the theoretical maximum strain with the values obtained experimentally (0.0064), the experimental value did not exceed the stated maximum strain value.

5. The tensile force provided by the FRP sheet should be greater than the tensile force the FRP sheet is required to resist for the design condition to be satisfied.

7.0 CONCLUSIONS AND RECOMMENDATIONS

7.1 Conclusions

This study presents an experimental investigation carried out to determine the bond behaviour of reinforced concrete strengthened with CFRP sheets. A DIC technique was used to obtain and analyze strain data obtained from this program. Based on the results obtained, the following conclusions can be drawn:

1. The double lap pull-out test is an appropriate method for testing the bond behaviour of CFRP sheet-to-concrete interface.
2. Accurate and comprehensive results were obtained using the DIC technique when compared to the use of traditional strain gauges.
3. Failure for all specimens was brittle and was due to debonding caused by the initiation of a wedge crack in the concrete at the loaded end of the FRP sheet.
7. Strain results showed that beyond a certain bond length known as the effective bond length, there was no further increase in force which the CFRP sheet could resist. As debonding failure propagated from the loaded end along the CFRP bond length, there was a corresponding movement of effective (development) length along the specimen over time.
8. An increase in bond length from 160 m to 240 mm did not cause a significant increase in ultimate load (12 % increase) and corresponding strain and bond stress values. Ultimate load and corresponding strain values decreased slightly (7%) when bond length was increased from 240 mm to 350 mm.

9. Bond stress values obtained from virtual strain gauges had a high discrepancy compared to the results obtained from the other two methods where local strains and maximum loads were used to determine the bond stress of the FRP sheet.
10. The bond-slip relationship curve from experimental results corresponded with the bond-slip relationship curve obtained using Popovic's 1973 model indicates a good amount of accuracy in the result obtained using the Popovic's model.

7.2 Recommendations

It is recommended that more studies be carried out using the DIC technique for collecting and analyzing data to further validate the efficiency of this method. Future studies should also involve determining the effect of concrete strength and other properties of the FRP sheet (FRP width and number of layers) on the bond behaviour of the FRP-to concrete interface. The behaviour of surface bonded FRP to reinforced concrete under high strain rates should also be studied. Other types of FRP materials such as glass, aramid and basalt fiber reinforced polymers should be considered in future experimental or analytical research with more than three bond lengths tested. Finite element analysis would be a useful tool in helping to understand the bond behaviour of FRP-to-concrete interface.

Although statistical analysis shows that the decrease in ultimate load when bond length was increased from 240 mm to 350 mm was not significant, it is recommended at further studies be carried out to ascertain why this occurred. Since the inadequacy of the bond strength between FRP-to-concrete interface has been identified, it is recommended that when FRP sheets are used to strengthen real life reinforced concrete members, physical anchorages may be installed to improve the interface bond strength of the retrofitted members.

REFERENCES

ACI (American Concrete Institute). (2008). Guide for the design and construction of externally bonded FRP systems for strengthening concrete structures. ACI 440.2 R-08, Farmington Hills, MI.

ACI (American Concrete Institute). (2008). Test Methods for Fiber-Reinforced Polymers (FRPs) for Reinforcing or Strengthening Concrete Structures. ACI 440.3 R-04, Farmington Hills, MI.

Ahmed, E, Sobuz H.R, Sutan, N.M (2011). Flexural Performance of CFRP Strengthened RC Beams with Different Degrees of Strengthening Schemes. International Journal of the Physical Sciences Vol. 6(9), pp. 2229-2238, 4 May 2011.

Ballinger C. A. (1991) Development of Composites for Civil Engineering. Advanced Composite Materials in Civil Engineering Structures. Proceedings of the Specialty Conference, ASCE, Reston VA.

Barre, S., Chotard, T. and Benzeggagh, M. (1996) Comparative study of strain rate effects on mechanical properties of glass fibre-reinforced thermoset matrix composite. Composites Part A Applied Science and Manufacturing, 1996; 27(12):1169–81.

Benloulo I.C, Rodriguez J, Martinez M, Galvez V. S. (1997). Dynamic tensile testing of aramid and polyethylene fiber composites. International Journal on Impact Engineering 1997;19(2):135-46.

Berver, E. W., Fowler, D. W., and King, J. J.(2001). Corrosion in FRP-wrapped concrete members. Structural Faults and Repair 2001.

Bisby, L., Take W.A., Caspary, A. (2007). Quantifying Strain Variation in FRP Confined Concrete Using Digital Image Correlation: Proof-of-Concept and Initial Results. International Institute for FRP in Construction. Asia-Pacific Conference on FRP in Structures (APFIS 2007)

Bizindavyi, L. and Neale, K. (1999). Transfer lengths and bond strengths for composites bonded to concrete. Journal of Composite Construction, 10.1061/(ASCE)1090-0268(1999)3:4(153), 153–160.

Brosens K. and Van Gemert, D. (1997). Anchoring Stresses between Concrete and Carbon Fibre Reinforced Laminates. Non-Metallic (FRP) Reinforcement for Concrete Structures, Vol. 1, Japan Concrete Institute, Japan, pp. 271-278.

Buyukozturk, O, Gunes, O., and Karaca E. (2004). Progress on understanding debonding problems in reinforced concrete and steel members strengthened using FRP composites. Construction Building Materials, 2004; 18(1):9–19.

Campbell, F.C. (2010). Structural Composite Materials. AMS international. United States of America.

Canadian Standard Association, (2002) S806-02 Design and construction of Building Components with Fibre-Reinforced Polymers, Toronto, ON, Canada, 2002.

CEN (European Committee for Standardization). (2005). Eurocode 8: Design of structures for earthquake resistance—Part 3: Assessment and retrofitting of buildings. EN 1998–3. 2004, Brussels, Belgium.

Chajes, M.J.; Finch, W.W.Jr.; Januszka, T.F.; and Thomson, T.A. (1996). Bond and Force Transfer of Composite Material Plates Bonded to Concrete. ACI Structural Journal, ACI, Vol. 93, No. 2.

Chen, J. F., and Teng, J. G. (2001). Anchorage strength models for FRP and steel plates bonded to concrete. Journal of Structural Engineering, 10.1061/(ASCE) 0733-9445(2001)127:7(784), 784–791.

Chiew S, Sun Q, Yu Y (2007). Flexural Strength of RC Beams with GFRP Laminates. Journal of Composites for construction. ASCE, September/October 2007.

CNR (National Research Council). (2004). Guide for the design and construction of externally bonded FRP systems for strengthening existing structures: Materials, RC and PC structures, masonry structures. CNR-DT 200/2004, Italian Research Council, Italian Advisory Committee on Technical Recommendations for Construction, Rome.

Correia, J. R. (2013). The New Frp Materials for Civil Engineering Structural Applications. 57th Meeting of the European Council of Civil Engineers (ECCE). Technical University of Lisbon.

Correlated Solutions (2010). The VIC 3D system. http://correlatedsolutions.com/vic-3d/

Dai J, Ueda T and Sato Y. (2007). Bonding Characteristics of Fiber-Reinforced Polymer Sheet-Concrete Interfaces under Dowel Load. Journal on Composite Construction 2007; 11: 138–148.

Dai, J.G., Ueda, T. and Sato, Y. (2005). Development of the Nonlinear Bond Stress-Slip Model of Fiber Reinforced Plastics Sheet-Concrete Interfaces with a Simple Method. ASCE, Journal of Composites for Construction, 9 (1, 52-62).

Daniel I. and Liber T. (1976) Strain rate effects on the mechanical properties of fiber composites. Report NASA CR-135087. Part 3.

Daniel, I., LaBedz, R. and Liber, T. (1981). New method for testing composites at very high strain rates. Exp Mech 1981; 21(2):71–7.

Davidson, J. S, Fisher, J. W, Hammons, M. I, Porter, J. R. and Dinan, R. J. (2005). Failure Mechanisms of Polymer Reinforced Concrete Masonry Walls Subjected to Blast. J Structural Engineering, 2005; 131(8):1194–205.

Dutton, M. (2012). Digital Image Correlation for Evaluating Structural Engineering Materials. MASc Thesis, Queen's University, Canada.

Esfahani, M. R., Kianoush, M. R. and Tajari, A. R. (2007). Flexural Behaviour of Reinforced Concrete Beams Strengthened by CFRP Sheets. Elsevier Limited, Engineering Structures 29 (2007) 2428–2444.

Eskandari H, Nemes J. (2000). Dynamic testing of composite laminates with a tensile split Hopkinson bar. Journal of Composite Materials.

Foroutan R, Nemes J, Ghiasi H, Hubert P. (2013). Experimental investigation of high strain-rate behaviour of fabric composites. Journal of Composite Structures 2013; 106:264-9.

Ghorbani, M, Mostofinejad, D, Hosseini, A. (2016). Experimental Investigation into Bond Behavior of FRP-to-concrete under Mixed-mode I/II Loading. Construction and Building Materials, Volume 132.

Gilat A, Goldberg R. K, Roberts G. D. (2002). Experimental study of strain-rate dependent behavior of carbon/epoxy composite. Journal on Composite Science and Technology, 62(10):1469-76.

Greco, W. (2009). Structural Impact Loading. Greensward N. Warrington, Pa. 18976.

Guo, Z. G., Cao, S. Y., Sun, W. M. And Lin, X. Y. (2005). Experimental Study on Bond Stress-Slip Behaviour Between FRP Sheets and Concrete. Proceedings of The International Symposium on Bond Behaviour of FRP in Structures. International Institute for FRP in Construction, 2005.

Hiroyuki Y and Wu Z. Analysis of Debonding Fracture Properties of CFS Strengthened Member Subject to Tension. In: Proceedings of Third International Symposium on Non-Metallic (FRP) Reinforcement for Concrete Structures, Sapporo, Japan, 1997, vol. 1, pp.287–294. Tokyo: Japan Concrete Institute

Huo, J., Liu, J., Dai, X., Yang, J., Yuan Lu, Y., Xiao, Y., ASCE, F. and Monti, G. (2016). Experimental Study on Dynamic Behavior of CFRP-to-Concrete Interface. American Society of Civil Engineers, DOI: 10.1061/ (ASCE) CC.1943-5614.0000677.

Jacob, G. C., Starbuck, J. M., Fellers, J. F., Simunovic, S. and Boeman, S. R. (2004). Strain Rate Effects on the Mechanical Properties of Polymer Composite Materials. Published online in Wiley InterScience (www.interscience.wiley.com). DOI 10.1002/app.20901.

Jadhav, A., Woldesenbet, E., Pang, S. (2003). High strain rate properties of balanced angleply graphite/epoxy composites. Composites, Part B 2003; 34(4):339–46.

Jacques, E. (2016). Characteristics of Reinforced Concrete Bond at High Strain Rates. Thesis submitted to the Faculty of Graduate and Postdoctoral Studies, Department of Civil Engineering Faculty of Engineering University of Ottawa.

Japan Concrete Institute (JCI). (2003). Technical Report of Technical Committee on Retrofit Technology. In: Proceedings of The International Symposium on Latest Achievement of Technology And Research on Retrofitting Concrete Structures, Pp. 4–42, Tokyo: Japan Concrete Institute, 2003.

Kabir, M. Z and Shafei, E. (2009). Analytical and Numerical Study of FRP Retrofited RC Beams Under Low Velocity Impact. Department of Civil and Environmental

Engineering, Amirkabir University of Technology, Tehran, Iran. Sharif University of Technology, Vol. 16, No. 5, pp. 415-428.

Karbhari, V. M. and Gao, Y. (1997). Composite jacketed concrete under uniaxial compression—verification of simple design equations. J. Mater. Civ. Eng., 9(4), 185–193.

Khalifa A, Gold, W. J, Nanni A, M. I. (1998). Contribution of Externally Bonded FRP to Shear Capacity of RC Flexural Members. Journal on Composite Construction 2(4):195–202.

Khalighi, Y. (2009). A Study of Bond Between Fibre Reinforced Polymer and Concrete under Quasi-Static and Impact Loading. A Thesis Submitted in Partial Fulfillment of the Requirements for the Degree of Doctor of Philosophy. The University of British Columbia.

Kim, D. and Sebastian, W. M. (2002). Parametric Study of Bond Failure in Concrete Beams Externally Strengthened with Fibre Reinforced Polymer Plates. Magazine of Concrete Research, 47–59.

Lee, S. and Moy, S. (2007). A Method for Predicting the Flexural Strength of RC Beams Strengthened with Carbon Fiber-reinforced Polymer. Journal of Reinforced Plastics and Composites. Sage Publications. DOI: 10.1177/0731684407079372

Lloyd A, Saatcioglu M, Tikka T.K (2011). Strengthening of Non-Seismic Columns subjected to Explosive Loading with External Longitudinal CFRP. 2nd International Engineering Mechanics and Materials Specialty Conference. June 2011

Lifshitz, J. and Leber, H. (1998) Response of fiber-reinforced polymers to high strain-rate loading in interlaminar tension and combined tension/shear. Composite Science Technology, 1998; 58(6):987–96.

Lu et al., (2007). Intermediate Crack Debonding in FRP-Strengthened RC Beams: FE Analysis and Strength Model. Journal of Composites for Construction ASCE 10.1061/ (ASCE) 1090-0268 (2007) 11:2.161.

Lu, X. Z., Teng, J. G., Ye, L. P., and Jiang, J. J. (2005). Bond-slip models for FRP sheets/plates bonded to concrete. Engineering structures 27(6), 920–937.

Malvar, L. J., ASCE, M., Kenneth B., Morrill and John E. Crawford, J. E. (2004). Journal of Composites for Construction, Vol. 8, No.4.

Meier, U. (1997). Post-strengthening by continuous fiber laminates in Europe. Proa, 3rd Int. Symp., Non-Metallic (FRP) Reinforcement forConcrete Struct., Vol. 1, Japan Concrete Institute, Tokyo, 41-56.

Mirmiran, A., Zagers, K. and Yuan, W. (2000). Nonlinear finite element modeling of concrete confined by fiber composites. Finite Elememt Analysis and Design, 35(1), 79–96.

Maeda, T., Asano, Y., Sato, Y., Ueda, T. and Kakuta, Y. (1997). A Study on Bond Mechanism of Carbon Fiber Sheet. Non-Metallic (FRP) Reinforcement for Concrete Structures, Vol. 1, Japan Concrete Institute, Japan, pp. 279-286.

Maalej M, Leong K.S (2005). Effect of Beam Size and FRP Thickness on Interfacial Shear Stress Concentration and Failure Mode of FRP-Strengthened Beams. Composites Science and Technology 65 (2005) 1148–1158.

Melin, L. G.; Asp, L. E. (1999). Composites A 1999, 30, 305

Nakaba, K., Toshiyuki, K., Tomoki, F. and Hiroyuki, Y. (2001) Bond Behaviour between Fiber Reinforced Polymer Laminates and Concrete. ACI Structural Journal; 98(3):359-67.

Nam, J., Kim, H., Kim, S., Yi, N. and Kim, J. J. (2009). Numerical Evaluation of The Retrofit Effectiveness for GFRP Retrofitted Concrete Slab Subjected to Blast Pressure. Elsevier Limited, Composite Structures 92 (2010) 1212–1222.

Neubauer U, Rostasy FS. Design Aspects of Concrete Structures Strengthened Wwth Externally Bonded CFRP-Plates. In: Forde MC, editor. Proc, 7th International Conference on Structural Faults and Repair. Edinburgh, UK: Engineering Technics Press; 1997. p. 109–18.

Niedermeier R. Envelope line of tensile forces while using externally bonded reinforcement. PhD thesis, Germany: TU München; 2000 (in German).

Oehlers, D.J. and Seracino, R. (2004), Design of FRP and steel plated RC structures, Adelaide, Australia, 2004, Elsevier, 228p.

Okoli, O. I and Smith, G. F. (1995) In Proceedings of Society of Plastics Engineers Annual Technical Conference (ANTEC), Advanced Polymer Composites Division, 1995, Vol.2, p. 2998 –3002.

Orton, S. L., Chiarito, V. P., Rabalais, C., Wombacher, M. and Rowell, S. P. (2014). Strain Rate Effects in CFRP Used For Blast Mitigation. Open Access Polymers, ISSN 2073-4360, www.mdpi.com/journal/polymers.

Otani, S. (1979). Nonlinear Dynamic Analysis of Reinforced Concrete Building Structures. Department of Civil Engineering, University of Toronto, Toronto, Ontario, Canada M5S 1A4. Received January 10, 1979.

Pan J, Chung T.C.F, Leung C.Y.K (2009). FRP Debonding from Concrete Beams under Various Load Uniformities. Advances in Structural Engineering 12(6) 2009.

Pham, T. and Hao, H. (2016). Review of Concrete Structures Strengthened with FRP Against Impact Loading. American Society of Engineers. Elsevier Structures, 10.1016.j istruc.2016.05.003, 59-70.

Popovics S. (1973). A numerical approach to the complete stress-strain relation for concrete. Cement Concrete Research 1973; 3:583–599.

Quantrill, R. J., Holloway, L. C. and Thorne, A. M. (1996). Experimental and Analytical Investigation of FRP Strengthened Beam Response: Part I. University of Surrey, Magazine of Concrete Resaerch, 1996, 48, No. 177, December 331-342.

Rahimi, H. and Hutchinson, A. (2001). Concrete Beams Strengthened with Externally Bonded FRP Plates. Journal of Composites for Construction, 2001, 5(1): 44-56.

Rodriguez, J., Chocron, I., Martinez, M. and Sanchez-Galvez, V. (1996) High strain rate properties of aramid and polyethylene woven fabric composites. Composites Part B 1996; 27(2):147–54.

Rotem, A. and Lifshitz, J. M. In Proceedings of the 26th Annual Technical Conference, Society for Plastics Industry, Reinforced Plastics/Composites Division, Washington, DC, 1971, Section 10-G, p. 1–10.

Ruiters, A. (2014). Analytical Behaviour of FRP Strengthened Reinforced Concrete Beams Under Low Velocity Impact Load Incorporating Rate Dependent Material Constitutive Models. Department of Civil engineering, University of Cape Town.

Sebastian, W. M. (2001). Significance of Midspan Debonding Failure in Frp-Plated Concrete Beams. Journal of Structural Engineering, Vol. 127, No. 7, July, 2001. ASCE, ISSN 0733-9445/01/0007-0792–0798. Paper No. 22479.

Setunge et al. (2002). Review of Strengthening Techniques Using Externally Bonded Fiber Reinforced Polymer Composites. CRC construction Innovation. Report 2002-005-C-01.

Shadravan, B. (2009). Investigation of Surface Bond Behaviour of FRP Sheets on Concrete and Masonry Substrates. A thesis submitted to the department of Civil Engineering, University of Ottawa, Ottawa, Ontario, Canada. Heritage Branch, 978-0-494-69115-1.

Shen, D, Shi, X., Ji, Y. and Yin, F. (2015). Strain Rate Effect on Bond Stress–Slip Relationship between Basalt Fiber-Reinforced Polymer Sheet and Concrete. Journal of Reinforced Plastics and Composites. Sage, 2015, Vol. 34(7) 547–563.

Shen, D, Shi, H., Ji, Y. and Yin, F. (2015). Strain Rate Effect on Effective Bond Length of Basalt FRP Sheet Bonded to Concrete. Article in construction and Building Materials. May 2015.

Shi, J., Zhu, H., Wu, Z. and Diab, H. (2012). Strain Rate Effect on The Bond of FRP Laminate concrete Interface. Journal of Fiber Reinforced Polymer.

Shokrieh, M. M, Omidi M. J. (2009). Tension behavior of unidirectional glass/epoxy composites under different strain rates. Composite Structures 2009;88(4):595-601

Sims, G. D. In Proceedings of the 6th International Conference on Composite Materials and 2nd European Conference on Composite Materials, Imperial College, London, 1988, Vol. 3, pp.3.494 –3.507.

Smith, S. T and Teng, J. G (2001). FRP-strengthened RC beams I: review of debonding strength models. Engineering Structures, Elsevier 24 (2002) 385–395.

Tanaka T. Shear resisting mechanism of reinforced concrete beams with CFS as shear reinforcement. Japan: Hokkaido University, 1996.

Teng, J. G., Chen, J. F., Smith, S. T. and Lam, L. (2002). FRP Strengthened RC Structures, Chichester, John Wiley and Sons.

Ueda T, Dai JG, Sato Y. (2003) A nonlinear bond stress-slip relationship for FRP sheet concrete interface. In Proc. of international symposium on latest achievement of technology and research on retrofitting concrete structures.

Wu, Z. S., and Niu, H. D (2000). Shear transfer along FRP-concrete interface in flexural members. J. Materials, Construction, Structures and Pavements, JSCE, 49 (662), 231-245.

Wu, Z. S., Yuan, H. and Niu, H. D. (2002). Stress Transfer and Fracture Propagation in Different Kinds of Adhesive Joints, ASCE Journal of Engineering Mechanics, 128(5):562-573.

Yao, J. Teng, J.G. and Chen, J.F. (2005). Experimental study on FRP to concrete bonded joints, Composites, 36 Part B 2005.

Yuan, H., Wu, Z. S. and Yoshizawa, H. (2001). Theoretical Solutions on Interfacial Stress Transfer of Externally Bonded Steel/Composite Laminates. JSCE Journal of Structural Mechanics and Earthquake Engineering, 18(1): 27-39.

Zhu, H., Wu, G., Shi, J., Liu C., And He, X. (2014). Digital Image Correlation Measurement of the Bond–Slip Relationship between Fiber-Reinforced Polymer Sheets and Concrete Substrate. Journal of Reinforced Plastics and Composites 2014, Vol. 33(17) 1590–1603

APPENDIX A

EXPERIMENTAL STATIC TEST RESULTS FOR CFRP SHEETS EXTERNALLY BONDED TO REINFORCED CONCRETE

A.1 Dimensions and Test Properties for Specimens L160-S

Specimens Dimensions:

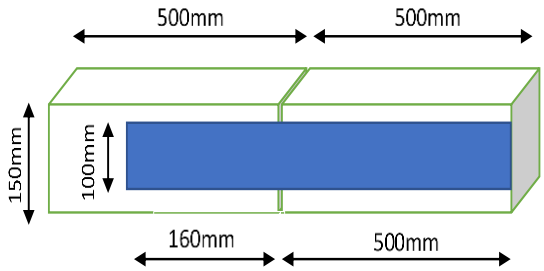

Figure A1.1: FRP Sheet Bonded to concrete Specimen for Specimens L160-S

Testing Machine: Baldwin Testing Machine

Date of Test: July 21st, 2017

Test Type: Double Lap Pull-out Bond Test

Bond Length:160mm

Loading Rate: 0.5mm/min

Picture time Interval: 400ms

A1.1 Results for Specimen L160-S-1

- Specimen Installed Prior to Testing

a) Front of Specimen b) Back of Specimen c) Side of Specimen

Figure A1.2: Views of Specimen L160-S-1 Installed in Testing Machine Prior to Testing

- Test Results

Pictures of Specimen after Testing:

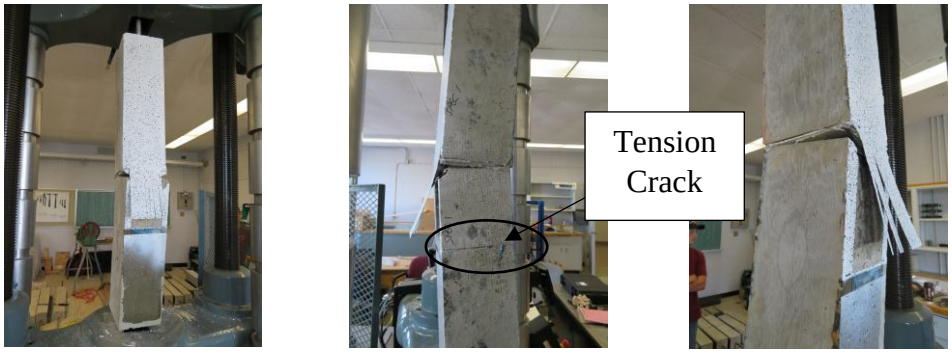

a) Front side b) Right Side c) Left side

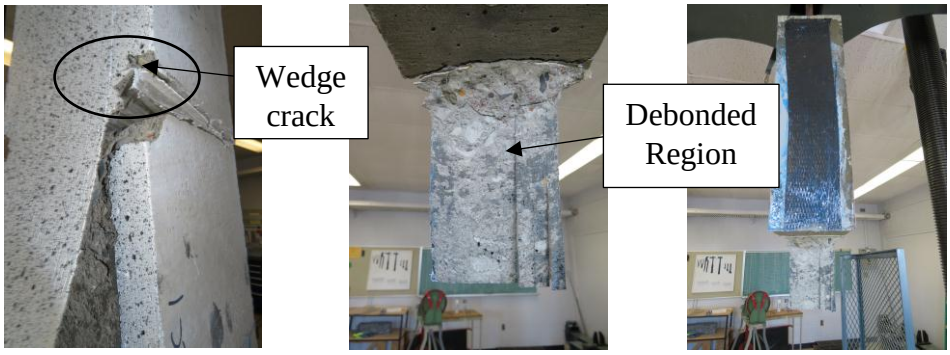

d) Wedge Failure e) Debonded Region f) Back Side

Figure A1.3: Views of Specimen L160-S-1 after Failure

Comments on Specimen L160-S-1 before and after Failure:

The following were observed after the specimen failed:

- The specimen experienced brittle failure accompanied by a loud noise
- As seen in Figure A1.3(a), failure took place on the speckled side of the specimen.
- Tension crack normal to the force was developed on the right side of the specimen but none was observed on the left side of the specimen.
- Concrete wedge crack developed at the loaded end of the specimen as seen in Figure A1.3(d)
- The CFRP sheet was well bonded to concrete because debonding occurred by shearing of concrete below the bonded surface as seen in Figure A1.3(e)
- The back side of the specimen failed due to buckling of the CFRP sheet immediately after the debonding failure of the front side took place as shown in Figure A1.3(f).

Analysis of Test Results

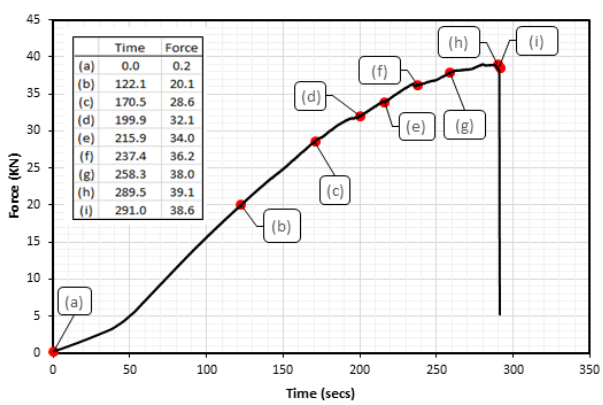

	Time	Force
(a)	0.0	0.2
(b)	122.1	20.1
(c)	170.5	28.6
(d)	199.9	32.1
(e)	215.9	34.0
(f)	237.4	36.2
(g)	258.3	38.0
(h)	289.5	39.1
(i)	291.0	38.6

Figure A1.4: Force versus Time curve for Specimen L160-S-1 Showing Key Points During the Test

Comments on Figure A1.4:

Points (a), (b) and (c) on the graph show the elastic behaviour of the specimen up to (d). A small decrease in force although not obvious occurred from (d) to (e) and from (f) to (g) due to the initiation of the wedge and tension cracks. Gradual increase in force took place until failure at (i).

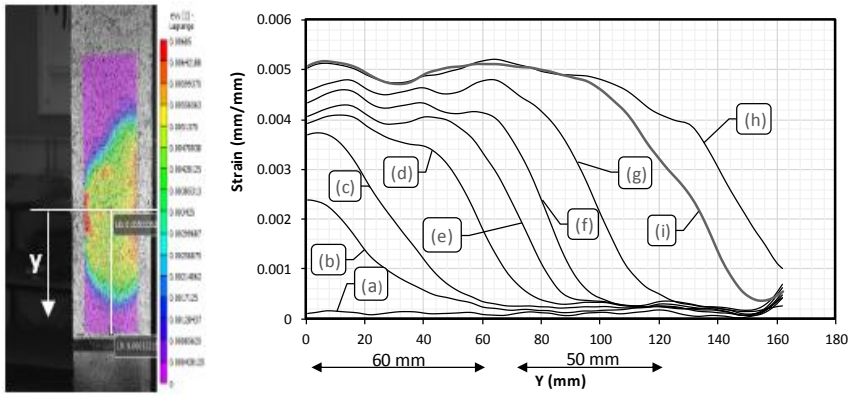

(a) (b)

Figure A1.5: (a) Contour Diagram Showing Position of Strain Inspector Line along the Bond Length of CFRP Sheet (b) Strain versus Distance along the Bond Length of CFRP Sheet at Times shown in Figure A1.4 for Specimen L160-S-1

<u>Comments on Figure A1.5:</u>

The strain values increased as the load increased over time. Curves (b) and (c) are elastic but as the curve moved to (d), the slope (effective bond length) began to shift towards the unloaded end of CFRP with flat segments at the loaded end. This indicates the initiation of cracks. At (h), there was a decrease in strain to (i) due to a corresponding decrease in applied load.

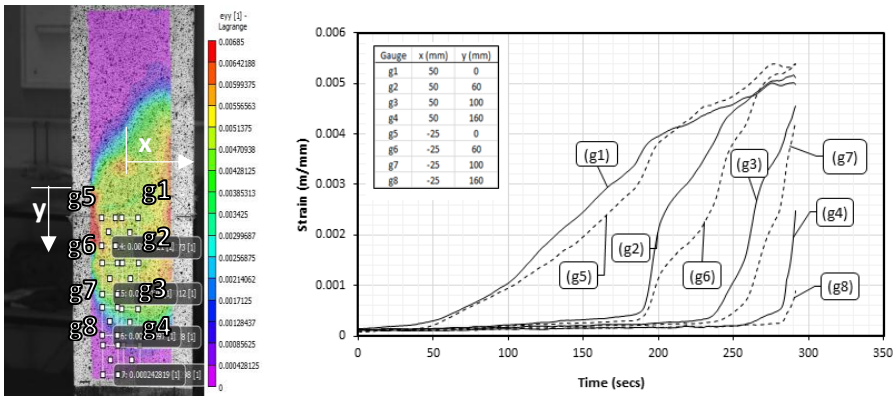

(a) (b)

Figure A1.6:(a): Contour Diagram Showing Position of 8 Gauges (b): Strain versus Time Curves of Specimen at Locations of Gauges as Indicated in the Contour Diagram in Figure A1.6(a) for Specimen L160-S-1

Comments on Figure A1.6:

Gauges (g1), (g2), (g3) and (g4) recorded higher strain values than (g5), (g6), (g7) and (g8) due to shear lag and load eccentricity effect. Strain at Gauges (g2) and (g6) started to increase after the redistribution of stresses caused by the initiation of the concrete wedge crack. There was no drop in strain until failure.

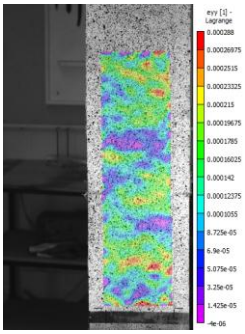

(a) ε_{yy} Dist. at T= 0 s

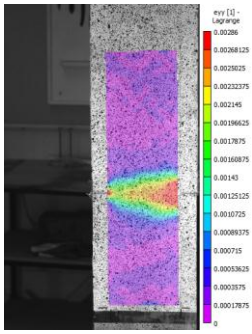

(b) ε_{yy} Dist. at T= 122 s

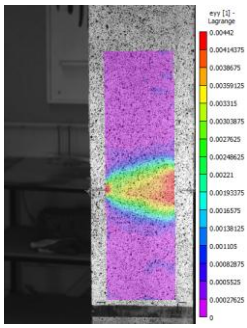

(c) ε_{yy} Dist. at T= 171 s

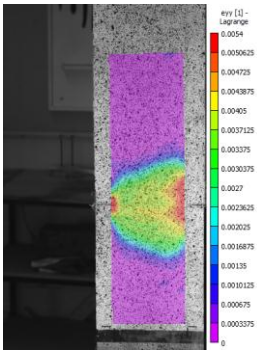

(d) ε_{yy} Dist. at T= 200 s

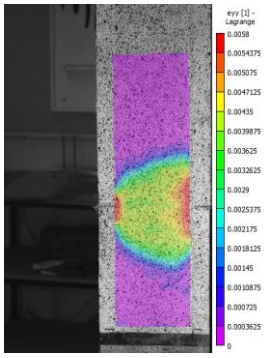

(e) ε_{yy} Dist. at T= 216 s

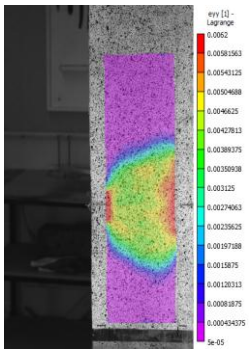

(f) ε_{yy} Dist. at T= 237 s

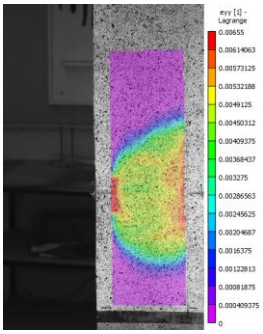

(g) ε_{yy} Dist. at T= 258 s

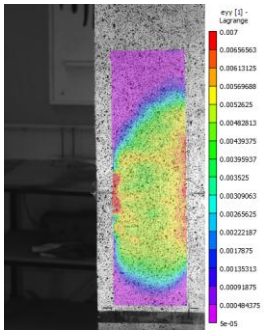

(h) ε_{yy} Dist. at T= 290 s

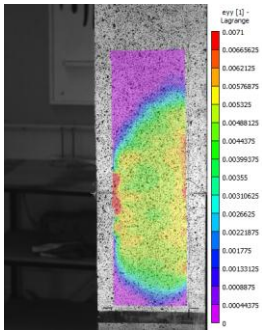

(i) ε_{yy} Dist. at T= 291 s

Figure A1.7: Strain Fields Showing distribution of longitudinal Strains (ε_{yy}) on CFRP Sheet at Different Times as Test Progressed to Failure for Specimen L160-S-1

Comments on Figure A1.7:

Contour diagrams show a gradual increase in longitudinal strain originating from the loaded section towards the unloaded section until failure. Shear lag effect was significant in the specimen as seen in the uneven distribution of strain along the width of the CFRP sheet. An asymmetry in strain field is observed which may be due to the load being transferred to the specimen at an eccentricity or due to the CFRP sheet not properly installed on the concrete prism.

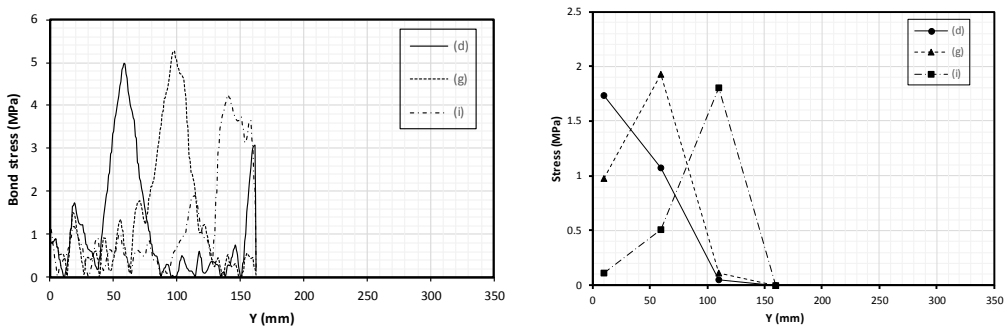

(a) (b)

Figure A1.8: Graph of Bond Stress along CFRP Bond Length of Specimen L160-S-1 using (a) Equation 5.2 (b) Equation 5.3

Comments on Figure A1.8:

Both curves show a similar trend where the maximum bond stress moved along the length of the CFRP sheet towards the unloaded region. This behaviour is like the strain profile where the active bond zone (development length) moved towards the unloaded end of the specimen. Equation 5.3 gave smoother curves due to the limitation in data points compared to curves obtained from Equation 5.2.

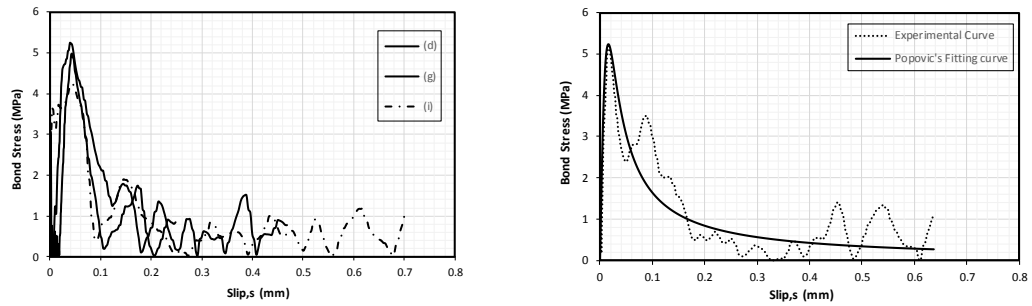

(a) (b)

Figure A1.9: Relationship between Bond Stress and Slip for Specimen L160-S-1 at varying Load Levels and the Corresponding Fitting Curve

Comments on Figure A1.9:

From Figure A1.9(a), the bond-slip relationship gives a parabolic curve with a steep increase at the initial stage of the test. The descending region correlates with the elastic strain distribution which moves along the bond length of the CFRP sheet as debonding cracks propagates towards the unloaded end.

A fitting model proposed by Popovic was used to fit the experimental bond-slip curve. There is a correlation between the curves as both follow the same parabolic trend as observed from Figure A1.9(b).

A1.2 Results for Specimen L160-S-2

- Specimen Installed Prior to Testing

a) Front of Specimen b) Back of Specimen c) Side of Specimen

Figure A1.10: Views of Specimen L160-S-2 Installed in Testing Machine Prior to Testing

- Test Results

Pictures of Specimen after Testing:

a) Front side b) Right Side c) Left side

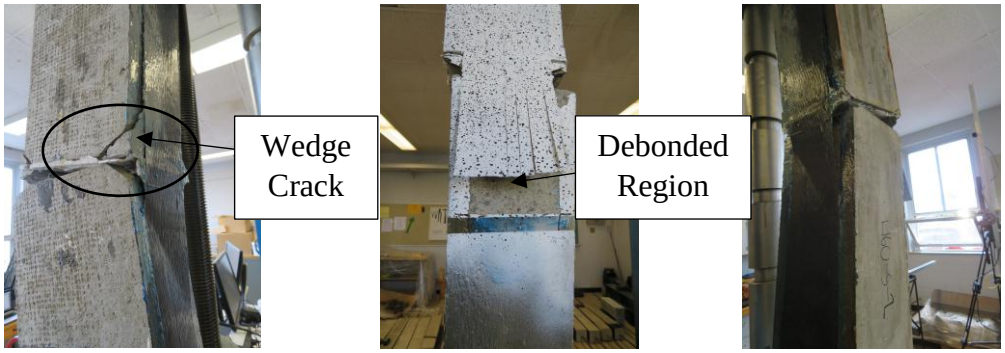

d) Wedge Crack e) Debonded Region f) Back Side

Figure A1.11: Views of Specimen L160-S-2 after Failure

Description of Specimen L160-S-2 after Failure

It was observed that the following happened to the specimen at/after failure:

- The specimen experienced brittle failure accompanied by a loud noise
- As seen in Figure A1.11(a), failure took place on the speckled side of the specimen.
- Tension crack normal to the force was developed on the right and left sides of the specimen but none was evident in the pictures indicated in Figures A1.11(b) and (c).
- Concrete wedge crack occurred at the critical section of the specimen as seen in Figure A1.11(d)
- CFRP sheet was well bonded to concrete because debonding occurred by shearing of concrete below the bonded surface as seen in Figure A1.11(e)
- The back side of the specimen failed due to buckling of the CFRP sheet immediately after the debonding failure of the front side took place as shown in Figure A1.11(f).

Analysis of Test Results

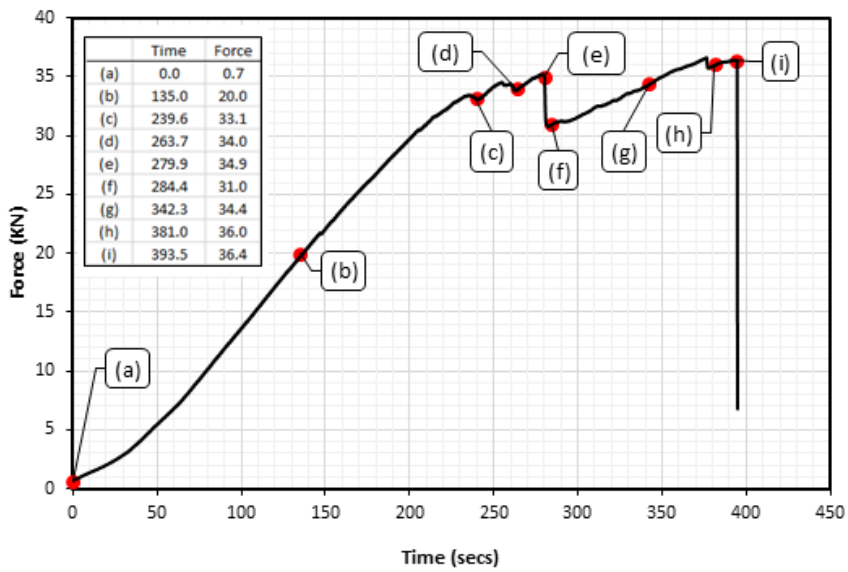

Figure A1.12: Force versus Time curve for Specimen L160-S-2 Showing Key Points During the Test

Comments on Figure A1.12:

Points (a), (b) and (c) on the graph show the elastic behaviour of the specimen. A small drop in force occurred from point (c) to (d) after which there was a force increase to point (e). A significant decrease in force took place from point (e) to (f) due to the initiation of the wedge crack at the critical section of the specimen. Gradual increase in force took place from point (f) to point (h) when the tension crack occurred. There was an increase in force to point (i) before failure took place.

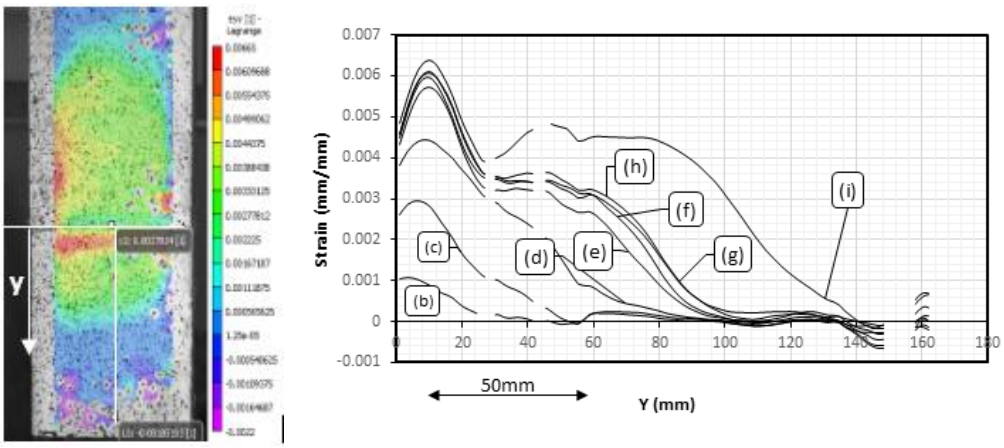

(a) (b)

Figure A1.13: (a) Contour Diagram Showing Position of Strain Inspector Line along the Bond Length of FRP Sheet (b) Strain versus Distance along the Bond Length of FRP Sheet at Times shown in Figure A1.12 for Specimen L160-S-2

Comments on Figure A1.13:

An anomaly in the strain curves at the critical section is observed. This may be due to the pair of prisms not properly aligned before installing the FRP sheet as observed before the test was carried out. The strain values increased as the load increased over time. Curves (b) and (c) are elastic but as the curve moved to (d), the slope (effective bond length) began to shift towards the unloaded end of FRP with almost flat segments at the loaded end. This indicates the initiation of wedge cracks and the propagation of debonding. Strain curves increased gradually until (i) before failure.

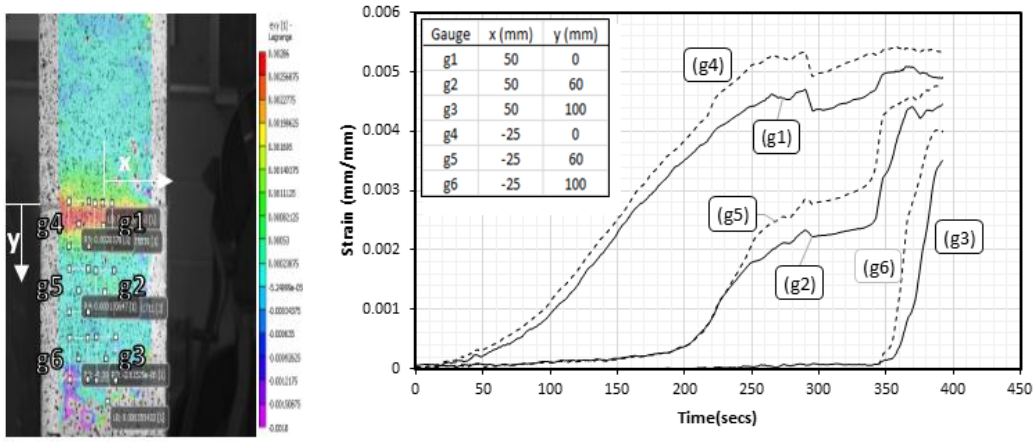

(a) (b)

Figure A.14:(a): Contour Diagram Showing Position of 6 Gauges (b): Strain versus Time Curves of Specimen L160-S-2 at Locations of Gauges as Indicated in the Contour Diagram in (a)

Comments on Figure A1.14:

Six gauges were used for this specimen because data was lost towards the unloaded end of the specimen. Gauges (g1), (g2) and (g3) recorded lower strain values than (g4), (g5) and (g6) due to shear lag and load eccentricity effect. Strain at Gauges (g3) and (g6) started to increase only after the redistribution of stresses caused by the initiation of the concrete wedge and tension cracks. There was no drop in strain until failure.

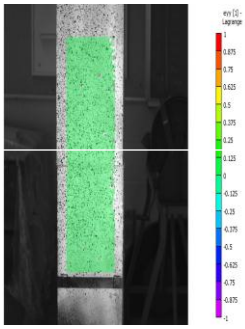

(a) ε_{yy} Dist. at T= 0 s

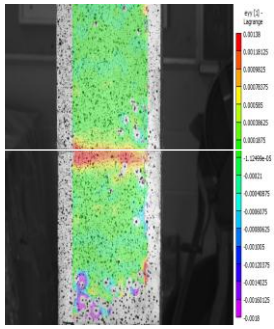

(b) ε_{yy} Dist. at T= 135 s

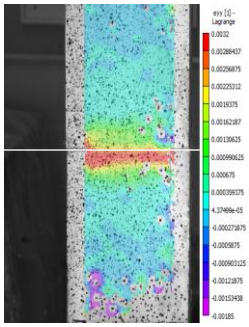

(c) ε_{yy} Dist. at T= 240 s

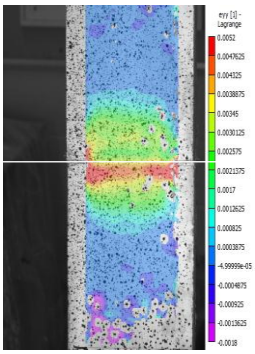

(d) ε_{yy} Dist. at T= 264 s

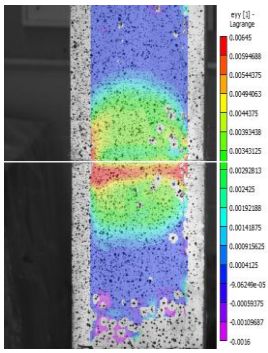

(e) ε_{yy} Dist. at T= 280 s

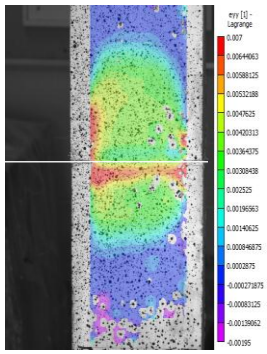

(f) ε_{yy} Dist. at T= 284 s

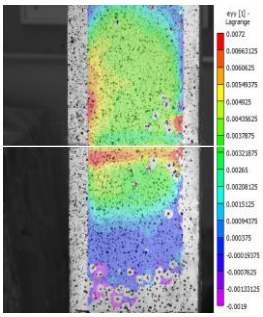

(g) ε_{yy} Dist. at T= 342 s

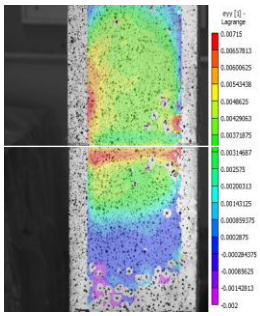

(h) ε_{yy} Dist. at T= 381 s

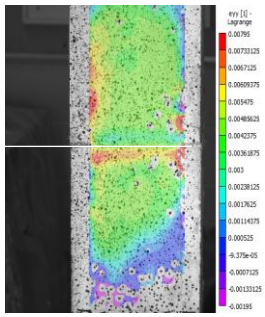

(i) ε_{yy} Dist. at T= 394 s

Figure A1.15: Strain Fields Showing distribution of Longitudinal Strains on FRP Sheet at Different Times as Test Progressed to Failure for Specimen L160-S-2

<u>Comments on Figure A1.15:</u>

Similar observation as in specimen L160-S-1 was observed here. Contour diagrams show a gradual increase in longitudinal strain originating from the loaded section towards the unloaded section until failure. The wedge crack and the tension crack did not show a significant effect on the strain values of the specimen. Shear lag effect was significant in the specimen as seen in the parabolic distribution of strain across the width of the CFRP sheet.

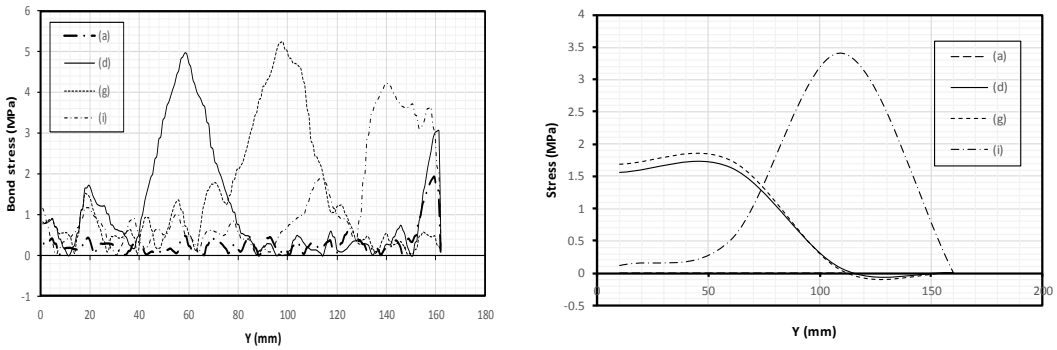

(a) (b)

Figure A1.16: Graph of Bond Stress along CFRP bond Length of Specimen L160-S-2 using (a) Equation 5.2 (b) Equation 5.3

<u>Comments on Figure A1.16:</u>

Both curves show similar trend where the maximum bond stress moved along the length of the CFRP sheet towards the unloaded section. Maximum bond stress moved along the bond length of the FRP sheet towards the unloaded region as debonding propagates. Equation 5.3 gave smoother curves due to the limitation in data points compared to curves obtained from Equation 5.2.

A1.3 Results for Specimen L160-S-3

- Specimen Installed Prior to Testing

a) Front of Specimen b) Back of Specimen c) Side of Specimen

Figure A1.17: Views of Specimen L160-S-3 Installed in Testing Machine Prior to Testing

- Test Results

Pictures of Specimen after Testing:

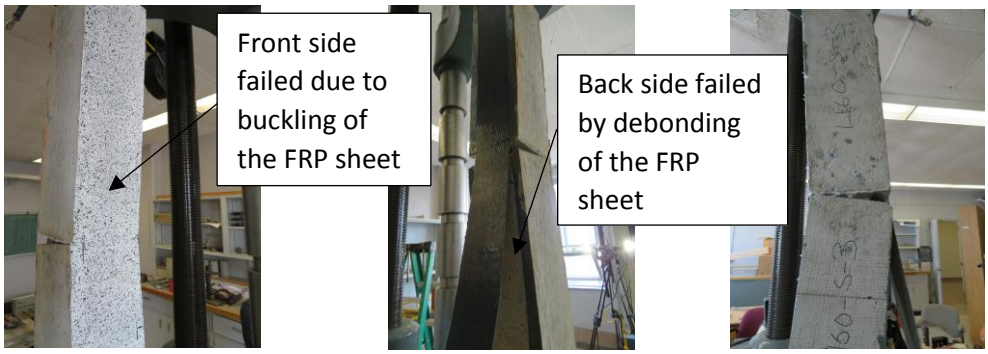

a) Front side b) Back Side c) Wedge Failure

Figure A1.18: Views of Specimen L160-S-3 after Failure

Description Specimen L160-S-3 after Failure

It was observed that the following happened to the specimen at/after failure:

- The specimen experienced brittle failure accompanied by a loud noise
- As seen in Figure A1.18(b), failure took place at back side of the specimen.
- Tension crack normal to the force was developed on the right and left sides of the specimen but none was evident in the pictures indicated in Figure A1.18.
- Concrete wedge failure occurred at the critical section of the specimen as seen in Figure A1.18(c)
- CFRP sheet was well bonded to concrete because debonding occurred by shearing of concrete below the bonded surface as seen in Figure A1.18(b)
- The speckled side of the specimen failed due to buckling of the FRP sheet immediately after the debonding failure of the back side took place as shown in Figure A1.18(a).

Analysis of Test Results

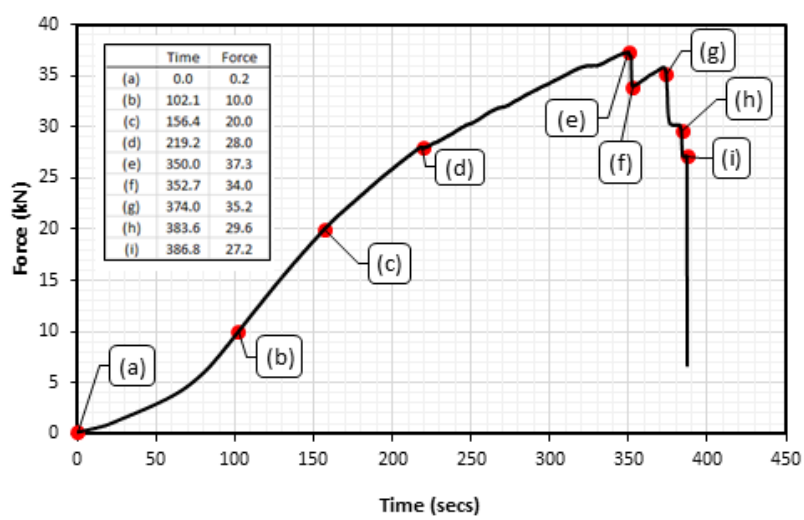

	Time	Force
(a)	0.0	0.2
(b)	102.1	10.0
(c)	156.4	20.0
(d)	219.2	28.0
(e)	350.0	37.3
(f)	352.7	34.0
(g)	374.0	35.2
(h)	383.6	29.6
(i)	386.8	27.2

Figure A1.19: Force versus Time curve for Specimen L160-S-3 Showing Key Points During the Test

Comments on Figure A1.19:

Points (a) to (d) show the elastic behaviour of the specimen. A decrease in force from point (e) to (f) can be observed due to propagation of the wedge crack. Load increased to point (g) and then decreased to point (i) before failure.

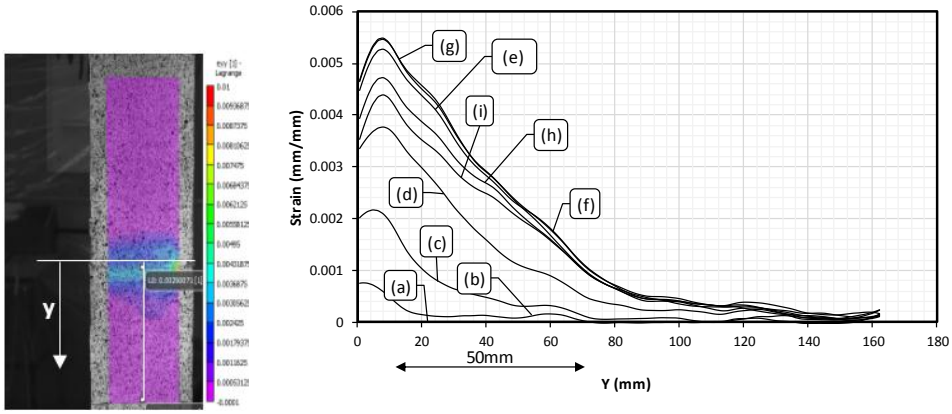

(a) (b)

Figure A1.20: (a) Contour Diagram Showing Position of Strain Inspector Line along the Bond Length of FRP Sheet (b) Strain versus Distance along the Bond Length of FRP at Times shown in Figure A1.19 for Specimen L160-S-3

Comments on Figure A1.20:

An anomaly in the strain curves at the critical section is observed. This may be due to the pair of prisms not properly aligned during the installation of the FRP sheets. The strain values increased as the load increased over time. The slope of the curves (effective bond length) began to shift towards the unloaded end of FRP sheet with almost flat segments at the loaded end that indicates the initiation of wedge cracks.

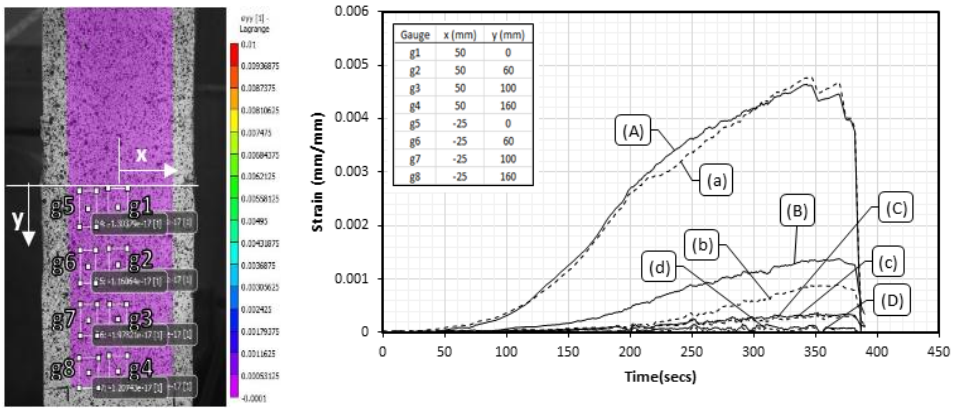

(a) (b)

Figure A1.21:(a) Contour Diagram Showing Position of 8 Gauges (b) Strain versus Time Curves of Specimen at Locations of Gauges as Indicated in the Contour Diagram in (a) for Specimen L160-S-3

Comments on Figure A1.21:

Generally, gauges (g1), (g2), (g3) and (g4) recorded higher strain values than (g5), (g6), (g7) and (g8) due to shear lag and load eccentricity effect. Strain at gauges (g1) and (g5) were significantly higher than those obtained from other gauges. This may be due to the FRP sheet on the back face of the specimen failing prematurely.

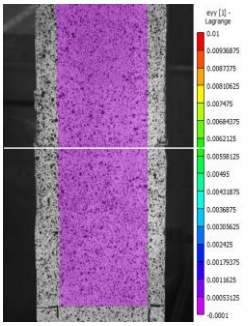

(a) ε_{yy} Dist. at T= 0 s

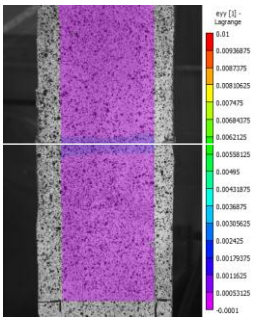

(b) ε_{yy} Dist. at T= 102 s

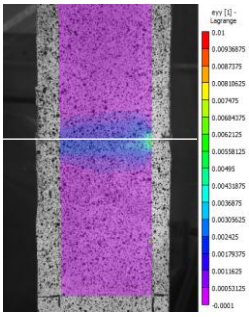

(c) ε_{yy} Dist. at T= 156 s

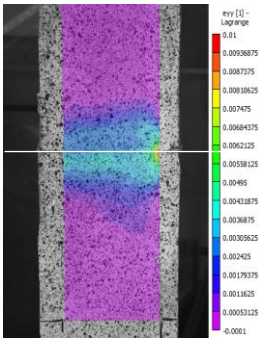

(d) ε_{yy} Dist. at T= 219 s

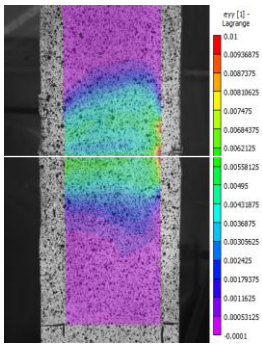

(e) ε_{yy} Dist. at T= 350 s

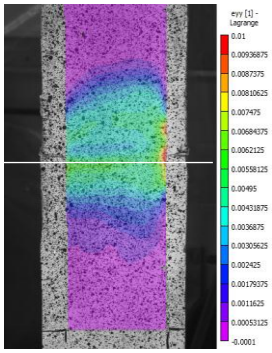

(f) ε_{yy} Dist. at T= 353 s

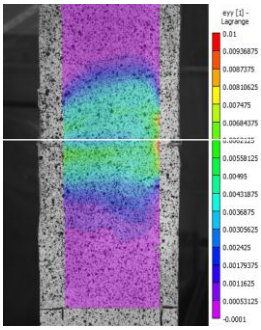

(g) ε_{yy} Dist. at T= 374 s

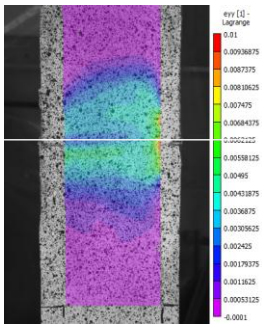

(h) ε_{yy} Dist.at T= 384 s

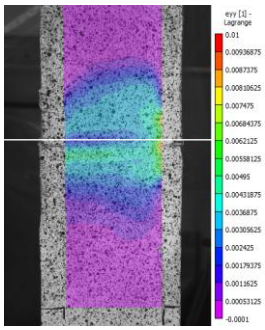

(i) ε_{yy} Dist.at T= 387 s

Figure A1.22: Strain Fields Showing distribution of longitudinal Strains on FRP Sheet at Different Times as Test Progressed to Failure for Specimen L160-S-3

Comments on Figure A1.22:

Contour diagrams show a gradual increase in longitudinal strain originating from the loaded region towards the unloaded region until failure. It is observed that only a fraction of the CFRP sheet being monitored by the DIC software was stressed before failure. Shear lag effect was not dominant in this specimen.

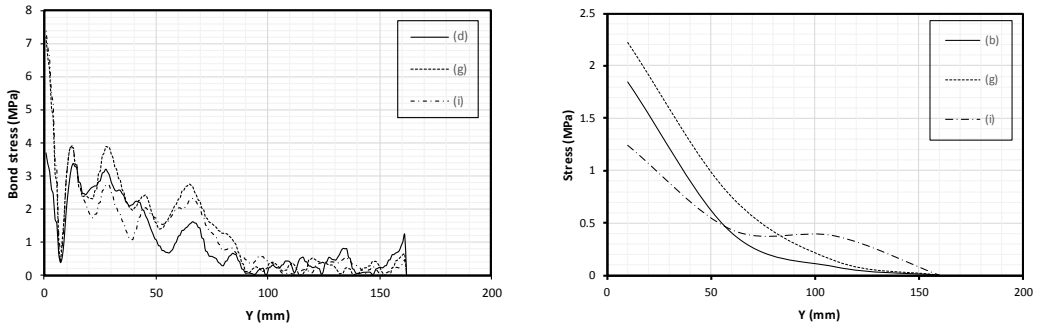

(a) (b)

Figure A1.23: Graph of Bond Stress along the CFRP Bond Length for Specimen L160-S-3 using (a) Equation 5.2 (b) Equation 5.3

Comments on Figure A1.23:

Shape of the curves in Figure A1.23(a) are similar to what was observed in specimens L160-S-1 and L160-S-2. Although not very evident in this specimen, the peak stress moved along the bond length of the CFRP sheet. Figure A!.23(b) however, does not give the expected shape of the curve for bond stress and bond length relationship.

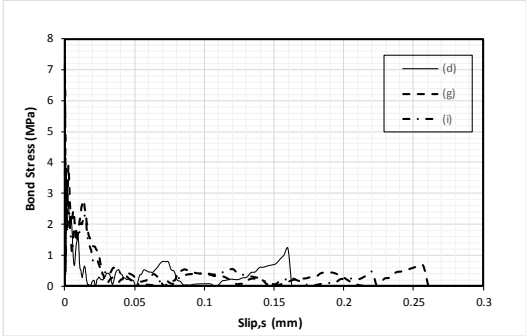

(a)

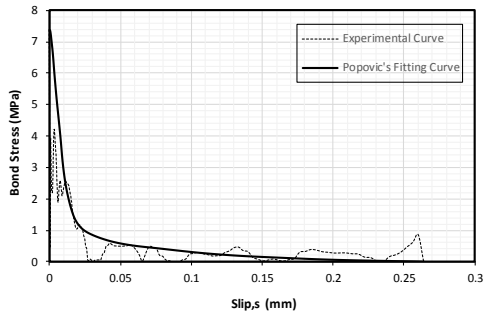

(b)

Figure A1.24: Relationship between Bond Stress and Slip for Specimen L160-S-3 at varying Load Levels and the Corresponding Fitting Curve

Comments on Figure 6.24

From Figure 6.24(a), the bond-slip relationship gives a curve with a sharp increase at the initial stage of the test as observed in previously discussed specimens. There is also a correlation between the fitting model proposed by Popovic and the experimental curve.

A.2 Dimensions and Test Properties for Specimens L240-S

Specimens Dimensions:

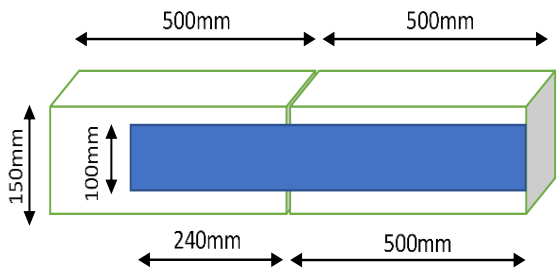

Figure A2.1: FRP Sheet Bonded to Concrete for Specimens L240-S

Testing Machine: Baldwin Testing Machine

Date of Test: July 21st, 2017

Test Type: Double Lap Pull-out Bond Test

Bond Length:240mm

Loading Rate: 0.5mm/min

Picture time Interval: 400ms

A2.1 Results for Specimen L240-S-1

- Specimen Installed Prior to Testing

a) Front of Specimen b) Back of Specimen c) Side of Specimen

Figure A2.2: Views of Specimen L240-S-1 Installed in the Machine Prior to Testing

- Test Results

Pictures of Specimen after Testing:

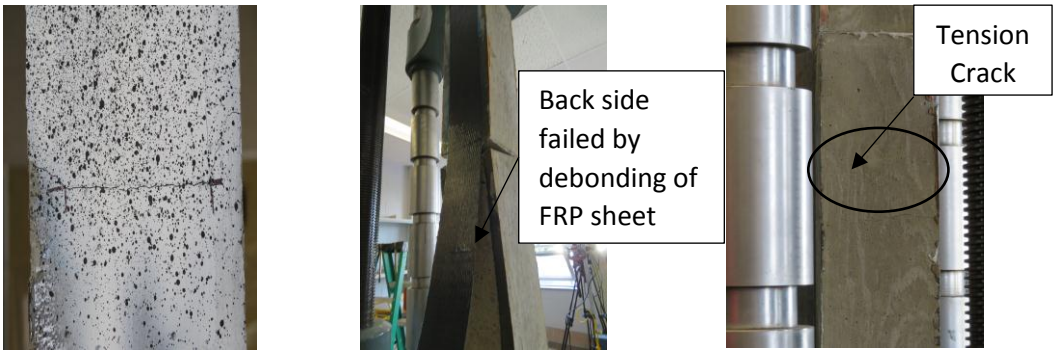

a) Front side b) Back Side c) Tension Crack

Figure A2.3: Views of Specimen L240-S-1 after Failure

Description Specimen L240-S-1 after Failure

It was observed that the following happened to the specimen at/after failure:

- The specimen experienced brittle failure accompanied by a loud noise
- As seen in Figure A2.3(b), debonding failure of FRP sheet took place on the back side of the specimen.
- Tension crack normal to the force was developed on the right and left sides of the specimen extending towards the face bonded by the speckled CFRP sheet.
- Concrete wedge crack developed at the loaded end of the CFRP sheet
- The CFRP sheet was well bonded to concrete because debonding occurred by shearing of concrete below the bonded surface.
- The front side of the specimen failed due to buckling of the CFRP sheet immediately after the debonding failure of the back side took place. Tension crack also caused debonding to occur at the unloaded end of the CFRP sheet on the front side.

Analysis of Test Results

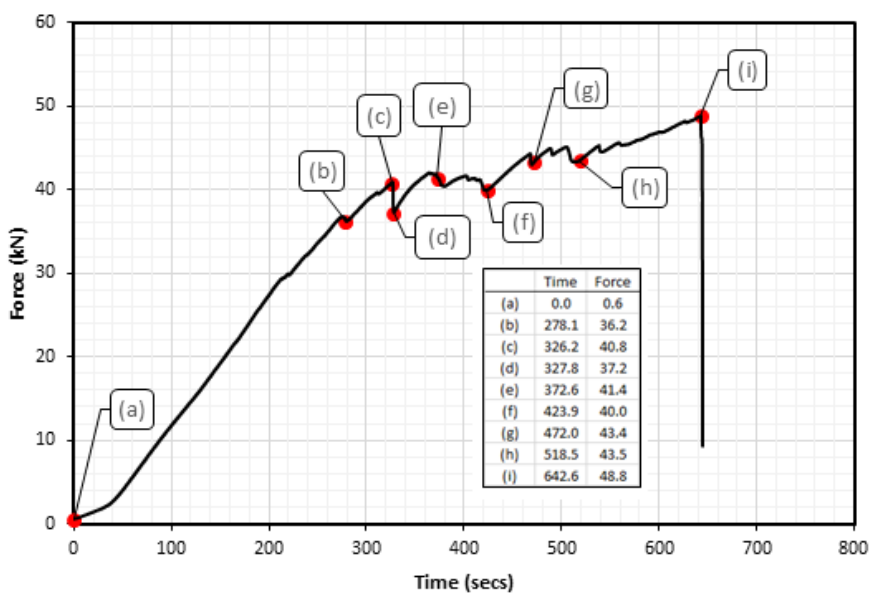

Figure A2.4: Force versus Time curve for Specimen L240-S-1 Showing Key Points During the Test

Comments on Figure A2.4:

Points (a) to (c) on the graph show the elastic behaviour of the specimen although a slight decrease in force occurred at point (b). A significant decrease in force occurred from point (c) to (d) after which there was a force increase to point (e). The applied force then increased gradually to point (i) with the force decreasing and gaining momentum in between. This fluctuation in force values may be due to the initiation of wedge and tension cracks on the prisms.

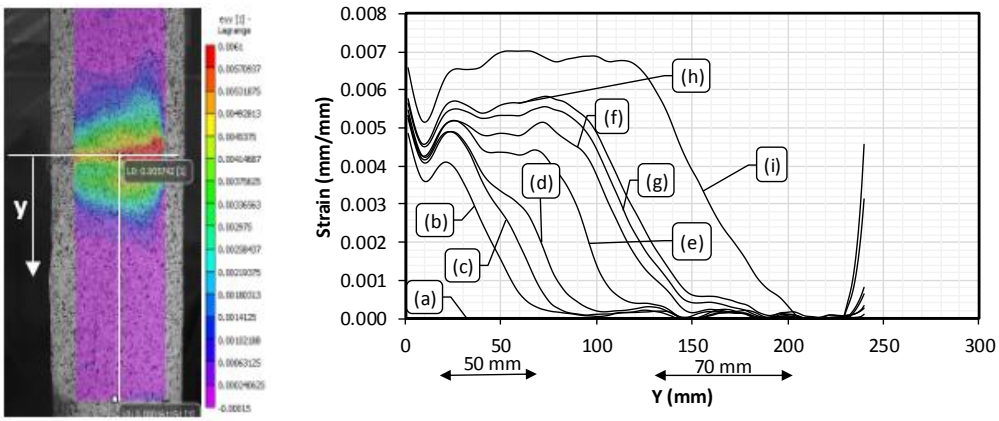

(a) (b)

Figure A2.5: (a) Contour Diagram Showing Position of Strain Inspector Line along the Bond Length of FRP Sheet (b) Strain versus Distance along the Bond Length of FRP Sheet at Times shown in Figure A2.4 for Specimen L240-S-1

Comments on Figure A2.5:

An anomaly in the strain curves at the loaded end of the FRP sheet is observed. This may be due to the pair of prisms not properly aligned as observed before the test was carried out. The strain values increased as the load increased over time. The shift in the active bond (development length) zone as the experiment proceeded is also observed in this CFRP sheet. Strain curves increased gradually to (i) before failure.

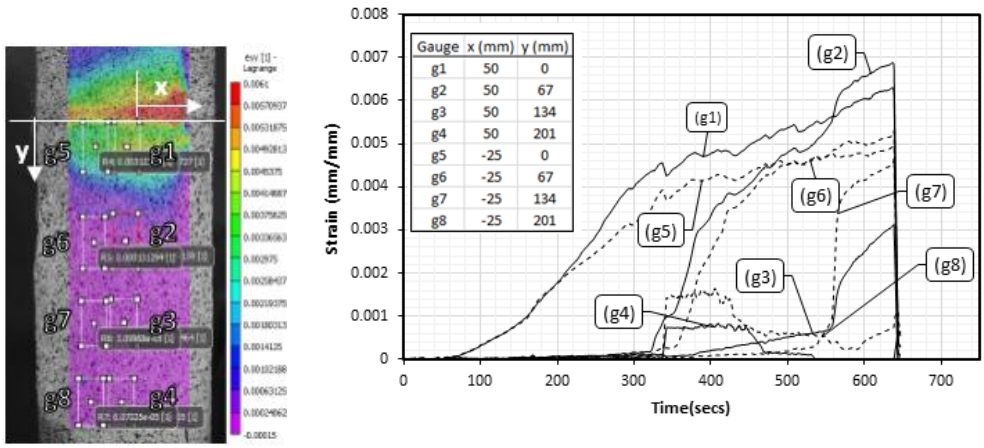

(a) (b)

Figure A2.6: (a) Contour Diagram Showing Position of 8 Gauges (b) Strain versus Time Curves of Specimen at Locations of Gauges as Indicated in the Contour Diagram in (a) for Specimen L240-S-1

<u>Comments on Figure A2.6:</u>

Gauges (g1) and (g2) recorded higher strain values than (g5) and (g6). However, gauges (g7) and (g8) recorded higher strain values than (g3) and (g4) due to shear lag and load eccentricity effect as stated before. Strain at Gauges (g2) and (g6), (g3) and (g7) and (g4) and (g8) only started to increase after the redistribution of stresses caused by the initiation of the concrete wedge and tension cracks.

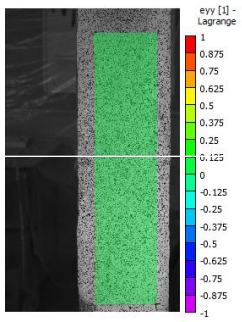

(a) ε_{yy} Dist. at T= 0 s

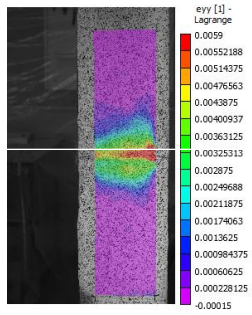

(b) ε_{yy} Dist. at T= 278 s

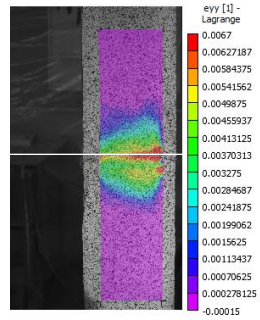

(c) ε_{yy} Dist. at T= 326 s

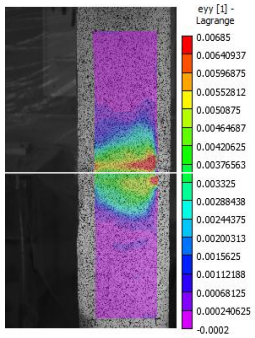

(d) ε_{yy} Dist. at T= 328s

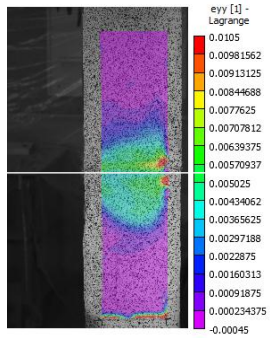

(e) ε_{yy} Dist. at T= 373 s

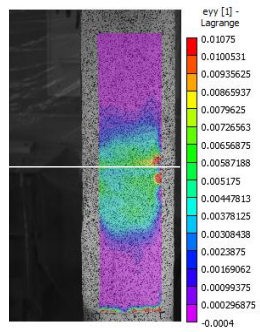

(f) ε_{yy} Dist. at T= 424 s

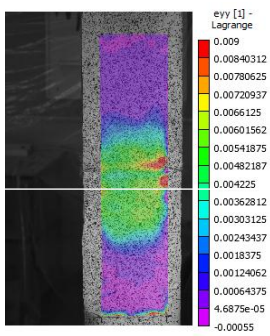

(g) ε_{yy} Dist. at T= 472 s

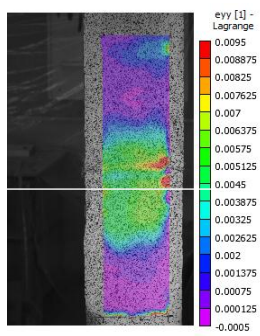

(h) ε_{yy} Dist. at T= 519 s

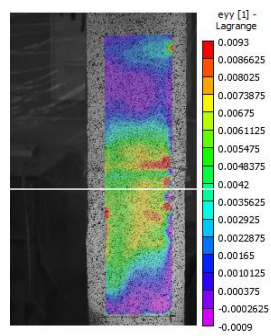

(i) ε_{yy} Dist. at T= 642 s

Figure A2.7: Strain Fields Showing the Distribution of Longitudinal Strains (ε_{yy}) on FRP Sheet at Different Times as Test Progressed to Failure for Specimen L240-S-1

<u>Comments on Figure A2.7:</u>

Contour diagrams show a gradual increase in longitudinal strain originating from the loaded end towards the unloaded end of the FRP sheet until failure. The tension crack at the end of the CFRP sheet caused stresses and subsequent plate end debonding to occur as seen in the figures. Shear lag effect was significant in the specimen as seen in the uneven distribution of strain along the width of the CFRP sheet.

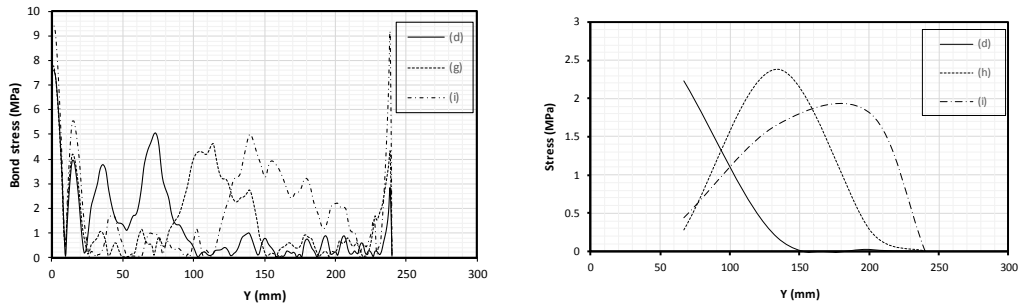

(a) (b)

Figure A2.8: Graph of Bond Stress along the CFRP Sheet Bond Length of Specimen L240-S-1 using (a) Equation 5.2 (b) Equation 5.3

Comments on Figure A2.8:

Curves in Figure A2.8(a) showed high stress values at the loaded and unloaded end of the FRP sheet, but this is not observed in Figure A2.8(b). Equation 5.3 gave smoother curves due to the limitation in data points compared to curves obtained from Equation 5.2 as earlier stated.

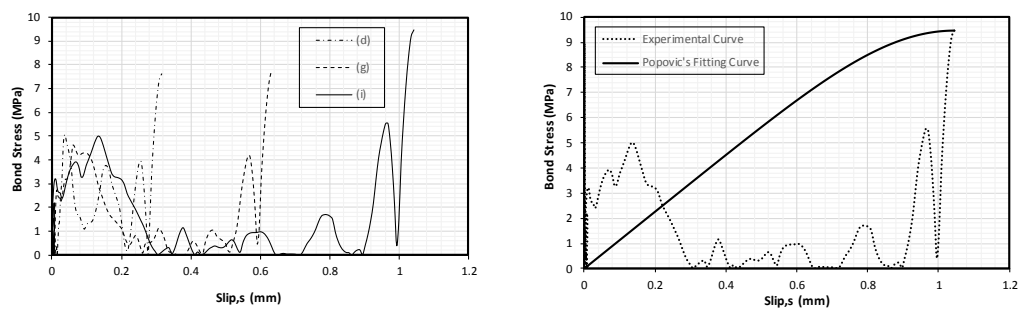

(a) (b)

Figure A2.9: Relationship between Bond Stress and Slip for Specimen L240-S-1 at varying Load Levels and the Corresponding Fitting Curve

Comments on Figure A2.9:

The Popovic's fitting cure does not correspond to the experimental values obtained. This may be due to experimental error because the CFRP sheet in this specimen failed on the back side.

A2.2 Results for Specimen L240-S-2

- Specimen Installed Prior to Testing

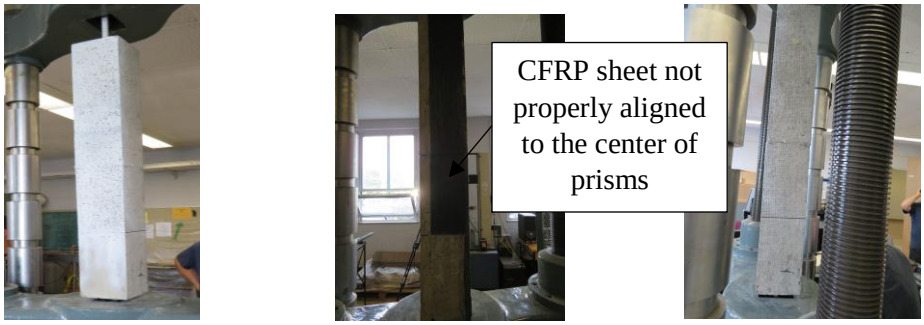

a) Front of Specimen b) Back of Specimen c) Side of Specimen

Figure A2.10: Views of Specimen L240-S-2 Installed in Testing Machine Prior to Testing

- Test Results

Pictures of Specimen after Testing:

a) Front side b) Right Side c) Left side

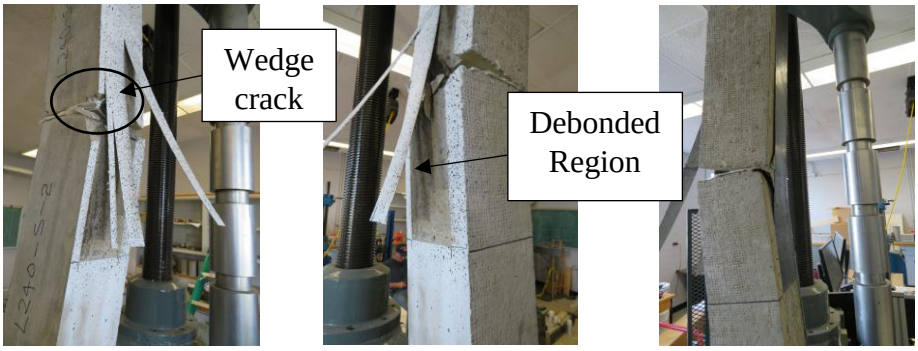

d) Wedge Failure e) Debonded Region f) Back Side

Figure A2.11: Views of Specimen L240-S-2 after Failure

Description of Specimen L240-S-2 before and after Failure:

Prior to testing, it was observed that the CFRP sheet was not properly aligned to the center of the pair of prisms. The CFRP sheet on the opposite side that was monitored was cut so that it is equal to the bond length to be studied. This was because specimens L160-S-3 and L240-S-1 failed on the longer side prematurely. It was observed that the following happened to the specimen at/after failure:

- The specimen experienced brittle failure accompanied by a loud noise
- As seen in Figure A2.11(a), failure took place on the speckled side of the specimen.
- Tension crack normal to the force was developed on the right and left sides of the specimen but not evident in the pictures provided.
- Concrete wedge crack occurred at the loaded end of the CFRP sheet as seen in Figure A2.11(d)
- The CFRP sheet was well bonded to concrete because debonding occurred by shearing of concrete below the bonded surface as seen in Figure A2.11(e)
- The back side of the specimen failed due to buckling of the FRP sheet immediately after the debonding failure of the front side took place as shown in Figure A2.11(f).

Analysis of Test Results

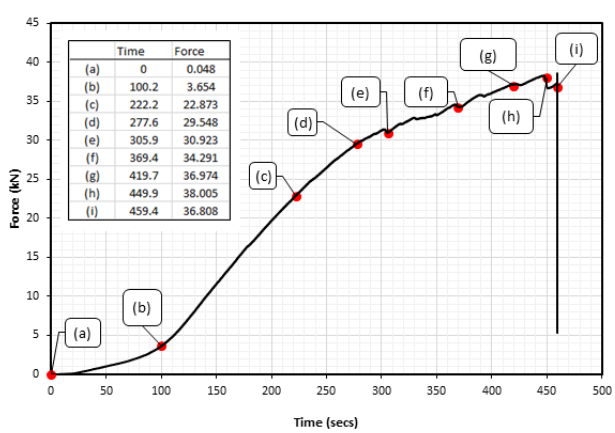

	Time	Force
(a)	0	0.048
(b)	100.2	3.654
(c)	222.2	22.873
(d)	277.6	29.548
(e)	305.9	30.923
(f)	369.4	34.291
(g)	419.7	36.974
(h)	449.9	38.005
(i)	459.4	36.808

Figure A2.12: Force versus Time curve for Specimen L240-S-2 Showing Key Points During the Test

Comments on Figure A2.12:

The increase in force was gradual except for some minimal fluctuation in force at points (e), (f), (g) and (h). Maximum load was at point (h) before failure occurred at point (i).

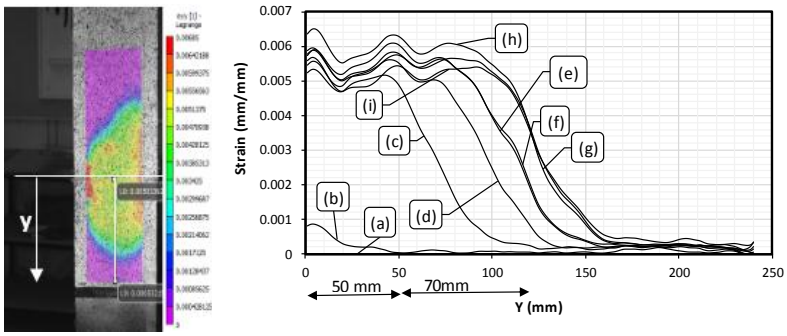

(a) (b)

Figure A2.13: (a) Contour Diagram Showing Position of Strain Inspector Line along the Bond Length of FRP Sheet (b) Strain versus Distance along the Bond Length of FRP Sheet at Times shown in Figure A2.12 for Specimen L240-S-2

Comments on Figure A2.13:

The strain values increased as the load increased over time. Curve (b) is elastic but as the curve moved to (c), the slope (effective bond length) began to shift towards the unloaded end of FRP sheet with flat segments at the loaded end. This indicates the initiation of wedge cracks. At (h), there was a decrease in strain to (i) due to a corresponding decrease in load.

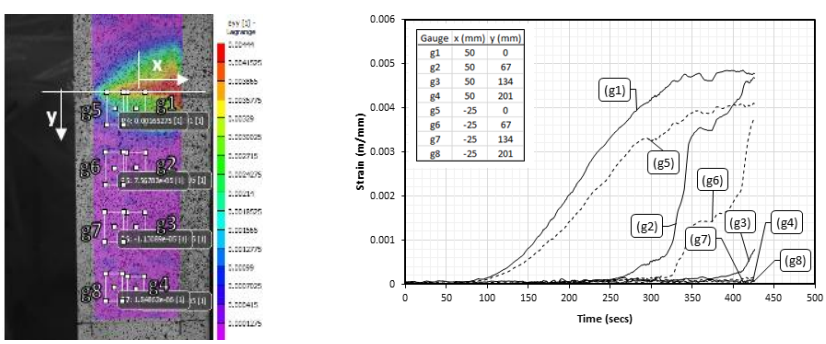

(a) (b)

Figure A2.14:(a): Contour Diagram Showing Position of 8 Gauges (b): Strain versus Time Curves of Specimen at Locations of Gauges as Indicated in the Contour Diagram in (a)for Specimen L240-S-2

Comments on Figure A2.14:

Gauges (g1), (g2), and (g3) recorded higher strain values than (g5), (g6) and (g7) due to shear lag and load eccentricity effect. Strain at Gauges (g6) and (g4) and (g8) did not experience a significant increase in strain from the zero position due to that region not being stress before premature failure of the FRP sheet on the back face of the specimen.

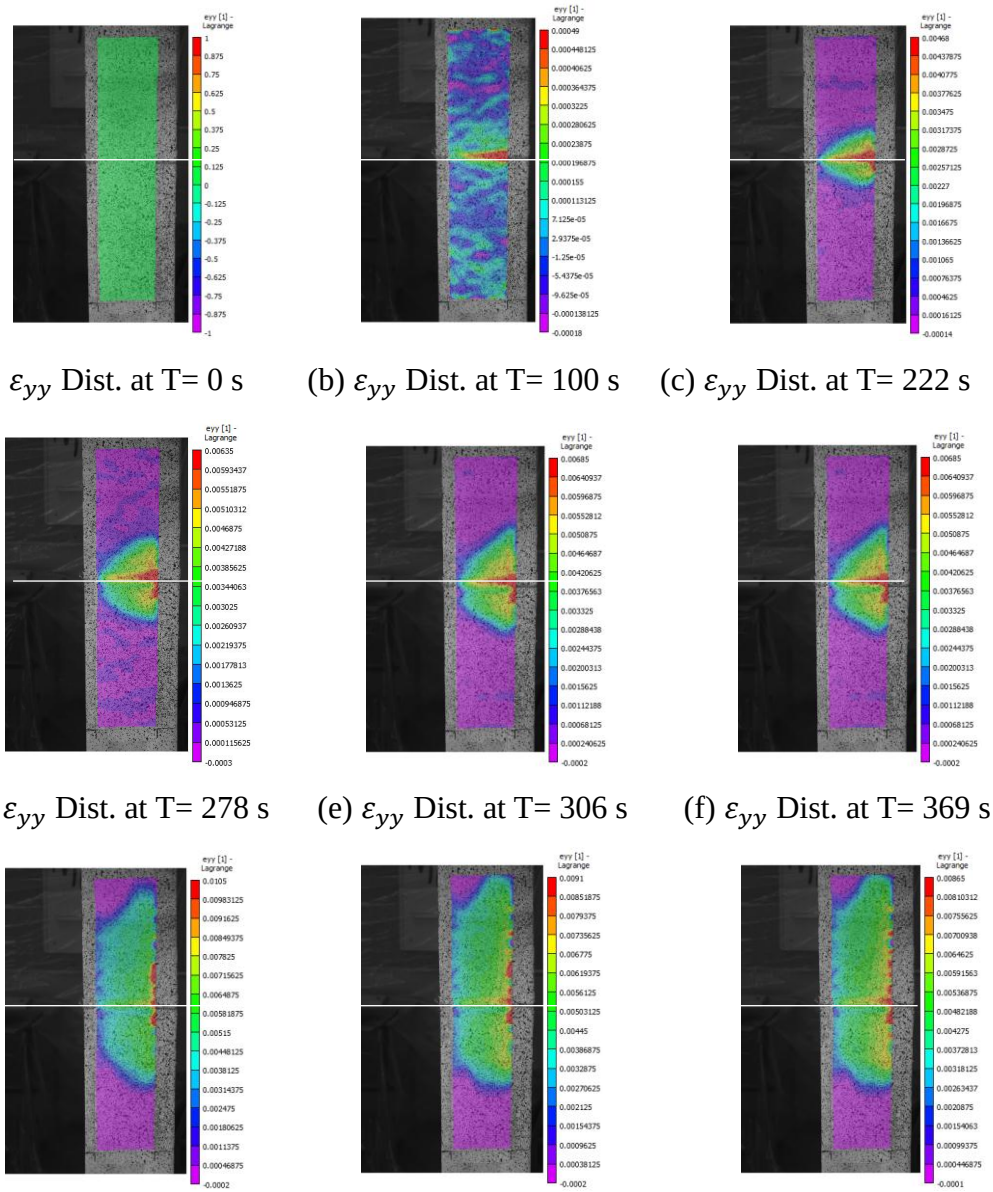

(a) ε_{yy} Dist. at T= 0 s (b) ε_{yy} Dist. at T= 100 s (c) ε_{yy} Dist. at T= 222 s

(d) ε_{yy} Dist. at T= 278 s (e) ε_{yy} Dist. at T= 306 s (f) ε_{yy} Dist. at T= 369 s

(g) ε_{yy} Dist. at T= 418 s (h) ε_{yy} Dist. at T= 450 s (i) ε_{yy} Dist. at T= 459 s

Figure A2.15: Strain Fields Showing distribution of longitudinal Strains on FRP at Different Times as Test Progressed to Failure for Specimen L240-S-2

Comments on Figure A2.15:

Contour diagrams show a gradual increase in longitudinal strain originating from the loaded section towards the unloaded section until failure. The wedge crack and the tension crack did not show a significant effect in the contour diagrams. Shear lag effect was significant in the specimen as seen in the parabolic distribution of strain across the width of the CFRP sheet.

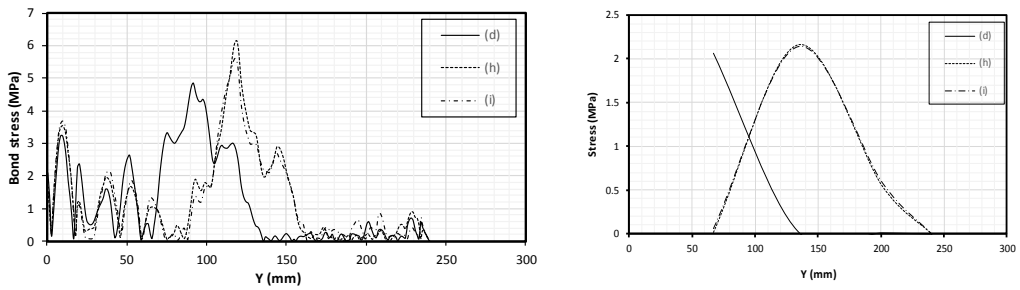

(a) (b)

Figure A2.16: Graph of Bond Stress along CFRP bond Length of Specimen L240-S-2 using (a) Equation 5.2 (b) Equation 5.3

Comments on Figure A2.16:

Both curves show similar trend where the maximum bond stress moved along the length of the CFRP sheet towards the unloaded end. This behaviour is like the strain profile where the active bond zone (development length) moved towards the unloaded end of the specimen. Equation 5.3 gave smoother curves due to the limitation in data points compared to curves obtained from Equation 5.2.

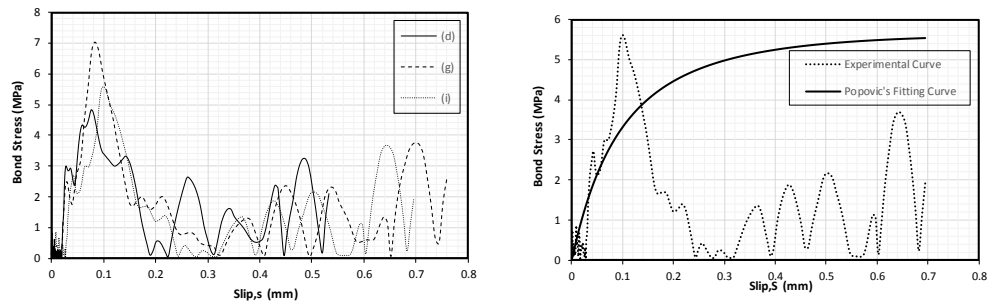

(a) (b)

Figure A2.17: Relationship between Bond Stress and Slip for Specimen L240-S-2 at varying Load Levels and the Corresponding Fitting Curve

<u>Comments on Figure A2.17:</u>

From Figure A2.17(a), the bond-slip relationship gives a curve with a sharp increase at the initial stage of the test. The descending region correlates with the elastic strain distribution which moves along the along the bond length of the CFRP sheet as debonding cracks propagates towards the unloaded end. There is a correlation between the curves as both follow the same trend as observed from Figure A2.17(b).

A2.3 Results for Specimen L240-S-3

- Specimen Installed Prior to Testing

a) Front of Specimen b) Back of Specimen c) Side of Specimen

Figure A2.18: Views of Specimen L240-S-3 Installed in Testing Machine Prior to Testing

- Test Results

Pictures of Specimen after Testing:

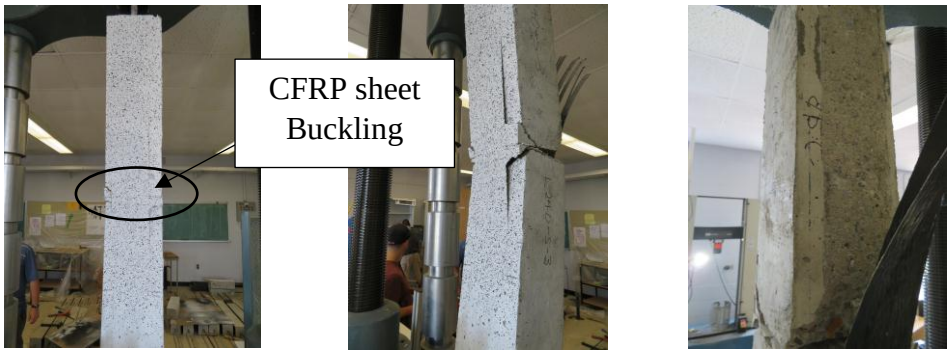

a) Front side b) Right Side c) Close-up of Back side

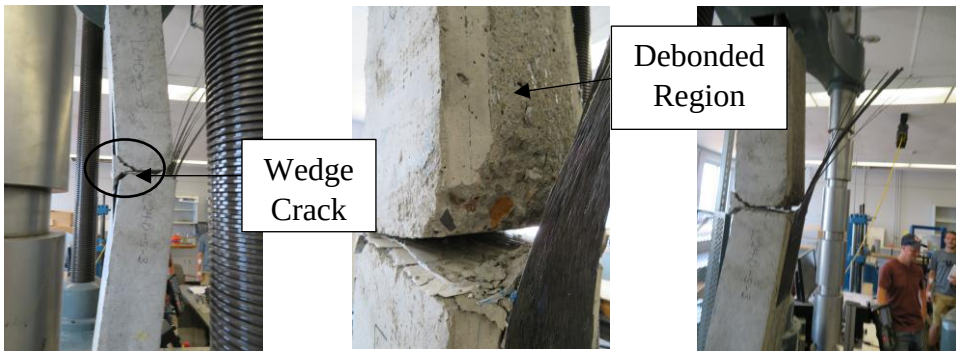

d) Wedge Failure e) Debonded Region f) Back Side

Figure A2.19: Views of Specimen L240-S-3 after Failure

Description Specimen L240-S-3 before and after Failure:

The CFRP sheet bonded to the back of the prims was not properly aligned to the center of the prisms before testing. It was observed that the following happened to the specimen at/after failure:

- The specimen experienced brittle failure accompanied by a loud noise
- As seen in Figure A2.19(c), failure took place on the CFRP sheet bonded to the back face of the specimen.
- Tension crack was not seen in this specimen which may be due to premature debonding failure.
- Concrete wedge crack occurred at the loaded end of the specimen as seen in Figure A2.19(d)
- The CFRP sheet was well bonded to concrete because debonding occurred by shearing of concrete below the bonded surface as seen in Figure A2.19(e)
- The front side of the specimen failed due to buckling of the FRP sheet immediately after the debonding failure of the front side took place.

Analysis of Test Results

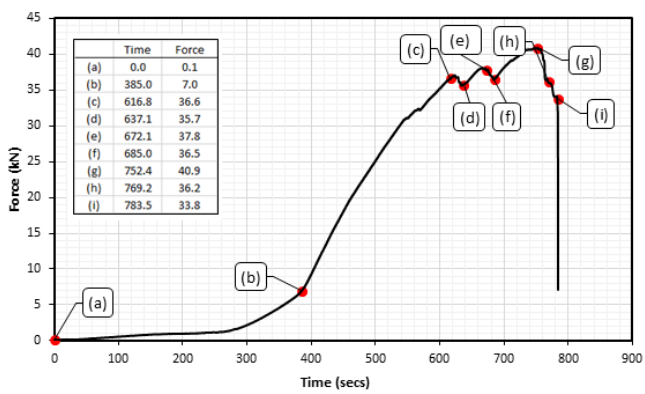

Figure A2.20: Force versus Time curve for Specimen L240-S-3 Showing Key Points During the Test

Comments on Figure A2.20:

Points (a), (b) and (c) on the graph show the gradual increase in force until the force decreased to point (d). The force increased to (e) and then dropped to point (f). A maximum force was attained at point (h) and then the force decreased to point (i) before failure.

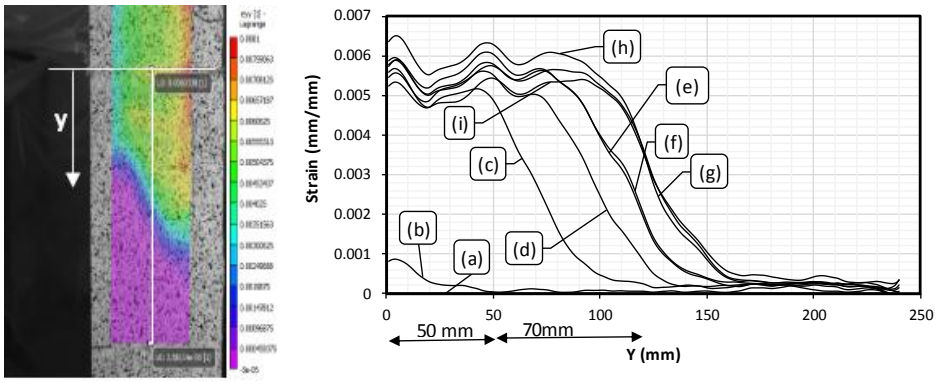

(a) (b)

Figure A2.21: (a) Contour Diagram Showing Position of Strain Inspector Line along the Bond Length of FRP Sheet (b) Strain versus Distance along the Bond Length of FRP Sheet at Times shown in Figure A2.20 for Specimen L240-S-3

Comments on Figure A2.21:

The strain values increased as the load increased over time. Curve (b) is elastic but as the curve moved to (c), the slope (effective bond length) began to shift towards the unloaded end of FRP with flat segments at the loaded end. This indicates the initiation of cracks. Maximum strain was at (h) with a decrease to (i) before failure.

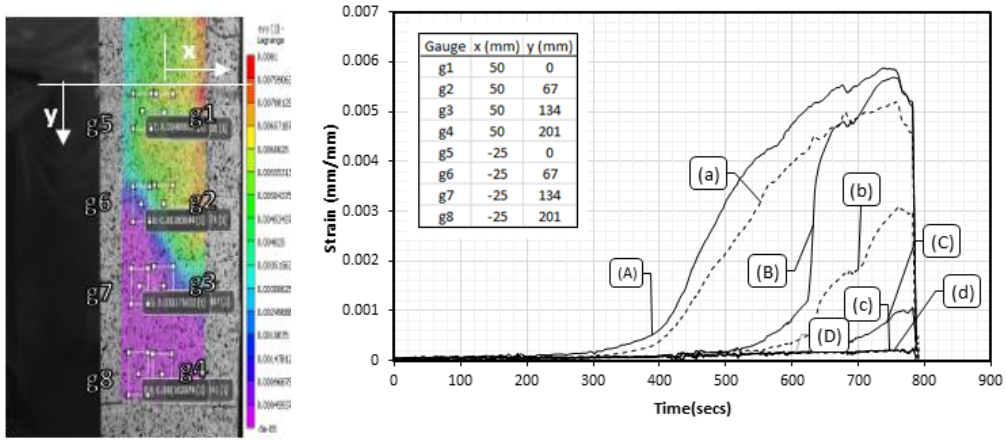

(a) (b)

Figure A2.22: (a) Contour Diagram Showing Position of 8 Gauges (b) Strain versus Time Curves of Specimen at Locations of Gauges as Indicated in the Contour Diagram in (a) for Specimen L240-S-3

Comments on Figure A2.22:

Gauges (g1), (g2) and (g3) recorded higher strain values than (g5), (g6) and (g7). Strain values in gauges (g4) and (g8) are almost equal as they recorded no significant amount of strain before failure. Difference in strain is due to shear lag and load eccentricity effect.

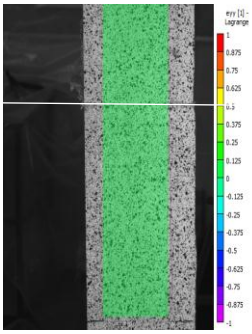

(a) ε_{yy} Dist. at T= 0 s

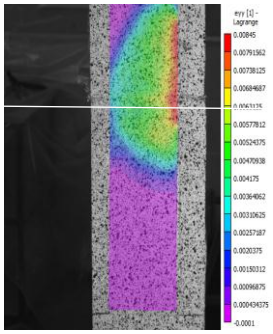

(b) ε_{yy} Dist. at T= 385 s

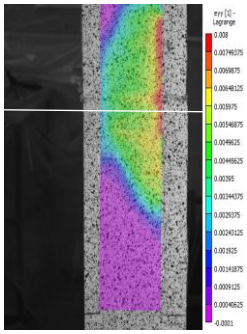

(c) ε_{yy} Dist. at T= 617 s

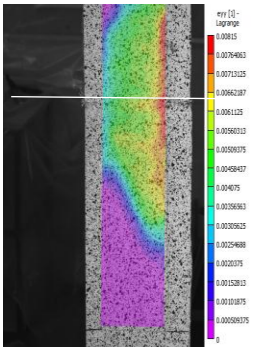

(d) ε_{yy} Dist. at T= 637 s

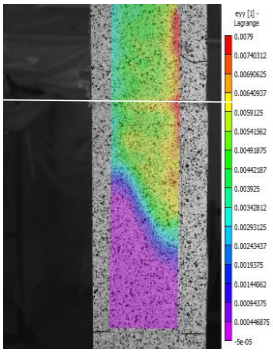

(e) ε_{yy} Dist. at T= 672 s

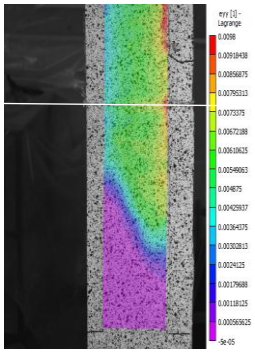

(f) ε_{yy} Dist. at T= 685 s

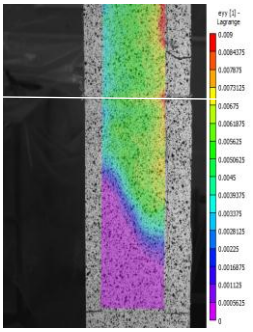

(g) ε_{yy} Dist. at T= 752 s

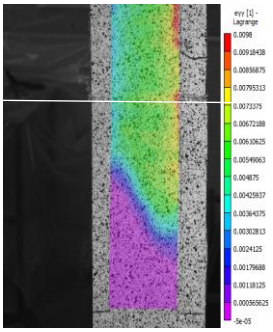

(h) ε_{yy} Dist. at T= 769 s

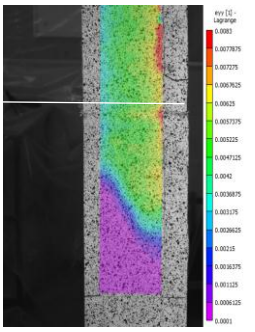

(i) ε_{yy} Dist. at T= 784 s

Figure A2.23: Strain Fields Showing distribution of longitudinal Strains (ε_{yy}) on the FRP Sheet at Different Times as Test Progressed to Failure for Specimen L240-S-3

Comments on Figure A2.23:

Contour diagrams show a gradual increase in longitudinal strain originating from the loaded end of the FRP sheet towards the unloaded end until failure. The shear lag and eccentricity effect are very evident in the diagrams presented as seen in the uneven distribution of strain along the width of the CFRP sheet.

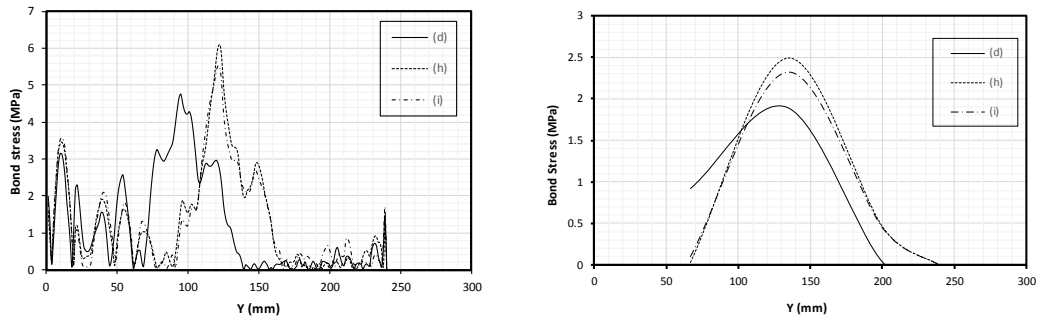

(a) (b)

Figure A2.24: Graph of Bond Stress along CFRP bond Length of Specimen L240-S-3 using (a) Equation 5.2 (b) Equation 5.3

Comments on Figure A2.24:

Both curves show similar trend where the maximum bond stress moved along the length of the CFRP sheet towards the unloaded end. This behaviour is like the strain profile where the active bond zone (development length) moved towards the unloaded end of the FRP sheet. Equation 5.3 gave smoother curves due to the limitation in data points compared to curves obtained from Equation 5.2.

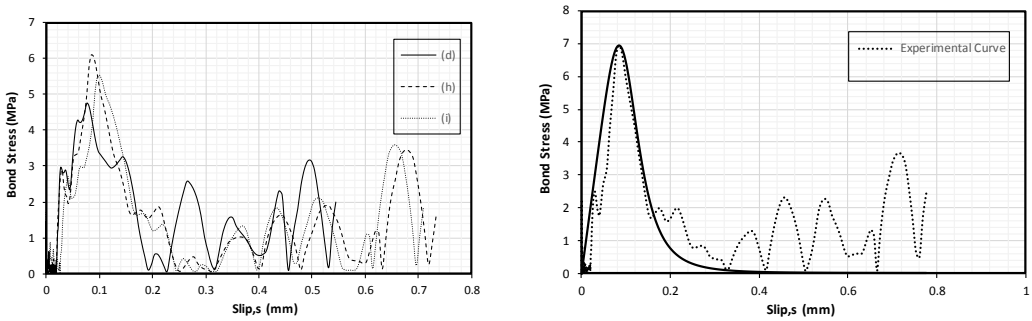

(a) (b)

Figure A2.25: Relationship between Bond Stress and Slip for Specimen L240-S-3 at varying Load Levels and the Corresponding Fitting Curve

Comments on Figure A2.25:

From Figure A2.25(a), the bond-slip relationship gives a curve with a sharp increase at the initial stage of the test. The descending region correlates with the elastic strain distribution which moves along the bond length of the CFRP sheet as debonding cracks propagates towards the unloaded end. There is a correlation between the experimental curve and the fitting curve as both follow the same parabolic trend as observed from Figure A2.25(b).

A.3 Dimensions and Test Properties for Specimens L350-S

Specimens Dimensions:

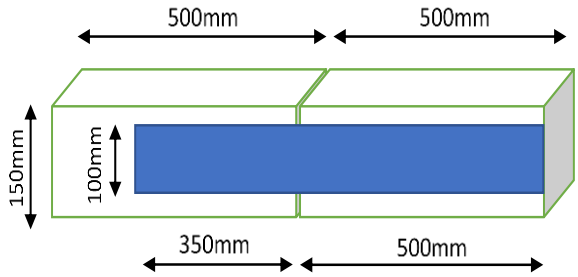

Figure A3.1: FRP Sheet Bonded to concrete for Specimens L350-S

Testing Machine: Universal Testing Machine

Date of Test: July 24th, 2017

Test Type: Pullout Bond Test

Bond Length:350mm

Loading Rate: 0.5mm/min

Picture time Interval: 400ms

Material Type: Concrete and FRP

A3.1 Results for Specimen L350-S-2

- Specimen Installed Prior to Testing

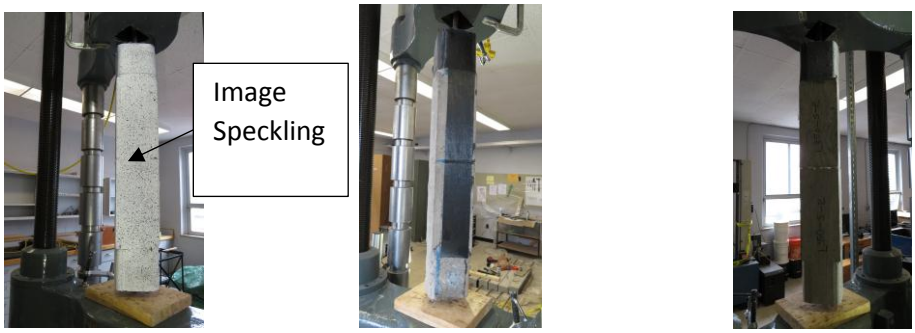

a) Front of Specimen b) Back of Specimen c) Side of Specimen

Figure A3.2: Views of Specimen L350-S-2 Installed in Testing Machine Prior to Testing

- Test Results

Pictures of Specimen after Testing:

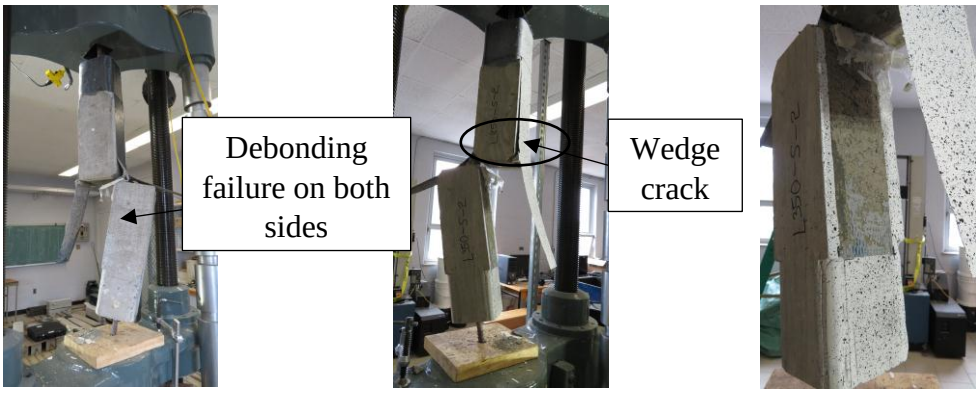

a) Front side b) Right Side c) Left side

Figure A3.3: Views of Specimen L350-S-2 after Failure

Description of Specimen L350-S-2 before and after Failure

Prior to the test, it was observed that the FRP sheets installed on opposite sides of the prism was offset from the center. It was observed that the following happened to the specimen after failure:

- The specimen experienced brittle failure accompanied by a loud noise
- As seen in Figure A3.3(a), failure took place on both sides of the specimen by debonding of the FRP sheets.
- Tension cracks were not observed in this specimen.
- Concrete wedge crack occurred at the loaded end of the FRP sheet as seen in Figure A3.3(b)
- The CFRP sheet was well bonded to concrete because debonding occurred by shearing of concrete below the bonded surface as seen in Figure A3.3(c)

Analysis of Test Results

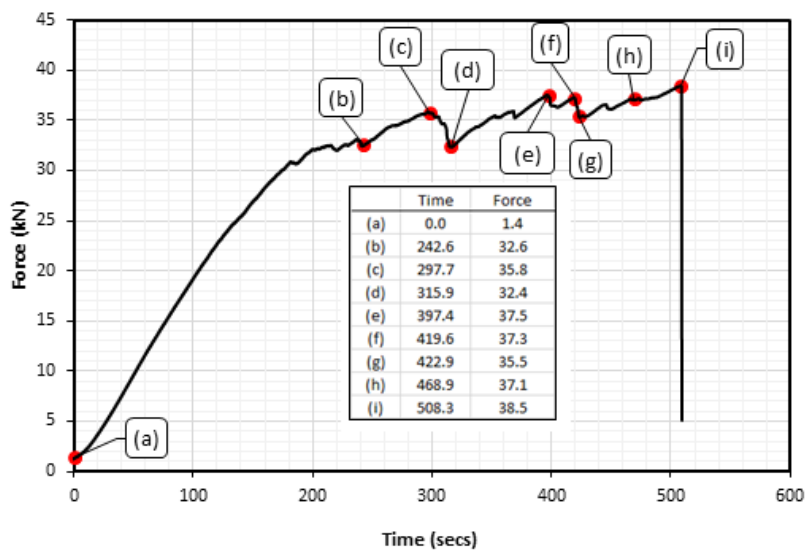

Figure A3.4: Force versus Time curve for Specimen L350-S-2 Showing Key Points During the Test

Comments on Figure A3.4:

The force increased over time during the test. Force values decreased and then increased at different times. A significant decrease in force was from point (c) to (d) which may have been due to the initiation of the wedge crack at the loaded end of the FRP sheet.

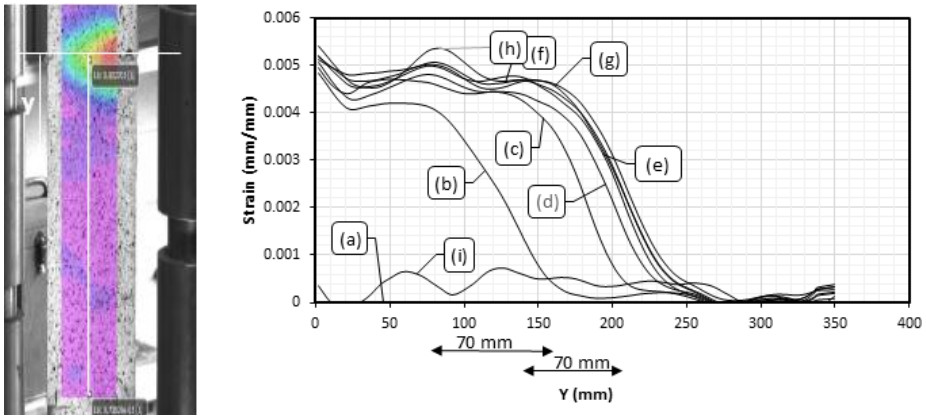

(a) (b)

Figure A3.5: (a) Contour Diagram Showing Position of Strain Inspector Line along the Bond Length of FRP Sheet (b) Strain versus Distance along the Bond Length of FRP Sheet at Times shown in Figure A3.4 for Specimen L350-S-2

<u>Comments on Figure A3.5:</u>

The strain values increased as the load increased over time. It is observed that the maximum strain was at (h) after which the strain values decreased to (i) before failure. The development length also moved towards the unloaded end of the FRP sheet as observed in other specimens.

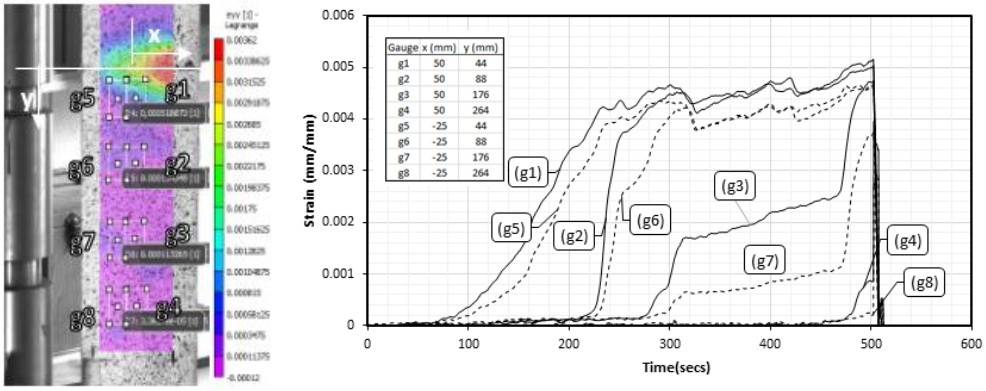

(a) (b)

Figure A3.6:(a) Contour Diagram Showing Position of 8 Gauges (b) Strain versus Time Curves of Specimen at Locations of Gauges as Indicated in the Contour Diagram in (a) for Specimen L350-S-2

Comments on Figure A3.6:

Gauges (g1), (g2), (g3) and (g4) recorded higher strain values than (g5), (g6), (g7) and (g8) due to shear lag and load eccentricity effect. All Gauges except gauges (g1) and (g5) started to increase only after the redistribution of stresses caused by the initiation of the concrete wedge crack.

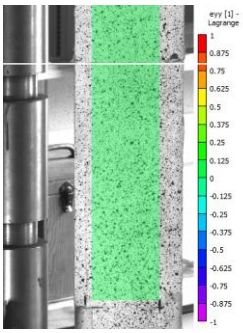

(a) ε_{yy} Dist. at T= 0 s

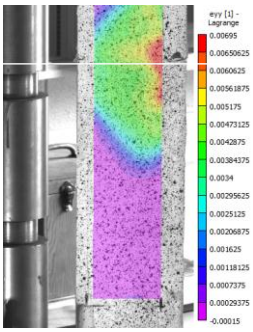

(b) ε_{yy} Dist. at T= 243 s

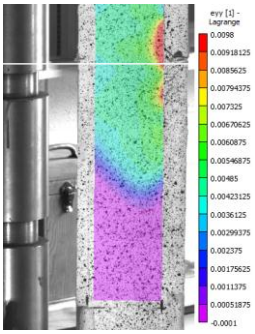

(c) ε_{yy} Dist. at T= 298 s

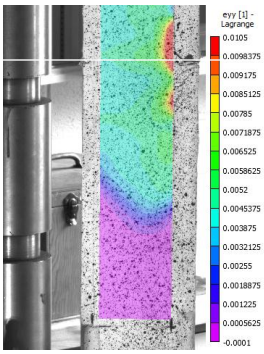

(d) ε_{yy} Dist. at T= 316 s

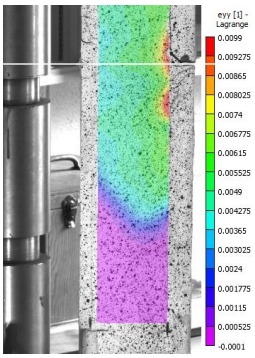

(e) ε_{yy} Dist. at T= 397 s

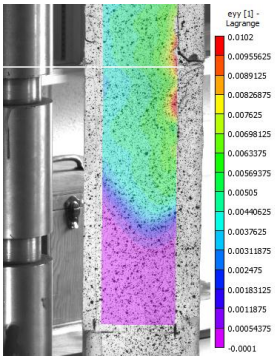

(f) ε_{yy} Dist. at T= 420 s

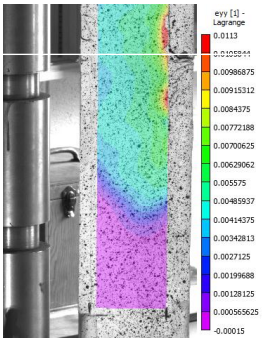

(g) ε_{yy} Dist. at T= 423 s

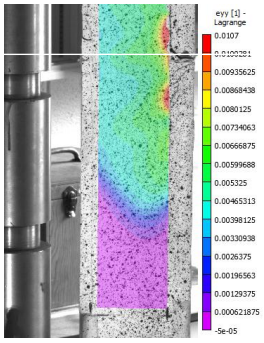

(h) ε_{yy} Dist. at T= 469 s

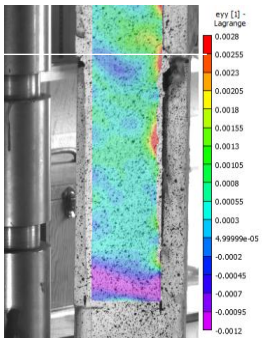

(i) ε_{yy} Dist. at T= 508 s

Figure A3.7: Strain Fields Showing distribution of longitudinal Strains (ε_{yy}) on FRP Sheet at Different Times as Test Progressed to Failure for Specimen L350-S-2

Comments on Figure A3.7:

Contour diagrams show a gradual increase in longitudinal strain originating from the loaded end towards the unloaded end of the FRP sheet until failure. Shear lag effect was significant in the specimen as seen in the uneven distribution of strain across the width of the CFRP sheet.

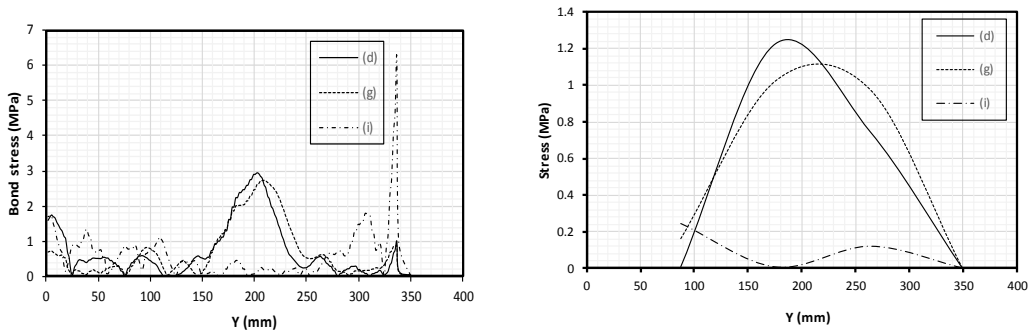

(a) (b)

Figure A3.8: Graph of Bond Stress along CFRP Sheet Bond Length of Specimen L350-S-2 using (a) Equation 5.2 (b) Equation 5.3

Comments on Figure A3.8:

Both curves show similar trend where the maximum bond stress moved along the length of the CFRP sheet towards the unloaded end. This behaviour is like the strain profile where the active bond zone (development length) moved towards the unloaded end of the specimen. Equation 5.3 gave smoother curves due to the limitation in data points compared to curves obtained from Equation 5.2.

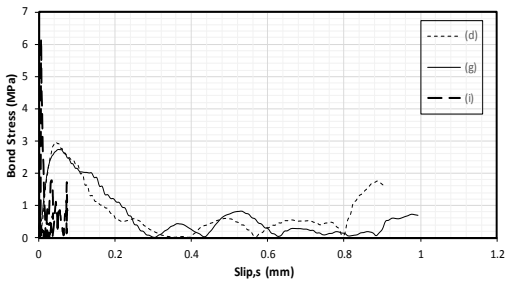

(a)

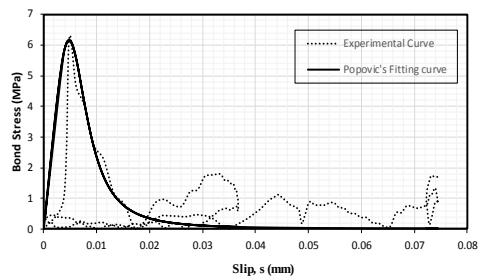

(b)

Figure A3.9: Relationship between Bond Stress and Slip for Specimen L350-S-2 at varying Load Levels and the Corresponding Fitting Curve

Comments on Figure A3.9:

From Figure A3.9(a), the bond-slip relationship gives a curve with a sharp increase at the initial stage of the test. The descending region correlates with the elastic strain distribution which moves along the bond length of the CFRP sheet as debonding propagates towards the unloaded end of the FRP sheet. There is a correlation between the experimental curve and the fitting curve as both follow the same trend as observed from Figure A3.9(b).

A3.2 Results for Specimen L350-S-3

- Specimen Installed Prior to Testing

a) Front of Specimen b) Back of Specimen c) Side of Specimen

Figure A3.10: Views of Specimen L350-S-3 Installed in Testing Machine Prior to Testing

- Test Results

Pictures of Specimen after Testing:

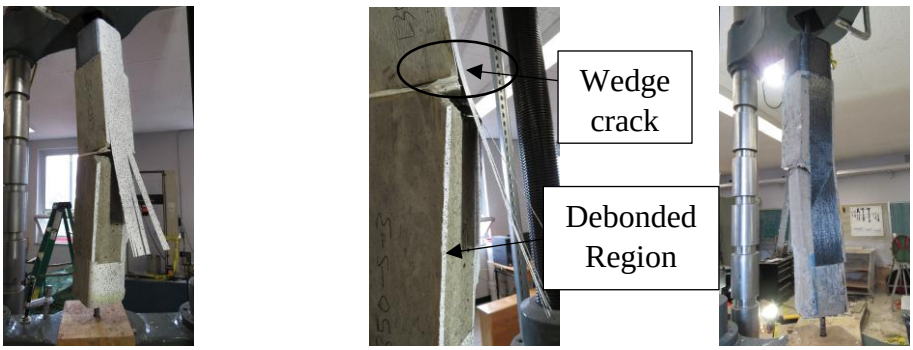

a) Front side b) Wedge Failure c) Black side

Figure A3.11: Views of Specimen L350-S-3 after Failure

Description of Specimen L350-S-3 before and after Test

Before the test, it was observed that the CFRP sheet installed on the prisms was not aligned to the center of the prisms. It was observed that the following happened to the specimen at/after failure:

- The specimen experienced brittle failure accompanied by a loud noise
- As seen in Figure A3.11(a), failure took place on the speckled side of the specimen.
- Tension crack was not observed on the concrete prisms.
- Concrete wedge crack occurred at the loaded end of the specimen as seen in Figure A3.11(b)
- The CFRP sheet was well bonded to concrete because debonding occurred by shearing of concrete below the bonded surface as seen in Figure A3.11(a)
- The back side of the specimen failed due to buckling of the FRP sheet immediately after the debonding failure of the front side took place as shown in Figure A3.11(c).

Analysis of Test Results

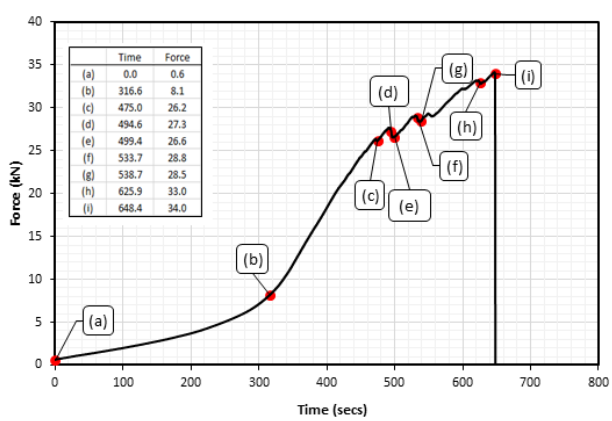

Figure A3.12: Force versus Time curve for Specimen L350-S-3 Showing Key Points During the Test

Comments on Figure A3.12:

Force increased with time. At point (d), there was a decrease in force to point (e) which then increased to point (i) before failure. The decrease in force is due to the initiation of wedge crack.

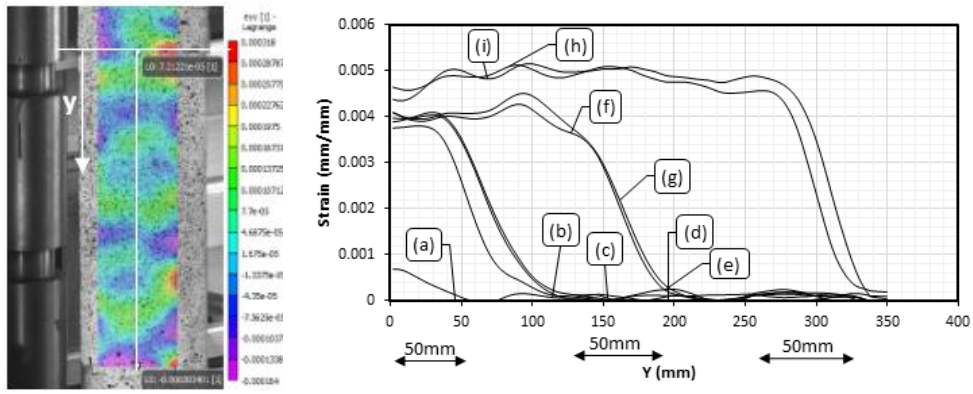

(a) (b)

Figure A3.13: (a) Contour Diagram Showing Position of Strain Inspector Line along the Bond Length of FRP Sheet (b) Strain versus Distance along the Bond Length of FRP Sheet at Times shown in Figure A3.12 for Specimen L350-S-3

Comments on Figure A3.13:

The strain values increased as the load increased over time. The slope (effective bond length) began to shift towards the unloaded end of FRP with flat segments at the loaded end indicating debonding. At (d), there was a decrease in strain to (e) due to a corresponding decrease in load.

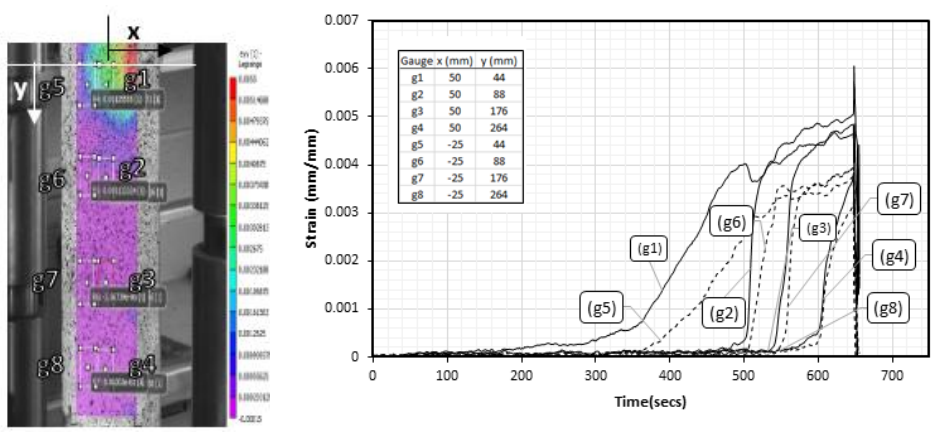

(a) (b)

Figure A3.14:(a) Contour Diagram Showing Position of 8 Gauges (b) Strain versus Time Curves of Specimen at Locations of Gauges as Indicated in the Contour Diagram in (a) for Specimen L350-S-3

Comments on Figure A3.14:

Gauges (g1), (g2), (g3) and (g4) recorded higher strain values than (g5), (g6), (g7) and (g8) due to shear lag and load eccentricity effect.

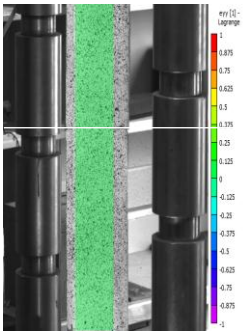

(a) ε_{yy} Dist. at T= 0 s

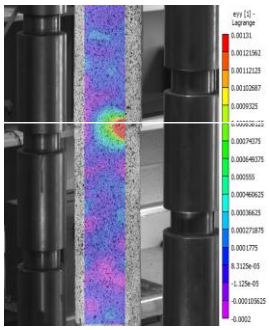

(b) ε_{yy} Dist. at T= 317 s

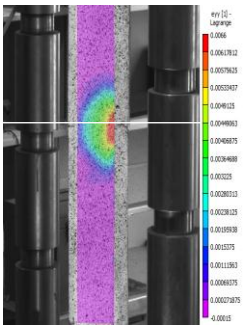

(c) ε_{yy} Dist. at T= 475 s

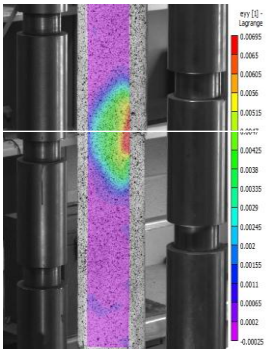

(d) ε_{yy} Dist. at T= 495 s

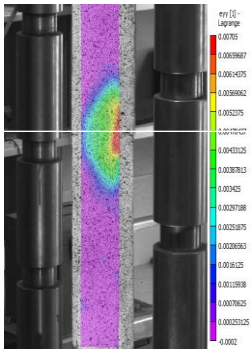

(e) ε_{yy} Dist. at T= 499 s

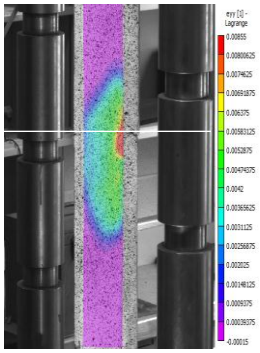

(f) ε_{yy} Dist. at T= 534 s

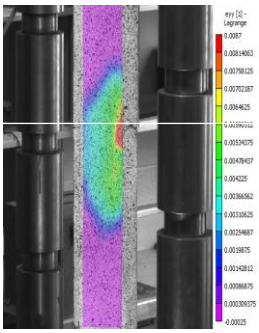

(g) ε_{yy} Dist. at T= 539 s

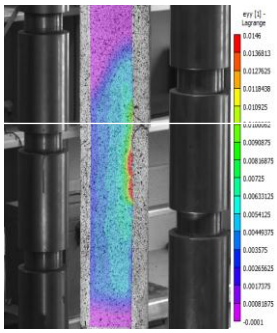

(h) ε_{yy} Dist. at T= 626 s

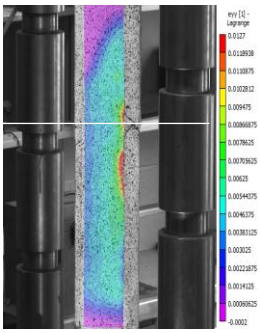

(i) ε_{yy} Dist. at T= 648 s

Figure A3.15: Strain Fields Showing distribution of longitudinal Strains (ε_{yy})on FRP Sheet at Different Times as Test Progressed to Failure for Specimen L350-S-3

Comments on Figure A3.15:

Contour diagrams show a gradual increase in longitudinal strain originating from the loaded end of the FRP sheet towards the unloaded end until failure. Shear lag effect was significant in the specimen as seen in the uneven distribution of strain across the width of the CFRP sheet.

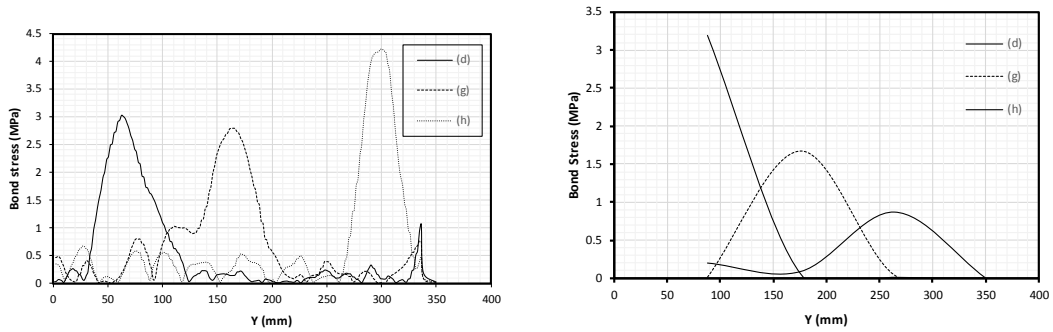

(a) (b)

Figure A3.16: Graph of Bond Stress along CFRP bond Length for Specimen L350-S-3 using (a) Equation 5.2 (b) Equation 5.3

Comments on Figure A3.16:

Both curves show similar trend where the maximum bond stress moved along the length of the CFRP sheet towards the unloaded end. This behaviour is like the strain profile where the active bond zone (development length) moved towards the unloaded end of the CFRP sheet. Equation 5.3 gave smoother curves due to the limitation in data points compared to curves obtained from Equation 5.2.

A3.3 Results for Specimen L350-S-4

- Specimen Installed Prior to Testing

a) Front of Specimen

b) Back of Specimen

c) Side of Specimen

Figure A3.17: Views of Specimen L350-S-4 Installed in Testing Machine Prior to Testing

- Test Results

Pictures of Specimen after Testing:

a) Front side

b) Right Side

c) Wedge Failure

Figure A3.18: Views of Specimen L350-S-4 after Failure

Description of Specimen L350-S-4 before and after Failure

FRP sheet was properly aligned to the center of the prisms. It was observed that the following happened to the specimen at/after failure:

- The specimen experienced brittle failure accompanied by a loud noise
- As seen in Figure A3.18(b), failure took place on the back side of the specimen.
- Tension crack normal to the force was not observed in this specimen.
- Concrete wedge crack occurred at the loaded end of the FRP sheet as seen in Figure A3.18(c)
- The CFRP sheet was well bonded to concrete because debonding occurred by shearing of concrete below the bonded surface.
- The front side of the specimen failed due to buckling of the FRP sheet immediately after the debonding failure of the back side took place as shown in Figure A3.18(a).

Analysis of Test Results

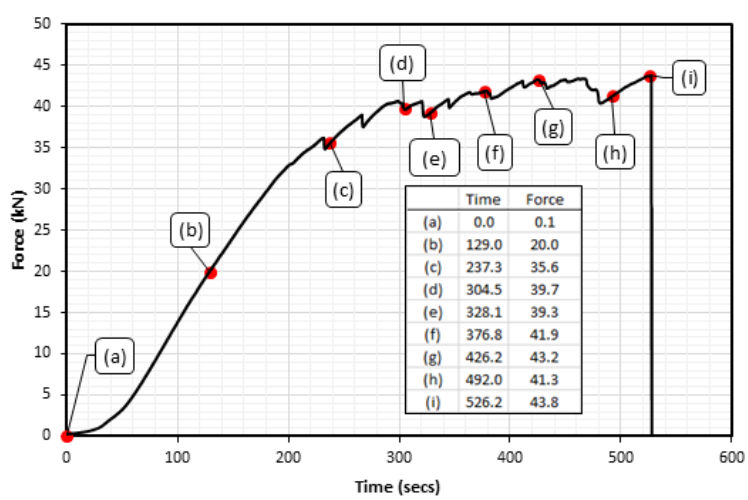

	Time	Force
(a)	0.0	0.1
(b)	129.0	20.0
(c)	237.3	35.6
(d)	304.5	39.7
(e)	328.1	39.3
(f)	376.8	41.9
(g)	426.2	43.2
(h)	492.0	41.3
(i)	526.2	43.8

Figure A3.19: Force versus Time curve for Specimen L350-S-4 Showing Key Points During the Test

Comments on Figure A3.19:

Force increased over time with the values increasing and decreasing from point (c) to (i) before failure. This may be due to the initiation of wedge crack on the concrete prisms.

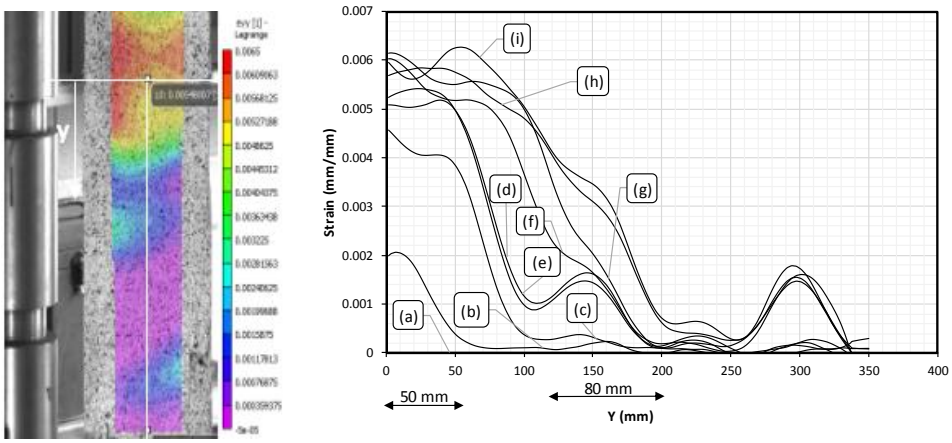

(a) (b)

Figure A3.20: (a) Contour Diagram Showing Position of Strain Inspector Line along the Bond Length of FRP Sheet (b) Strain versus Distance along the Bond Length of FRP Sheet at Times shown in Figure A3.19 for Specimen L350-S-4

<u>Comments on Figure A3.20:</u>

The strain values increased as the load increased over time. The slope (effective bond length) began to shift towards the unloaded end of the FRP sheet with flat segments at the loaded end. This indicates the initiation of wedge cracks. Strain increased before failure at (i).

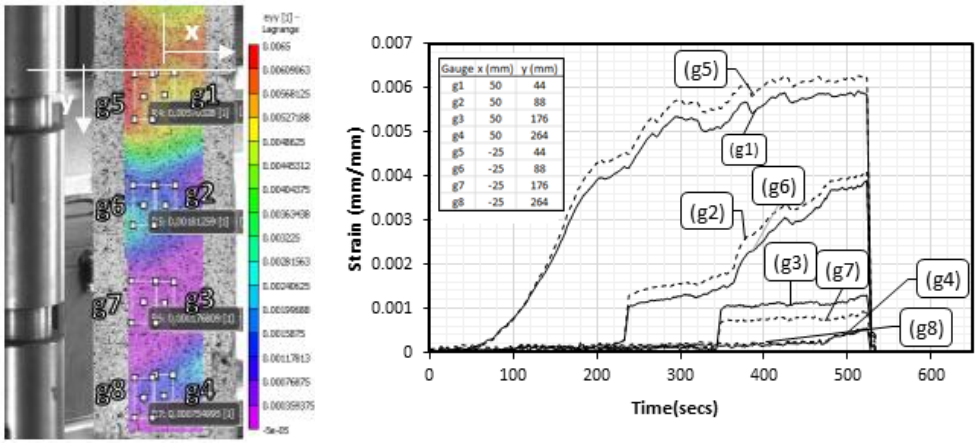

(a) (b)

Figure A3.21:(a) Contour Diagram Showing Position of 8 Gauges (b) Strain versus Time Curves of Specimen at Locations of Gauges as Indicated in the Contour Diagram in (a) for L350-S-4

Comments on Figure A3.21:

Gauges (g1), (g2), (g3) and (g4) recorded higher strain values than (g5), (g6), (g7) and (g8) due to shear lag and load eccentricity effect. Strain values at Gauges (g1) and (g5) started to increase before others picked up over time.

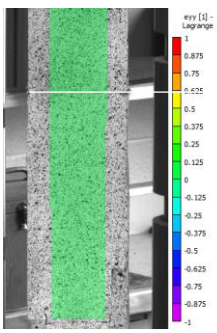

(a) ε_{yy} Dist. at T= 0 s

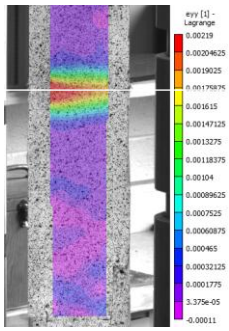

(b) ε_{yy} Dist.at T= 129 s

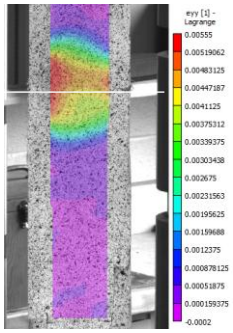

(c) ε_{yy} Dist. at T= 237 s

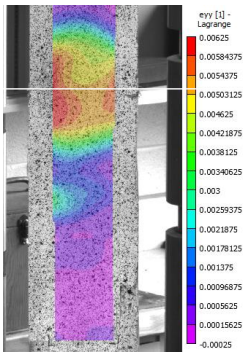

(d) ε_{yy} Dist. at T= 305 s

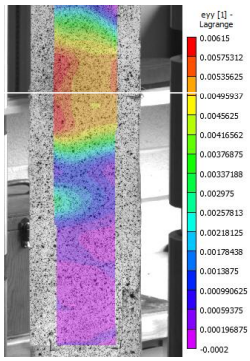

(e) ε_{yy} Dist. at T= 328 s

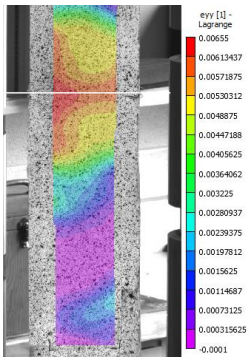

(f) ε_{yy} Dist. at T= 377 s

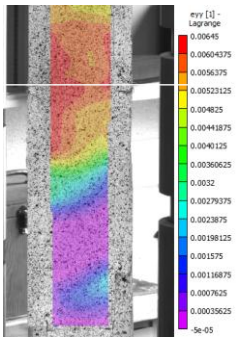

(g) ε_{yy} Dist. at T= 426 s

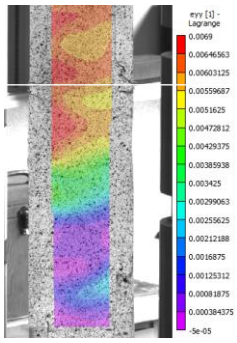

(h) ε_{yy} Dist. at T= 492 s

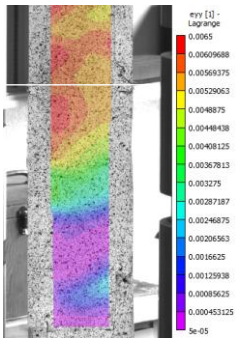

(i) ε_{yy} Dist. at T= 526 s

Figure A3.22: Strain Fields Showing the Distribution of Longitudinal Strains (ε_{yy}) on FRP at Different Times as Test Progressed to Failure for Specimen L350-S-4

Comments on Figure A3.22:

Contour diagrams show a gradual increase in longitudinal strain originating from the loaded section towards the unloaded end of the FRP sheet until failure. Shear lag effect was significant in the specimen as seen in the parabolic distribution of strain across the width of the CFRP.

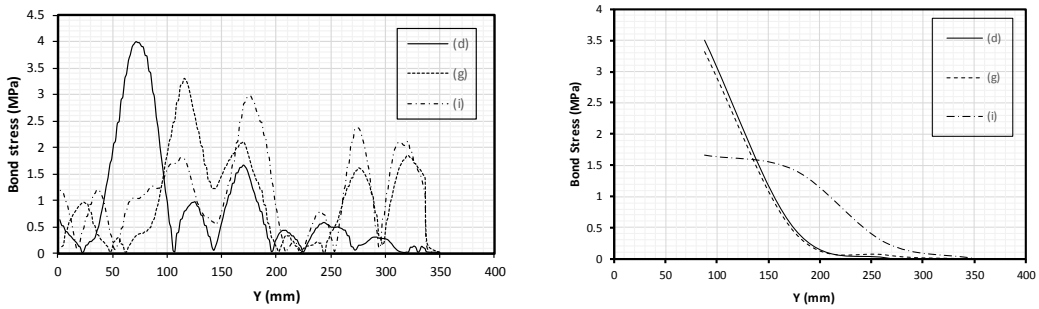

(a) (b)

Figure A3.23: Graph of Bond Stress along CFRP bond Length of Specimen L350-S-4 using (a) Equation 5.2 (b) Equation 5.3

Comments on Figure A3.23:

Figure 6.72(a) showed similar trend as observed for other specimens while Curves from Equation 5.3 did not show similar trend as observed in other specimens.

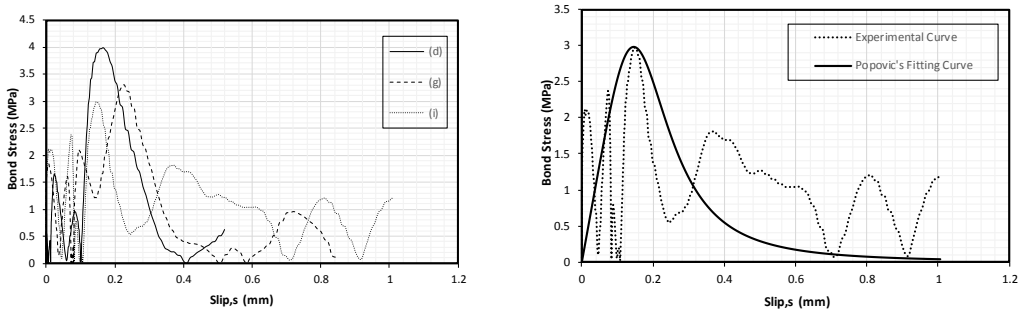

(a) (b)

Figure A3.24: Relationship between Bond Stress and Slip for Specimen L350-S-4 at varying Load Levels and the Corresponding Fitting Curve

Comments on Figure A3.24:

From Figure A3.24(a), the bond-slip relationship gives a curve with a sharp increase at the initial stage of the test. The descending region correlates with the elastic strain distribution which moves along the along the bond length of the CFRP as debonding cracks propagates towards the unloaded end. There is a correlation between the experimental curve and the fitting curve as observed from Figure A4.24(b).

CURRICULUM VITAE

Candidate's full name: Emmanuella Oluwatoyin Atunbi

Universities attended:

- Bachelor of Science in Civil Engineering: University of Ilorin, Ilorin, Nigeria (September 2009-June 2014)
- Publications: N/A
- Conference Presentations: N/A